RECOGNITION AND MONITORING OF HUMAN MOTIONS USING RF SIGNALS

Doktora Tezi

Can UYSAL

Eskişehir, 2020

RECOGNITION AND MONITORING OF HUMAN MOTIONS USING RF SIGNALS

Can UYSAL

DOKTORA TEZİ

Elektrik-Elektronik Mühendisliği Anabilim Dalı
Danışman: Doç. Dr. Tansu FİLİK

Eskişehir
Eskişehir Teknik Üniversitesi
Lisansüstü Eğitim Enstitüsü
AĞUSTOS 2020

Bu tez çalışması, BAP Komisyonu tarafından kabul edilen 20DRP022 numaralı proje kapsamında desteklenmiştir.

ÖZET

İNSAN HAREKETLERİNİN RF SİNYALLERİ KULLANARAK TANIMLANMASI VE İZLENMESİ

Can UYSAL

Elektrik-Elektronik Mühendisliği Anabilim Dalı
Elektromanyetik Alanlar ve Mikrodalga Tekniği Bilim Dalı
Eskişehir Teknik Üniversitesi, Lisansüstü Eğitim Enstitüsü, Ağustos 2020

Danışman: Doç. Dr. Tansu FİLİK

Bu tezde, iç ortam ve duvar arkası sağlık takibi ve aktivite tanıma uygulamaları için kablosuz radyo-frekans (RF) sinyallerinin potansiyelleri araştırılmıştır. Elektromanyetik dalgaların yayılım yolu üzerindeki veya yakınındaki hareketli veya sabit nesneler alınan RF sinyallerin dalga biçimini etkilemektedir. Son dönemlerde, bu RF sinyalleri, literatürdeki düşme tespiti, yaşamsal işaret takibi, aktivite tanıma gibi farklı sağlık hizmeti uygulamaları için incelenmektedir. Sağlıklı insanlar için bile, yaşamsal işaretlerden biri olan solunum hızını (RR) gerçek zamanlı olarak izlemek hayat kurtarıcı olabilmektedir. Koronavirüs hastalığı 2019'un (COVID-19) erken dönemde solunumla ilgili hafif semptomlara neden olduğu bildirilmektedir. Huzurevleri ve evlerindeki insanların solunum hızlarının temassız bir yöntemle sürekli olarak izlenmesi yakın gelecekte daha önemli olacaktır. Bu tezde ilk uygulama olarak temassız yaşamsal solunum hızı izleme seçilmiş ve üç farklı sinyal modeli ve yeni yöntemler önerilmiştir. Önerilen sistemde, yüksek çözünürlüklü altuzay-tabanlı parametrik spektral kestirim yaklaşımları, rotasyonel değişmezlik tekniği ile sinyal parametrelerinin kestirimi (ESPRIT) ve çoklu sinyal sınıflandırması (MUSIC), ve ardışık bağlanımlı hareketli ortalama (ARMA) modeli-tabanlı Quinn ve Fernandes (QF) tekniği solunum hızı kestirim algoritmaları olarak sunulmaktadır. Önerilen temassız solunum hızı izleme sisteminin kısıtlı veriyle çok yüksek doğruluğa sahip sonuçlara ulaştığı ve literatürde yaygın olarak kullanılan referans periodogram yönteminden üstün olduğu gerçek dünya ayarları ve ölçümleriyle yapılan deneylerle gösteril-

mektedir. Standart ortak kokusuz Kalman filtresi (JUKF) yöntemi de bu yeni ve zaman açısından kritik problem için modifiye edilmiştir ve önerilen modifiye JUKF (ModJUKF) yönteminin zamanla değişen solunum hızı senaryosunda pencereleme-tabanlı yöntemlere göre düşük bir hata oranına ulaştığı deneylerde gösterilmiştir.

İkinci uygulama olarak, duvar arkası (TTW) statik/hareketli insan tespiti problemi araştırılmıştır. İnsan solunumunun neden olduğu çok küçük yansımalar kullanılarak duvar arkasındaki statik insanın varlığının tespiti literatürde ilk defa önerilmekte/ kullanılmaktadır. Önerilen makine öğrenimi tabanlı yöntemin, çift duvar arkası senaryosunda hem statik hem de hareketli insanın tespiti için %99'un üzerinde doğruluk elde ettiği çeşitli deneylerle gösterilmektedir. Önerilen sistemin makine öğrenimi modelini yeniden eğitmeden yeni bir ortamda kullanılabileceği gerçek deneylerle de doğrulanmaktadır.

Son uygulama 26 harfi RF sinyallerini kullanarak sınıflandıran cihazsız havaya-yazma tanıma sistemi olan bir insan-makine etkileşimi uygulamasıdır. Önerilen sistem, el hareketi tanıma için literatürde ilk kez Ayrık Kosinüs Dönüşümü (DCT) katsayılarını ayırtedici özellikler olarak kullanmaktadır. Önerilen sistemde, sınıflandırma doğruluğunu iyileştirmek için kullanılan polarizasyon çeşitliliğini sağlamak için iki-kanallı alıcıda zıt kutuplu (yatay ve dikey) antenler kullanılmaktadır. Önerilen sistemin havaya-yazılmış 26 harfin sınıflandırılmasında %95.15 doğruluğa ulaştığı ve oldukça yeni WiFi tabanlı havaya-yazma tanıma yaklaşımlarından daha iyi performans gösterdiği gerçek ölçümlere yapılan deneylerle gösterilmektedir.

Tüm bu uygulamalarda, kablosuz RF sinyalleri düşük maliyetli yazılım tabanlı radyo (SDR) modulleri ile üretilmekte ve alınmaktadır. Sunulan sistemler, gerçekçi senaryolarla uyumlu, farklı sayıda gönüllüden toplanan gerçek ölçümlerle gerçekleştirilen çeşitli deneylerle doğrulanmıştır.

Anahtar Sözcükler: RF sinyalleri, duvar arkası, sağlık hizmetleri, solunum hızı kestirimi, temassız, Kalman filtre, makine öğrenmesi, statik insan tespiti, insan-makine etkileşimi, cihazsız, havaya-yazma tanıma, Ayrık Kosinüs Dönüşümü, yazılım-tabanlı radyo.

ABSTRACT

RECOGNITION AND MONITORING OF HUMAN MOTIONS USING RF SIGNALS

Can UYSAL

Department of Electrical and Electronics Engineering
Programme in Electromagnetic Fields and Microwave Technique
Eskişehir Technical University, Institute of Graduate Programs, August 2020

Supervisor: Assoc. Prof. Dr. Tansu FİLİK

In this thesis, the potentials of radio frequency (RF) signals are investigated for indoor and through-the-wall (TTW) health monitoring and activity recognition applications. The moving or stationary objects on or near the propagation path of electromagnetic waves affects the received RF signals waveform. Recently, these RF signals are examined in literature for different healthcare applications, such as fall detection, vital sign monitoring, etc., and activity recognition. It can be life-saving to monitor the respiratory rate (RR), one of the vital signs, even for healthy people in real-time. It is reported that coronavirus disease 2019 (COVID-19) causes mild respiratory symptoms in the early stage. It is more important to continuously monitor the RR of people in nursing homes and houses with noncontact methods. In this thesis, the noncontact vital RR monitoring is chosen as the first application and three different signal models and new methods are proposed. In the proposed system, the high resolution subspace-based parametric spectral estimation approaches, estimation of signal parameters by rotational invariance technique (ESPRIT) and multiple signal classification (MUSIC), and auto-regressive and moving average (ARMA) model-based techniques are presented as the RR estimation algorithms. It is shown by the experiments with real-world settings and measurements that the proposed noncontact RR monitoring system achieves very accurate results with the limited number of observations and outperforms the periodogram method commonly used as the benchmark in the literature. The standard joint unscented Kalman filter (JUKF) method is also modified for this new and time-critical problem and it is shown in the experiments

that the proposed modified JUKF (ModJUKF) method attains a low error rate according to the windowing-based methods in the time-varying RR scenario.

As the second application, TTW static/moving human detection problem is investigated. The presence detection of the static human behind the wall using minute reflections caused by human breathing is the first time proposed/used in the literature. It is shown in various experiments that the proposed machine learning-based method achieves over 99% accuracy for the detection of both static and moving human in double TTW scenario. It is also validated with the real experiments that the proposed system can be used in a new environment without retraining the machine learning model.

The last application is a human-machine interaction application which is a device-free air-writing recognition system that classifies 26 capital letters using RF signals. The proposed system uses the Discrete Cosine Transform (DCT) coefficients as discriminative features for the first time for gesture recognition. The oppositely polarized (i.e. horizontal and vertical) antennas are used in the two-channel receiver to provide polarization diversity that is exploited to improve the classification accuracy. It is shown with experiments conducted with real measurements that the proposed system, which achieves 95.15% accuracy in the classification of 26 air-written letters, outperforms the fairly new WiFi-based air-writing recognition approaches.

In all these applications, RF signals are generated and captured by low-cost software-defined radio (SDR) modules. The presented systems are validated through various experiments conducted with real measurements collected from different numbers of volunteers and from different places compatible with realistic scenarios.

Keywords: RF signals, through-the-wall, healthcare, respiratory rate estimation, non-contact, Kalman filter, machine learning, static human detection, human-machine interactions, device-free, air-writing recognition, Discrete Cosine Transform, software-defined radios.

14/08/2020

STATEMENT OF COMPLIANCE WITH ETHICAL PRINCIPLES AND RULES

I hereby truthfully declare that this thesis is an original work prepared by me; that I have behaved in accordance with the scientific ethical principles and rules throughout the stages of preparation, data collection, analysis and presentation of my work; that I have cited the sources of all the data and information that could be obtained within the scope of this study, and included these sources in the references section; and that this study has been scanned for plagiarism with "scientific plagiarism detection program" used by Eskişehir Technical University, and that "it does not have any plagiarism" whatsoever. I also declare that, if a case contrary to my declaration is detected in my work at any time, I hereby express my consent to all the ethical and legal consequences that are involved.

. . . . . .

Can UYSAL

ACKNOWLEDGMENTS

I would like to express my sincere gratitude to my supervisor, Assoc. Prof. Dr. Tansu Filik, for all the support and mentoring during my graduate studies. Dr. Filik always has motivated and guided me to pursue the goals against all the odds. He is a very special and precious teacher for me.

I would like to thank Prof. Dr. Ömer Nezih Gerek and Assist. Prof. Dr. Efnan Şora Günal for their valuable suggestions throughout the whole period and for their time in the Progress Committee meetings. I also want to thank Prof. Dr. Mehmet Tankut Özgen, Assoc. Prof. Dr. Evren Ekmekçi, and Assoc. Prof. Dr. Yılmaz Kalkan for their comments and suggestions in order to improve the quality of the thesis.

I would like to thank Mustafa Demirtaş, Asım Önder, Onur Kılınç, Burak Batmaz, Ahmet Murat Türk, Mustafa Gökçe who helped in collecting the respiratory rate measurements, and also Altan Onat for his contributions to the thesis. I also thank Burak Benligiray for preparing the thesis template.

I would like to thank TUBİTAK for their financial support with a scholarship during my doctorate education.

Finally, I want to thank my family and my wife Sultan Uysal for their support and love.

I would like to dedicate this thesis to my dear daughter Defne. I love her more than anything.

Can UYSAL

August 2020

TABLE OF CONTENTS

LIST OF TABLES

LIST OF FIGURES

ABBREVIATIONS

ARMA	Auto Regressive and Moving Average
CSI	Channel State Information
DCT	Discrete Cosine Transform
DWT	Discrete Wavelet Transform
ESPRIT	Estimation of Signal Parameters by Rotational Invariance Technique
HMI	Human Machine Interaction
JUKF	Joint Unscented Kalman Filter
KNN	K-Nearest Neighbor
LOS	Line of Sight
MAE	Mean Absolute Error
ModJUKF	Modified Joint Unscented Kalman Filter
MUSIC	Multiple Signal Classification
QF	Quinn and Fernandes
RR	Respiratory Rate
RF	Radio Frequency
RSS	Received Signal Strength
SDR	Software Defined Radio
SNR	Signal-to-Noise Ratio
SVM	Support Vector Machines
TTW	Through The Wall
UWB	Ultra-wideband

1. INTRODUCTION

In this thesis, sensing, recognition and, monitoring of moving objects in a noncontact manner using radio-frequency (RF) signals are investigated. The moving or stationary objects on or near the propagation path between the transmitter (TX) and the receiver (RX) affect the received RF signals. It is experimentally observed that the amplitude and phase of received RF signals which are affected by the moving or stationary objects in the environment are correlated to the objects. Thus, it can be possible to achieve meaningful inferences such as detection of human presence, monitoring of vital signs, and recognition of micro-level gestures by analyzing the received signal parameters. Some other technologies such as audio and vision based techniques are widely used in literature for human activity and gesture recognition, vital sign monitoring, etc. But the use of RF signals for these purposes is a new and challenging problem for literature.

In this thesis, three main practical applications using RF signals are considered. The noncontact RR monitoring is chosen as the first application and three different signal models and new methods are proposed. In the proposed system, the high resolution subspace-based parametric spectral estimation approaches, ESPRIT and MUSIC, and ARMA model-based QF technique are presented as the RR estimation algorithms. The standard JUKF method is also modified for this new and time-critical problem. As the second application TTW static/moving human detection problem is investigated. The presence detection of the static human behind the wall using minute reflections caused by human breathing is the first time proposed/used in the literature. The last application is a human-machine interaction application which is a device-free air-writing recognition system that classifies 26 capital letters using RF signals. The proposed system uses the DCT coefficients as discriminative features for the first time in the literature for gesture recognition. In the proposed system, the oppositely polarized (i.e. horizontal and vertical) antennas are used in the two-channel receiver to provide polarization diversity that is exploited to increase the classification accuracy. In all these applications, RF signals are generated and captured by low-cost SDR modules. SDR modules that are reconfigurable and easy to control provide fine-grained signal measurements. The presented systems are validated through various experiments conducted with real measurements collected from

different numbers of volunteers, compatible with realistic scenarios.

1.1. Motivation and Objectives

This section provides an overview of the main motivations and objectives of the thesis.

- Respiratory Rate Monitoring

Elderly monitoring systems are becoming widespread with the increase in the elderly population around the world, and continuous monitoring of respiratory rate (RR) is vital, especially for those who live alone and suffer from respiratory diseases. Especially, the infection with severe acute respiratory syndrome (SARS), Middle East respiratory syndrome (MERS), and coronavirus disease 2019 (COVID-19) can cause a severe viral respiratory illness. The traditional RR monitoring methods require physical contact with the human body [1]. These contact-based methods, such as capnography or impedance pneumography, are used especially in clinical environments and require dedicated healthcare professionals [2]. There are also some other methods that use the physiological signals such as electrocardiography (ECG) [3], polysomnography (PSG), photoplethysmography (PPG) [4, 5]. Alternatively, some wearable sensor-based solutions such as microphones and accelerometers operating in non-clinical settings have emerged [6, 7]. In addition, sleep mattresses with pressure sensors are used for RR monitoring. In all these contact-based systems, some special sensing modules are required that limit patient mobility and comfort, and this is not suitable especially for long-term and remote patient monitoring at home or in nursing homes. Contactless monitoring the health status of patients with the infectious diseases mentioned above is very important since both preventing the spread of the disease and reducing the vital risk of the relevant healthcare staff. In addition to these wireless sensing systems, other noncontact methods which are using different technologies such as visual are also investigated in literature. However, vision-based systems have some disadvantages such as requiring daylight and line-of-sight propagation, and violating the privacy of private life. The main motivation is the use a new sensing technology (wireless) that will eliminate all the above disadvantages.

- Recognition of Moving Objects Using Machine Learning Techniques

In recent years, there has been an increasing interest in machine learning-based human sensing using RF signals instead of visual and audio (acoustic) signals. In this context the

studies, using radio propagation characteristics as features, increases. RF-based human sensing techniques aim to recognize information about humans such as presence, location, moving trajectory, activity, gesture, identity, vital sign, etc. using RF signals. In this scope, presence detection of static/moving human through the wall and device-free air-writing recognition which is one of the applications of human-machine interactions are quite new and challenging problems.

Through-the-Wall Human Detection: Through-the-wall (TTW) systems are useful for monitoring and detecting non-cooperative people. Such a system that can detect the presence of a non-cooperative person behind a wall can be used by law enforcement for better planning in hostage rescue operations. In addition, it can be used in home health-care services to monitor the health status of the elderly. In a post-disaster emergency, first responders can use such a system to detect the presence of people under the avalanche or debris. In such cases, people have significantly limited movement capabilities or they may lie unconsciously completely motionless. Therefore, detection of the motionless (static) human through the wall has significant importance especially for after disaster scenarios. In these emergency situations, using active systems where a controlled RF signal is emitted, and the received signal is analyzed to detect presence of a live human are effective since using opportunity signals, such as WiFi is not possible. Traditional RF-based methods use ultra-wideband (UWB) radar technology for the presence detection of human. These systems that occupy very high bandwidth require specific devices and big antennas. Existing human detection solutions utilize the analysis of RF signals that are affected by human movements. RF signals attenuate as they pass through the wall since some of them reflect from the wall. Therefore, TTW static human detection using RF signals is a very challenging problem. Periodic chest/abdominal movements caused by breathing can be used to separate the presence of static human from the empty environment.

Air-Writing Recognition: In recent years, the requirements of human-machine interactions (HMI) are increasing, especially for smart home, and industrial applications, gaming, and virtual reality world, etc. Traditional methods such as a keyboard and touch screen will not be preferred in the future's entertainment, home, and industrial applications. Other device-based methods require the user to wear a special sensor such as Data Glove or to hold a controller such as Wiimote for air-writing. Contactless (device-free) techniques such as air-writing, gesture recognition, speech recognition are becoming more

popular. These contactless techniques are widely using visual and acoustic technologies. Air-writing recognition using RF waves is a very challenging problem since the RF waveforms of the same letter are never identical even if the letters are written by the same person. The potentials of RF waves for human-machine interactions such as air-writing, which is defined as the user writing letters or words in the air, are investigated in this thesis.

The main objective of this thesis is to develop noncontact respiratory rate monitoring system for three different signal model, and machine learning approaches for through-the-wall presence detection of static/moving human based on human breathing and gesture (letters written in the air) recognition using RF signals.

1.2. Overview of Human Sensing Technologies

This section provides a general overview of the current sensing technologies used in human or moving object sensing systems. Basically, it is possible to categorize these technologies into two groups according to the sensor type: device-free and device-based sensing [8]. Device-based systems use a physical sensing module attached to the human body. These methods utilize on-body wearable sensors (accelerometer, gyroscope, pulse oximeter, thermal sensor, etc.) to sense the movements of body parts [9, 10, 11]. Although wearable sensors based systems offer low-cost solutions, they have some disadvantages. When wearable systems are used, the measuring devices are directly attached to the human body. For example, wearing a noise probe, wearing a chest band or lying on a private bed can disturb people. However, elder patients may forget to wear these sensors, and children may remove or lose them. Also baby's skin may be irritated by these sensors due to being worn on their bodies. On the other hand, device-free sensing systems can be categorized into three groups: 1) vision-based, 2) ambient sensors-based, 3) RF-based. Vision-based methods take advantage of camera to record the video sequence and sensing the human using computer vision algorithms [12, 13]. But these methods are completely dependent on daylight and have high computational cost. There is also violation of the privacy of private life. In the ambient sensors-based methods, the data received from physical sensors in the fixed position in the environment such as pressure sensor, vibration sensor, passive infrared (PIR) sensor, etc. are used [14, 15, 16]. These methods require specific sensing modules and have some disadvantages such as energy

consumption and deployment cost.

In recent years, RF-based methods for human sensing have emerged [17, 18, 19]. RF signals are reflected, scattered and attenuated by the human body. For this reason, these signals are influenced by the presence and/or movements of the human on the propagation path between the transmitter and the receiver. In all applications, the effect of the presence/movements of human to the propagation channel of the radio signals is analysed. Compared to other sensing methods, RF based methods do not require a physical sensing module, as they only benefit from wireless communication features. Thus, the deployment cost is removed, energy consumption for sensing and data transmission is reduced, and the right of privacy is protected.

1.3. Contributions

The key contributions of the thesis can be summarized into three parts as follows,

- An RF-based noncontact respiratory monitoring system is proposed in Chapter 3.
  - A new RF-based noncontact RR monitoring system is proposed. The covariance matrix model-based superior high resolution spectrum estimation methods, ESPRIT and MUSIC, are applied to RR estimation for the first time in this thesis. The system includes a simple motion detection algorithm based on adaptive thresholding to eliminate the effects of the large-scale body movements on the RR estimation. It is shown that high resolution techniques achieve very low error rate with the limited number of data and significantly improve the RR estimation accuracy according to the benchmark method (periodogram) in literature [20, 21].
  - A novel modification to the JUKF method is proposed for the real-time estimation and tracking of RR, which is called ModJUKF. Due to the nonlinear structure of the RR estimation problem with respect to the measurement hereby, a new and novel modification is proposed in this thesis to transform measurement errors into parameters errors by using the hyperbolic tangent function. The proposed method reduces the computational complexity and improves the accuracy according to the standard JUKF method. In addition,

ModJUKF achieves the highest accuracy among the windowing-based common methods in the time-varying RR scenario [22].

- An efficient RF-based noncontact sleep monitoring system is proposed. ARMA model based frequency estimation algorithm, Quinn and Fernandes (QF) method is firstly adapted and used for the RR estimation. The proposed noncontact system can successfully separate body movements (turnovers), breath holding (apnea) and breathing cases with the sleep event detection method [23].

- A machine learning-based system for TTW presence detection of static/moving human using RF signals is presented in Chapter 4 [24].
  - The presence detection of the static human using minute reflections caused by human breathing for the double TTW scenario is the first time proposed in the literature. Double TTW is a more challenging scenario where both transmitter and receiver are placed in different rooms from the one in which the human exists.
  - Periodic chest movements caused by breathing cause a periodic change in the received signal. The RR estimates obtained using this periodicity are used to distinguish the presence of a static human from a human-free environment. In addition, variance, which has great potential to separate dynamic and static conditions, is used to detect the presence of moving human.
  - It is shown in various experiments that the proposed system achieves over 99% accuracy for the detection of both static and moving human in double TTW scenario. It is also validated with the experiments conducted in realistic scenarios that the proposed system can be used in a new environment without retraining the model.

- A machine learning-based air-writing recognition system that classifies 26 capital letters using RF signals is presented in Chapter 4. The presented system does not require any wearable sensor or hand-held controller for writing the letters in the air [25].
  - In the proposed system, the oppositely polarized (i.e. horizontal and vertical)

antennas are used in the two-channel receiver to provide polarization diversity that is exploited to improve the classification accuracy.

  - The proposed system uses the DCT coefficients as discriminative features for the first time in the literature for air-writing recognition. These spectral features are more efficient than conventional time-domain features which cannot distinguish subtle letter gestures.
  - The proposed system also includes a letter segmentation stage that uses a thresholding-based method to identify the data segments which contain air-writing.

- The proposed system utilizes the narrowband unmodulated continuous wave signals captured by powerful low-cost SDR modules which provide flexibility and versatility to the users [20, 21, 22, 23, 24, 25].

1.4. Thesis Outline

In this section, the organization and overview of the contents of the subsequent chapters of the thesis are presented.

In Chapter 2, the background of RF sensing concept is provided. The chapter begins with the basics of the electromagnetic wave propagation. Then the received signal models are given and how a moving object affects the RF signal is discussed. RF-based monitoring and sensing technology is described and the application areas of this technology are briefly discussed. Finally, background information for different types of RF signals that are used on the purpose of RF sensing are provided.

In Chapter 3, the noncontact respiratory rate (RR) monitoring system using RF signals is presented. First, basics of respiration are given and the effects of respiration to RF signal are shown. Then the mathematical formulations of the breathing signal are considered. Three different signal models are presented. Next, the preprocessing steps that are required to prepare the data are discussed. The motion detection algorithm used for the eliminate the effects of the large-scale body movements on the RR estimation and sleep event detection algorithm used to separate the cases during sleep are presented. Then, the RR estimation methods are presented and the experimental results are given to validate the accuracy of the presented methods.

In Chapter 4, machine learning-based applications are considered. First, TTW presence detection system for both static and moving human is presented. The extracted features used by the classifier are described. Various experimental results are given to demonstrate the effectiveness and robustness of the presented TTW human detection system. Then, a machine-learning based air-writing recognition system that classifies 26 capital letters using RF signals is presented. The basics of antenna polarization and effect of the polarization diversity are discussed. In addition, a letter segmentation algorithm to identify the data segments which contain air-writing activity is presented. Then, DCT-based features that are fed into the machine learning algorithm to generate a model are described. Finally, the performances of the proposed air-writing recognition system are extracted.

In Chapter 5, the conclusion of the thesis is given.

2. BACKGROUND & RELATED WORK

2.1. Background

RF signals are electromagnetic waves whose frequency range can vary from 3 kHz to 300 GHz. Electromagnetic waves are exposed to some effects while propagating in space. Some of these effects are reflection, refraction, absorption and scattering [26]. For example, a radio wave can propagate through an object, but some of the wave will be reflected on the object surface, and some of its energy will be absorbed by the body. In addition, the propagation of waves depends on the frequency. At high RF frequencies, the wavelength of the waves is at the millimeter level, so the scattering of the wave is almost non-existent and the dominant effects are the reflection and absorption of the waves, which leads to the attenuation of the wave energy [27]. The advantage of using RF signals is that they pass through non-metallic materials, thereby enabling the human body to be sensed from behind the wall. RF-based monitoring methods do not require line-of-sight path.

Another important factor in the propagation of radio waves is multipath propagation. The transmitted radio signals are reflected from many different moving or static objects. Different versions of the transmitted signal reaching the receiver in different ways are called multipath components. The effect of the multipath changes according to the distribution of intensity, propagation time and bandwidth of the transmitted signal [26]. The random phase and amplitudes of different multipath components cause fluctuations in signal strength. Multipath causes attenuation in power (in general), delay in time, shift in phase and frequency [27].

Fig. 2.1 shows an illustration of typical radio channel propagation between a transmitter and a receiver. The received signal consists of line-of-sight (LOS) component and multipath components like wall and human body reflections. While the wall reflection is caused by static objects, the body reflection is caused by a moving object.

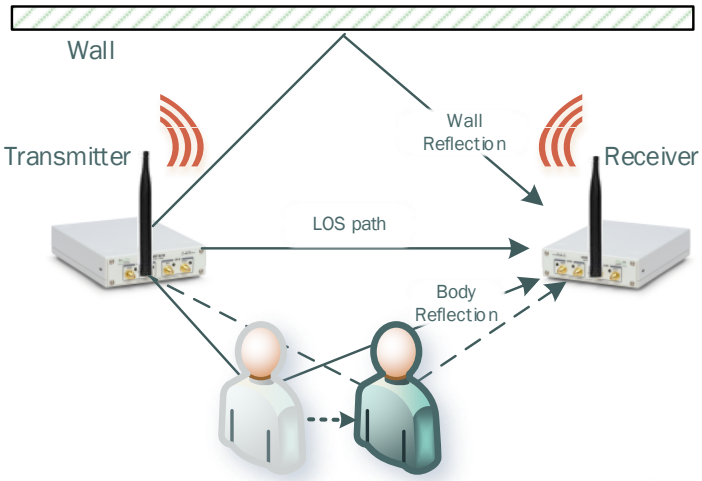

Figure 2.1: Illustration of typical radio channel propagation.

2.2. Radio Channel Measurements

The radio channel between the transmitter and the receiver can be modeled as a linear time-varying filter with the impulse response as follows [28] ,

$$h(t,\tau) = \sum_{i=1}^{N} \alpha_i(t)\delta\left(\tau - \tau_i(t)\right) e^{j\theta_i(t)} \tag{2.1}$$

where N is the number of multipath and i is the path index. $\alpha_i(t)$, $\theta_i(t)$, and $\tau_i(t)$ are time-varying amplitude, phase and time-delay of the i^{th} path, respectively. $\delta(.)$ is the delta function. This model is valid for wideband channels (i.e. Ultra-wideband (UWB) transceivers) [29]. Narrowband devices cannot receive multipath signals individually, instead they only measure magnitude and phase [30]. Multipath signals cause fluctuations in the received signal magnitude and phase in narrowband systems. When an unmodulated continuous wave is emitted from the transmitter, the received signal excluding noise is measured as the sum of all multipath components which resulting in complex baseband voltage as follows [31],

$$V(t) = \sum_{i=1}^{N} |\alpha_i(t)| e^{j(\theta_i(t)+2\pi\tau_i(t))} \tag{2.2}$$

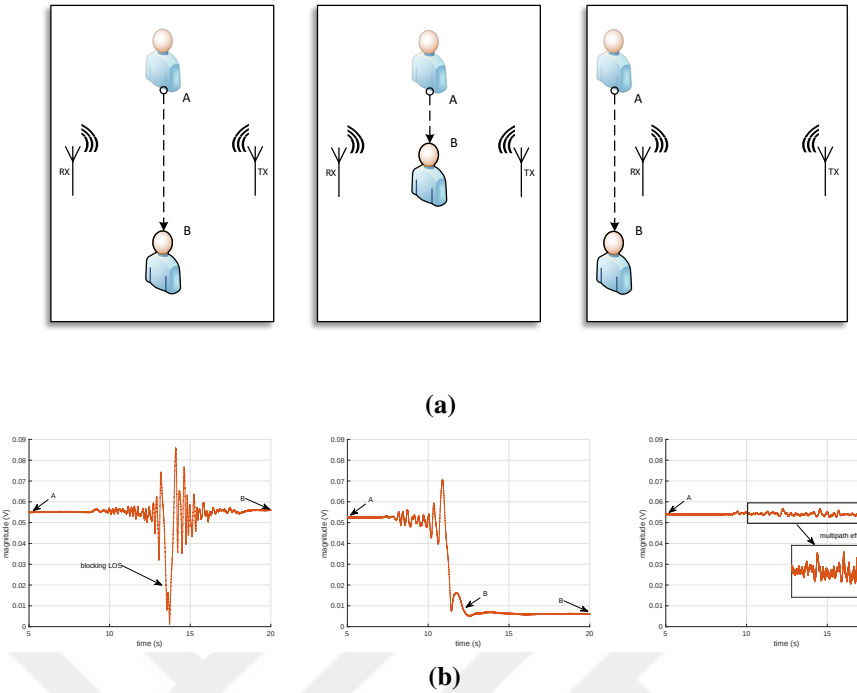

Figure 2.2: (a) Three scenarios to demonstrate the effect of moving objects to RF signals. (b) The changes in RF signal magnitude during the scenarios.

Then, the output of the channel, $y(t)$ is obtained as below,

$$y(t) = V(t) + n(t) \tag{2.3}$$

where $n(t)$ is complex-valued additive Gaussian measurement noise. In our system, low cost software defined radio (SDR) modules, which are easy to control and reconfigure, are used as the radio transmitter and receiver. SDR modules offer higher number of degrees of freedom and provide flexibility and versatility to the users. In this thesis, we use SDR modules as narrowband transceivers as we preferred the unmodulated continuous wave (CW) signal as the monitoring signal. In this way, there is no need for a time synchronization and an isolation between the transmitter and the receiver. Since the monitoring signal is a continuous signal, we also get rid of the main disadvantages of the standard Wi-Fi technology such as sampling jitters, etc. Although the impulse response approach has the capability to resolve individual multipaths better than narrowband systems. These wideband systems also require very high bandwidth and a time synchronization between the transmitter and the receiver, which increases the system cost and complexity.

2.3. Effect of Moving Objects to RF Signals

RF signals are affected by the human body while propagating in the air. A human body reflects or attenuates the RF signals. Therefore, the presence or movements of the human changes the radio channel between the transmitter and the receiver. Thus, it can be possible to have information about the presence, location, or some characteristics of the human in the environment by analyzing the RF signal patterns and characteristics. The main factors that affect the radio signal propagation in indoors are the multipath effects and blocking the LOS path. Blocking the LOS path causes a sharp drop in the magnitude of the signal. Additionally, depending on the phase value of $V(t)$ in (2.2), multipath components can increase (in-phase) or decrease (out-of-phase) the magnitude of the signal. These factors are explored in three different scenarios that are shown in Fig 2.2(a). In these scenarios, the person leaves point A and reaches point B and waits there until the end of the measurement. The changes in RF signal magnitude during these scenarios are shown in Fig. 2.2(b). In the first scenario, the person moves along the corridor between the receiver and the transmitter. When the person comes to the LOS path, the signal magnitude drops dramatically. Then, the signal magnitude rises back to its former level as the person continues to walk and moves away from LOS path. In the second scenario, unlike the first scenario the person waits at this point after he blocks to the LOS path. As the LOS path is blocked, a sharp decrease in the signal magnitude is observed, similar to the first scenario. Afterward, since the person continues to stay in the same position, the signal magnitude does not change. In the third scenario, the apparent factor that effects the signal is multipath. In this scenario, the person walks behind the receiver, not along the corridor between the receiver and the transmitter, here, blocking LOS path is out of scope. As seen, slight fluctuations are shown up due to the multipath effect. It is reported that the amount of these fluctuations has a linear relationship with the total power in multipath components influenced by the movements in the environment [32].

2.4. RF-Based Monitoring Technologies and Applications

Radio Frequency (RF) sensing has been one of the topics that have become popular in recent years. In this approach, the aim is to obtain information from that environment or people by monitoring the ambient RF signals. According to the recent researches, changes

in the transmission path of RF signals can be used as a powerful sensing tool for noncontact measurement systems. The most important factor that highlights this approach is that monitored people do not need to wear any sensors or wireless devices on them. Therefore, it has attracted a lot of attention lately. RF signals are used in many applications such as human activity recognition, occupancy estimation, vital sign monitoring, indoor localization, fall detection and gesture recognition. Application areas in RF-based monitoring are given in Table 2.1. Both specifically designed radio signal sources like Software Defined Radio (SDR) and wireless technologies like WiFi, Zigbee, Bluetooth can be used for RF sensing.

Table 2.1: Application Areas in RF Sensing.

Task	*Application Areas*
Human Activity Recognition[8] **Gesture Recognition[17]**	Home Automation Gaming Health-care Robotics Security (surveillance) Shopping
Vital Sign Monitoring[19]	Search and rescue Patient monitoring Emergency response
Presence Detection[33]	Home automation Intrusion detection Border protection
Occupancy Estimation[34]	Smart building management Smart transportation Emergency response Shopping Search and rescue
Fall Detection[35]	Assisted living Elderly monitoring

2.4.1. Sensing Techniques

In this section, background information for different types of RF signals that are used on the purpose of RF sensing, such as WiFi, SDR-based, and radar are provided.

WiFi is a standard communication technology that provides connecting devices such as personal computers, smartphones, gaming consoles, etc. with each other in a

wireless manner. The frequency bands of WiFi are 2.4 GHz and 5 GHz. WiFi signals exist in many indoor and outdoor environments. Therefore, it is widely preferred in many RF sensing applications [36]. WiFi-based systems generally use coarse-grained received signal strength indicator (RSSI) [37] and fine-grained channel state information (CSI) [18, 38] measurements of the signal. RSS measurements are easily provided by commercial devices. However, since these measurements have low time and bit resolution, their accuracies are limited. RSS values are integers therefore have high quantization errors. In addition, RSS measurements are susceptible to environmental changes. Unlike RSS, CSI have fine-grained information and high resolution [39]. CSI describes how an RF signal propagate from the TX(s) to the RX(s) and reveals the combined effect of, for instance, scattering, fading, and power decay with distance [40]. CSI involves both phase and amplitude information of 30 subcarriers. However, CSI is provided by only specific network interface cards (NIC) such as Intel 5300, Atheros 9580 which are available for a limited number of PC models.

Software defined radio (SDR) which is powerful and low-cost specialized hardware provides high flexibility and versatility to the users. SDR modules that are reconfigurable and easy to control provide fine-grained signal measurements, such as amplitude and phase. The main advantage of the SDR module is that, unlike standard devices using WiFi, it can adjust the signal configurations such as transmission mode, carrier frequency, modulation type, bandwidth, etc. In addition, since the sampling frequency of SDRs is relatively high, it is possible to obtain actual channel instead of only tracking RSSI [41]. Unlike CSI which can only be collected from Wi-Fi signals, this approach can be applied to any RF system. Likewise, it does not have any limitation about signal characteristics. SDR modules are preferred in many applications such as gesture recognition [42], vital sign monitoring [43, 44], activity recognition [41, 45], and indoor localization [46].

Radar techniques can also be used for RF sensing [47]. Most widely used radar techniques in RF sensing applications are continuous-wave (CW) radar [48, 49], ultra wideband (UWB) radar [50, 51, 52], frequency-modulated CW (FMCW) radar [43]. These radars are active radars where a radar waveform is transmitted from the transmitter and this signal is expected to return by reflecting from the target. Passive radar systems do not have their own transmitter, they use existing signals from other sources to extract information about the target. CW radars usually measure Doppler shift of the reflected

signal. These radars which are widely used for vital sign monitoring [48] or target localization [49] which utilize displacement measurements. FMCW radars ensure sweeping the carrier frequency along the bandwidth. This technique requires very high bandwidth. They use the frequency difference between the transmitted and reflected signal, which corresponds to object range. These radars are preferred for some applications including gesture recognition, respiratory rate monitoring [43], and multi-target localization[53]. UWB radars take advantage of ultra-short pulses less than 1 ns [50]. These radars can cope with multipath interference thanks to ultra short pulses. However, the range of these radars is low as they send low energy signals. UWB radars are widely used for patient and vital sign monitoring applications [51, 52].

3. NONCONTACT RESPIRATORY RATE MONITORING

3.1. Introduction

Elderly monitoring systems are becoming widespread and continuously monitoring of respiratory rate (RR), especially for those living alone and suffering from respiratory diseases is vital [54]. Especially, the infection with severe acute respiratory syndrome (SARS), Middle East respiratory syndrome (MERS) and COVID-19 can cause a severe viral respiratory illness. The conventional RR monitoring methods which require physical contact with the human body restrict the movements and comfort of a person. These contact-based methods such as capnography or impedance pneumography are used especially in clinical environments [1]. There are also some other methods that use the physiological signals such as electrocardiography (ECG) [3], polysomnography (PSG), photoplethysmography (PPG) [4] and the sleeping mattresses consisting the piezoelectric, the capacitance and the fiber optic pressure sensors [55]. These conventional contact-based methods are not suitable especially for long-term monitoring at home or nursing homes since they restrict people's movements and prevent them from performing their daily activities. Noncontact (device-free) RR monitoring methods are developed for eliminating the disadvantages of contact-based systems especially in-home care services.

In recent years, radio-frequency (RF)-based noncontact health monitoring methods which use the electromagnetic wave propagation models, have begun to attract more attention especially for monitoring houses, workplaces, and even for clinic environments. RF signals which are noncontact and are already present in homes, are preferred for health monitoring methods such as fall detection [56], human activity recognition [41] and indoor localization [57]. Since these methods annihilate the disadvantages of the contact-based methods, they provide great innovation to the area of interest. For accurate RR estimation, radar-based methods are proposed in literature which use Frequency Modulated Carrier Waves (FMCW) radar [58, 59], Doppler radar [60, 61, 62, 63] and Ultra Wide Band (UWB) radar [52, 51, 64, 65]. FMCW radars measure the distance between the chest wall and the transceiver device. This technique requires very high bandwidth since the chest displacements are in millimeters and it also requires sophisticated devices

to ensure sweeping the carrier frequency along the high bandwidth. In addition, Doppler and UWB radars measure the relative speed changes and displacements during breathing. UWB radars ensure a system with high range-resolution since they transmit very short pulses. These radars also require very high bandwidth and a time synchronization between the transmitter and the receiver, which increases the system cost and complexity. Doppler radars have low power consumption and simple radio architecture. But in the presence of multiple subjects, their accuracy decrease.

In addition to radar specific methods, there exist many other RF-based vital signs monitoring studies which use the standard radio signals known as wireless fidelity (Wi-Fi) technology. In [19, 66, 37], the received signal strength (RSS) measurements of Wi-Fi signals are used for health monitoring. In [19], they use RSS data from many wireless network links to extract the RR. However, the RSS measuring devices (indicators) have a limited number of quantization levels and therefore offer a low resolution with the high noise level. In real cases, these measurements can be easily disrupted by environmental factors. In [67, 68, 18, 38, 69, 70, 71, 72], the channel state information (CSI) of Wi-Fi signals, which is more sensitive than RSS, is used for RR monitoring. In [67, 68, 18], the periodic chest movements caused by breathing are sensed by using CSI data during sleep. In [38], the authors use the RR estimates for the detection of moving and stationary subjects. In [69], a theoretical approach that demonstrates the effect of human breathing on Wi-Fi signals is presented. While these methods use the amplitude of CSI to extract the RR, in [71, 72], the phase difference between the two receiver sensors is also used. In addition to these noncontact RF-based methods, some other technologies such as audio [73] and vision [74], [75] based techniques are also used for noncontact RR estimation. In this study, unlike the above radar-based methods and the standard Wi-Fi-based techniques, we preferred the unmodulated continuous wave (CW) signal as the monitoring signal. In this way, there is no need for a time synchronization and an isolation between the transmitter and the receiver sensors. Since the monitoring signal is a continuous signal, we also get rid of the main disadvantages of the standard Wi-Fi technology such as sampling jitters, etc.

It is observed in literature that the magnitude of received signal changes periodically due to inhaling/exhaling cycle of a person in between the RF propagation path. In order to estimate the periodicity, namely respiratory rate both the time and frequency domain

methods are used in literature. The time domain methods are based on estimating the intervals of the peaks or zero-crossings of the periodic signals [76, 77]. Frequency domain spectrum estimation techniques are widely used for RR estimation such as in [19, 66, 37, 68, 18, 38, 69, 43, 44]. Since these methods have no signal model assumption, they can be classified as non-parametric spectral estimation techniques. The frequency resolution and the accuracy of these methods are restricted with the collected data size. On the other hand, the periodicity (RR) in breathing signals are timely varying, so it is also required to reduce the data size for sensitively tracking the sudden changes. These non-parametric methods also fail to distinguish multiple subjects with close respiratory rates due to the limited resolution.

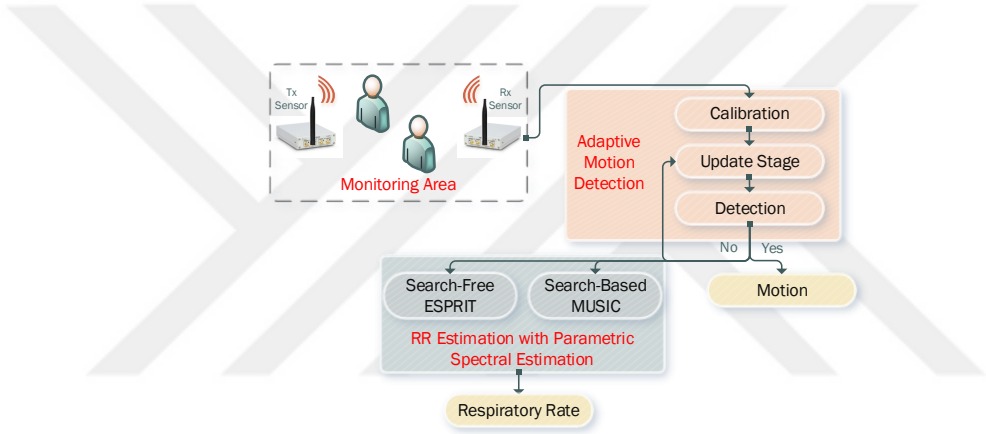

Figure 3.1: The general organization of the proposed RF-based noncontact RR estimation system using Model 1.

In this chapter, the problem of noncontact RR estimation is investigated. Three RF-based RR estimation methods are presented. The general organization schemes of the presented RR estimation methods which use an unmodulated continuous wave (CW) signal as the monitoring signal are shown in Fig. 3.1, Fig.3.2, and Fig. 3.3, respectively. The new system uses low cost software defined radios (SDR) as the transmitter and the receiver sensors. The presented methods which exploit the periodic patterns caused by breathing on RF signals are derived from three different signal models for the noisy breathing signal. First, the high resolution subspace techniques, estimation of signal parameters by rotational invariance technique (ESPRIT) [78] and multiple signal classification (MUSIC) [79], which are derived from covariance matrix model are used for the noncontact RR estimation. The system includes a simple motion detection algorithm based on adap-

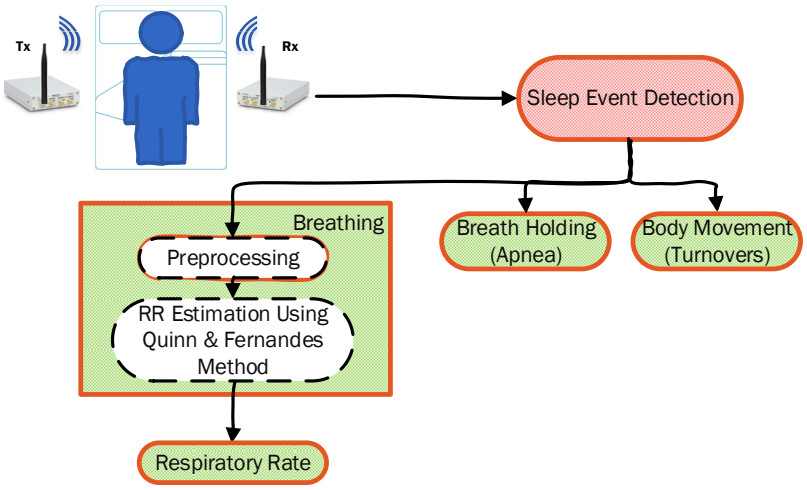

Figure 3.2: The organization of the proposed respiratory rate (RR) estimation system using Model 2.

tive thresholding to eliminate the effects of the large-scale body movements on the RR estimation. The proposed system is validated with real data collected using ten participants and realistic scenarios that examine the practical factors affecting RR estimation performance. It is shown that the high resolution techniques achieve very low error rate with the limited number of data and significantly improve the RR estimation accuracy according to the benchmark (periodogram) method in literature. Second, the ARMA (2,2) model-based Quinn and Fernandes (QF) [80] method is firstly adapted and used for the noncontact RR monitoring during sleep. The QF method treats as a filter which iteratively annihilates the RR. In addition, we use the same setup with a new sleep event detection method which can separate the breath-holding (apnea), body movements (turnovers) and deep sleep (breathing only) cases during sleep using a variance-based simple thresholding technique. It is shown with the experiments conducted with the real measurements that although the QF method has poor initial estimates provided by an inefficient estimator for limited data such as the periodogram, it produces accurate estimates with the limited number of data. These methods derived from the first two models benefit from the windowing approach where the RR is stationary along the window length. RR is a time-varying parameter. Assuming the RR as a longtime constant causes delays in monitoring the parameter; this can be a critical problem in emergencies. Although the subspace techniques reduce the latency and improve the accuracy according to the periodogram, a

real-time tracking is still an important requirement.

In the end, the nonlinear model-based Kalman Filter (KF) approach which is capable of estimating and tracking the RR with a low steady-state error is proposed. For real-time monitoring, we modify the standard joint unscented Kalman filter method which uses third-order state-space model. The KF is an optimal filter for linear systems and widely used in control, robotics, navigation systems, target tracking, and communication systems [81]. But, most of the real systems can not be modelled as linear systems such as biomedical systems [82, 83], neural networks [84], and smart grids [85, 86]. For these inherent nonlinear systems, extended Kalman Filter (EKF), which provides an approximation to optimal estimation, is developed [87, 88]. In EKF, since the first-order linearization is applied to the nonlinear model, the mean and covariance of the approximations highly deviate from their actual values. This may cause poor estimation performance and even divergence of the filter. To overcome this problem, the Unscented Kalman Filter (UKF) is developed [89, 90]. It is evaluated in many KF applications that UKF outperforms EKF [91, 92]. In UKF, true mean and covariance values are captured by using the deterministic sigma points. The UKF and its variants are successfully used in various fields such as attitude estimation [93], target tracking [94], power systems [95, 96], vehicle navigation [97, 98, 99].

The problem of estimating the vital signs such as RR is difficult due to the inherent nonlinearity of the problem. It is required to find the most appropriate KF approach for the RR monitoring problem. There are other types of KF besides UKF for nonlinear models such as particle KF [100], cubature KF [101, 102, 103], and ensemble KF [104]. All these types of KFs are proposed to solve the problems especially when the model's state and/or parameter dimensionality is high. Similarly, the other variants of UKF such as iterative one in [105], provides better state and covariance estimation when the dimensionality is high and the system is too complicated. Some other recent versions of UKF in [106, 107, 108] are proposed to give more robust results when there are outliers, incorrect states and measurements. But, in our case since the RR state-space model can be formulated with two states and one parameter, the standard UKF and the modification of standard joint UKF (JUKF), which is widely used for parameter estimation [109, 110, 111, 112, 113], are considered. In [114], it is shown that the modification for JUKF, decreases the computational complexity which is called as modified joint un-

scented Kalman filter (MJUKF). Both JUKF and MJUKF are based on unscented transformation [114, 115, 116, 117]. In JUKF, the parameters are combined with the state vector and estimated together with the states [118]. Thus, the computational complexity of the JUKF increases depending on the number of parameters. In MJUKF, the parameters are separated from the state-space and updated based on the transformation of errors between measurements and transformed sigma points into parameter errors. Thus, MJUKF reduces the computational complexity significantly according to the JUKF while parameter estimates converge. However, it is clear that the modification proposed in [114] works for nonlinear systems in which a linear transformation between measurements and parameters is achieved. Due to the nonlinear structure of the parameter estimation problem with respect to the measurement hereby, a new and novel modification which is sketched in Fig. 3.3 is proposed and presented in this chapter. A hyperbolic tangent function (i.e. $\tanh$) is firstly considered to transform measurement errors into parameter errors. Similar functions (e.g. hyperbolic sine, sigmoid, rectified linear unit function etc.) are generally used as activation functions in artificial neural network concept, [119, 120]. As stated in [120], such activation functions have two critical drawbacks, firstly outputs can be limited to a finite range, and secondly, they provides non-linearity for any function. Depending on the noise level of the measurements and with appropriate selection of the filter parameters, ModJUKF can surpass JUKF in terms of accuracy [114]. We collected signals from healthy volunteers to obtain performances of the proposed real-time monitoring method. It is shown in the experiments conducted with the real measurements taken using healthy volunteers that the proposed new real-time noncontact RR esti- mation and tracking ModJUKF method reduces the computational complexity and improves the accuracy according to the standard JUKF method. In addition, ModJUKF achieves the highest accuracy among the windowing-based common methods in the time-varying RR scenario.

3.2. Respiration

3.2.1. Basics of Respiration

Respiration is the process of human's taking oxygen in the air and releasing carbon dioxide to the air to survive. It consists of two phases as inhalation and exhalation as seen in

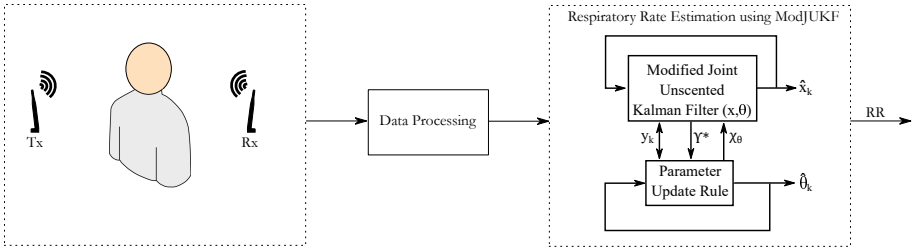

Figure 3.3: The organization of the proposed noncontact real-time respiratory rate tracking system using Model 3.

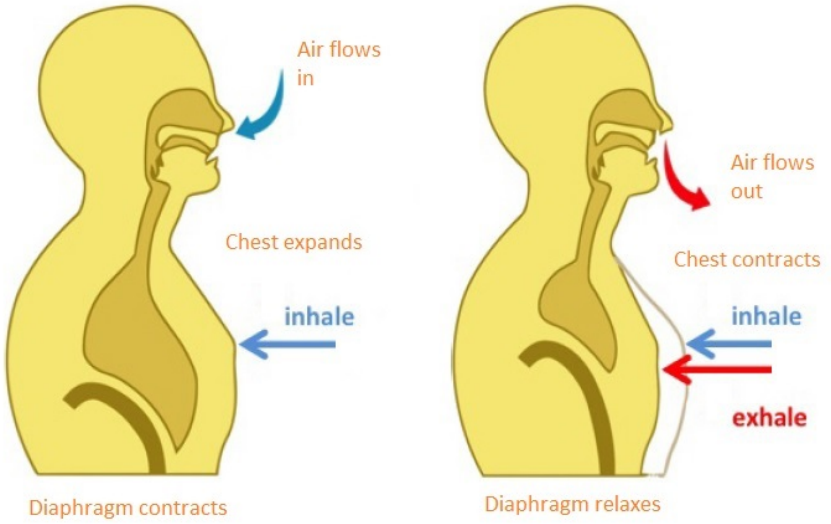

Figure 3.4: Inhalation and exhalation phases [43]

Table 3.1: The processes during respiration.

During Inhalation	During Exhalation
diaphragm contracts	diaphragm relaxes
chest expands	chest contracts
air flows in	air flows out
volume increases	volume decreases
pressure decreases	pressure increases

Fig. 3.4. During inhalation, air is inhaled through the mouth or nose and travels towards the lungs. In the meantime, the chest wall expands, the diaphragm contracts and the chest volume increases. During exhalation, this process works in the opposite direction, and it continues cyclically. The processes during inhalation and exhalation are given in Table 3.1. In a healthy adult the number of breaths per minute is between 12-20, 16-22 in children, and 18-40 in infants.

3.2.2. Effect of Respiration to RF Signal

In this section, the effects of the respiration to the RF signals are investigated. Alongside the large-scale movements like running, walking, etc., even micro-level movements like gestures or chest/abdomen movements caused by breathing affect the RF signal. Fig. 3.5 shows an example of the changes that occur in the radio channel during breathing. The displacement of the chest wall along the anteroposterior dimension is approximately 4.2 mm $\sim$ 5.4 mm at the normal breathing and 12.6 mm at the deep breathing [69, 121]. The chest wall expands outwards when the air is inhaled and contracts inwards when the air is exhaled, as expected. These arguments are also observed and verified with real measurements in our laboratory. The person sitting on the chair over the LOS path holds his breath (after inhalation) between the 17^{th} and 30^{th} seconds. Then he continues to breathing until the 43^{rd} second. Afterwards, he holds his breath again (after exhalation) between the 43^{rd} and 52^{nd} seconds. As shown in Fig. 3.5 (b), these planned movements can be easily monitored with variations on the received signal magnitude. Fig. 3.5 (a) shows the magnitude of the received signal when there is no moving object in the environment of interest. In this case, the signal amplitude is almost stable as seen. The received RF signal's magnitude level changes with inhaling/exhaling of the person and this causes a periodicity on the received signal due to the breathing movements. Even though the received signal is

affected by the ambient noise, it preserves its periodic structure. The proposed respiratory monitoring methods in this thesis estimate the respiratory rate taking advantage of periodicity of the received signal.

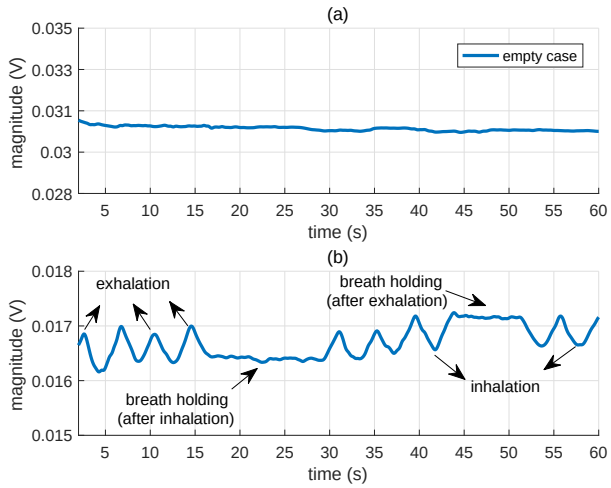

Figure 3.5: The effect of the exhalation, inhalation and breath holding to the received signal.

3.3. Breathing Signal Model

The received RF signal, affected by the breathing motion of an adult which is on or near the propagation path between the radio transmitter and the receiver, is called as the breathing signal. In this section, the mathematical formulations of the breathing signal are considered. During breathing, the chest movements of an adult who stands on/near the propagation path of the RF signal variate the magnitude and phase of the received signal. These variations on the received signal's magnitude can be modeled as a sinusoidal function depending on the periodical change of the chest movements. When there is no movement (or no person) in monitoring area between transmitter and receiver sensors, the sampled version of the magnitude of received complex-value baseband signal in (2.3) written as the following,

$$y_k = |r_k| = \mu_k + v_k \qquad k = 1, \ldots, N \tag{3.1}$$

where k is discrete time index and N denotes the collected sample number. μ_k is the time-varying DC component (average) value of the received signal and v_k is assumed as a

white Gaussian random process to represent random fluctuations. If there is a movement in the monitoring area, the magnitude of the received signal can be modeled as,

$$y_k = \mu_k + x_k + v_k \qquad k = 1, \ldots, N \tag{3.2}$$

where, x_k is the signal due to movement. In case of a stationary adult(s) lying or sitting in the monitoring area, x_k signal can be modeled as sum of the sinusoidal signals due to periodic breathing movements,

$$x_k = \sum_{i=1}^{n} A_i \cos(2\pi f_{R_{i,k}} k T_s + \phi_i) \qquad k = 1, \ldots, N \tag{3.3}$$

where A, ϕ are the amplitude and phase of the sinusoidal signal, respectively. n denotes the number of sinusoidal signals (subjects) and is known in advance, T_s is the sampling period and i is the signal (subject) index. f_{R_k} which is time-varying frequency is the RR of an adult who stands on the propagation path of the radio signal.

3.3.1. Model 1: Covariance Matrix Model

m samples are collected from the received breathing signal that is defined in (3.2) as follows,

$$\mathbf{y} = \begin{bmatrix} y_k \\ y_{k-1} \\ \vdots \\ y_{k-m+1} \end{bmatrix} = \mathbf{A} \begin{bmatrix} x_{1,k} \\ \vdots \\ x_{n,k} \end{bmatrix} + \begin{bmatrix} v_k \\ v_{k-1} \\ \vdots \\ v_{k-m+1} \end{bmatrix}, \tag{3.4}$$

where x_k is the sinusoidal source signal, n denotes the number of sinusoidal signals (subjects), $\mathbf{A}$ is a manifold matrix related with the frequency and its content is shown as,

$$\begin{aligned} \mathbf{a}(f) &= [1 \;\; e^{-j2\pi f} \ldots e^{-j(m-1)2\pi f}]^T \qquad (m \times 1) \\ \mathbf{A} &= [\mathbf{a}(f_1) \;\; \ldots \;\; \mathbf{a}(f_n)] \qquad (m \times n), \end{aligned} \tag{3.5}$$

where m, which is a positive integer, is the number of samples in the sequence and also known as the model order of the covariance matrix. The covariance matrix of $\mathbf{y}$ is defined as,

$$\mathbf{R} = E\{\mathbf{y}\mathbf{y}^H\} \qquad (m \times m), \tag{3.6}$$

where $(.)^H$ is the conjugate transpose operator and $E\{.\}$ is the expectation operator. With the performing of eigen decomposition of $\mathbf{R}$, the ordered eigenvalues are obtained as $\lambda_1 \geq \lambda_2 \geq ... \geq \lambda_m$. A set of orthonormal eigenvectors corresponding to $\{\lambda_1, ..., \lambda_n\}$ are defined as $\{s_1, ..., s_n\}$ and the orthonormal eigenvectors associated with $\{\lambda_{n+1}, ..., \lambda_m\}$ are defined as $\{g_1, ..., g_{m-n}\}$. When the eigenvalues of $\mathbf{R}$ are sorted in decreasing order, the eigenvectors corresponding to the largest n eigenvalues span the signal subspace, and the eigenvectors corresponding to the remaining $m - n$ eigenvalues span the noise subspace [122]. The eigenvectors span the signal and noise subspaces are shown in the following,

$$\begin{aligned} \mathbf{S} &= [\mathbf{s}_1, ..., \mathbf{s}_n] \qquad (m \times n), \\ \mathbf{G} &= [\mathbf{g}_1, ..., \mathbf{g}_{m-n}] \qquad (m \times (m-n)), \end{aligned} \tag{3.7}$$

where $\mathbf{S}$ and $\mathbf{G}$ represent the signal and noise subspace, respectively.

3.3.2. Model 2: ARMA Model

We consider one subject case for this model. For the estimation of the respiratory rate of a stationary adult, the received signal in (3.2) without a DC component can be written as the following,

$$y_k = A\cos(w_R k T_s + \phi) + v_k \tag{3.8}$$

If y_k satisfies (3.8), an ARMA (2,2) model equation can be defined as,

$$y_k - 2\cos(w_R T_s) y_{k-1} + y_{k-2} = v_k - 2\cos(w_R T_s) v_{k-1} + v_{k-2} \tag{3.9}$$

where the unknown parameter, w_R, can be estimated by an ARMA-based technique. There is no closed form solution for w_R in (3.9).

3.3.3. Model 3: Third-Order State-Space Model

The state-space equations are defined as,

$$\mathbf{x}_k = \mathbf{f}(\mathbf{x}_{k-1}) + \mathbf{w}_k \tag{3.10}$$

$$\psi_k = g(\mathbf{x}_k) + v_k \tag{3.11}$$

where (3.10) and (3.11) are state and measurement models, with nonlinear $\mathbf{f}$ and g functions, respectively. $\mathbf{w}_k \approx N(0, \mathbf{Q})$ and $v_k \approx N(0, R)$ are uncorrelated noise on states and measurement, respectively. $\mathbf{Q}$ and R are the state and measurement noise covariances, respectively.

The respiratory frequency (rate) of breathing signal in (3.8) is time-varying and can be called as *instantaneous frequency* [123] and rewritten as,

$$x_{1,k} = A\cos(\Phi_k + \phi). \tag{3.12}$$

where third–order state space representation of the signal is given as a rotating vector in Cartesian plane and projections of this rotating vector is given as the states $x_{1,k}$ and $x_{2,k}$, and its angular velocity equals to the instantaneous frequency $x_{3,k} = \Omega_k$. The constant frequency case is expressed as:

$$\Omega_k = \Phi_k - \Phi_{k-1}. \tag{3.13}$$

The noise free relations of state model in (3.10) can be expressed as,

$$\begin{aligned} x_{1,k} &= \cos(x_{3,k-1})x_{1,k-1} - \sin(x_{3,k-1})x_{2,k-1}, \\ x_{2,k} &= \sin(x_{3,k-1})x_{1,k-1} + \cos(x_{3,k-1})x_{2,k-1}, \\ x_{3,k} &= x_{3,k-1}, \end{aligned} \tag{3.14}$$

and the measurement model in (3.11) can be explicitly rewritten as,

$$\psi_k = x_{1,k} + v_k, \tag{3.15}$$

3.4. Preprocessing Steps

In this section, we discuss data preprocessing procedures. In order to make the respiratory rate estimation algorithm properly with real measurements, some preprocessing steps are required. In this section, the basic pre-processing steps such as DC blocking filter, outlier removal, and downsampling are briefly summarized.

3.4.1. Real-Time Recursive DC Blocking Filter

As shown in Fig. 3.6. (a) the DC (mean) value of the breathing signal is changing with time. In state-space formulations in Model 3, the sinusoidal waveform with time-varying frequency in (3.12) is defined without a DC component. The presence of the DC component disrupts the built-in model and consequently prevents the estimated parameters from converging to the correct value. Thus, DC components do not contain any information about the respiratory rate and must be filtered out from the received signal. To get rid of zero frequency component, a simple method which subtracts the average of the signal from the signal itself can be used. However, this method is not suitable for real-time applications since it requires batch data for computing the average, and also fails since the DC component changes over time. Alternatively, in this study, a recursive DC blocking filter [124, 125] which can operate in real-time is preferred. The transfer function of the system in the Z-domain is written as,

$$H(z) = \frac{1 - z^{-1}}{1 - pz^{-1}}, \tag{3.16}$$

where p is a coefficient, $0 < p < 1$, and the difference equation of DC blocking filter is given as,

$$y_k = \psi_k - \psi_{k-1} + py_{k-1}, \tag{3.17}$$

where ψ_k is the measurement data in (3.15) and y_k is the filtered measurement data. The initial value, y_0, is selected as a very small number close to zero for not creating an offset.

Fig. 3.6 (a) & (b) show an example of the received RF signal before and after passing through the DC blocking filter, respectively. In real measurements, the received signal may also have a trend not caused by respiratory rate as shown in Fig. 3.6 (a) due to the time-varying DC components. These trends can cause nonlinearity that adversely affects transient time that is the time for the system to converge the correct parameter. By using DC blocking filter, the trend of the signal alongside the DC component is also eliminated as shown in Fig. 3.6 (b). UKF assumes white Gaussian noise distributions on states and measurements but for this practical application it can not be always possible. Instead of applying some complex methods in [106, 107, 108] to overcome this problem, the measurements can be processed by recursive DC blocking filter. So besides getting rid

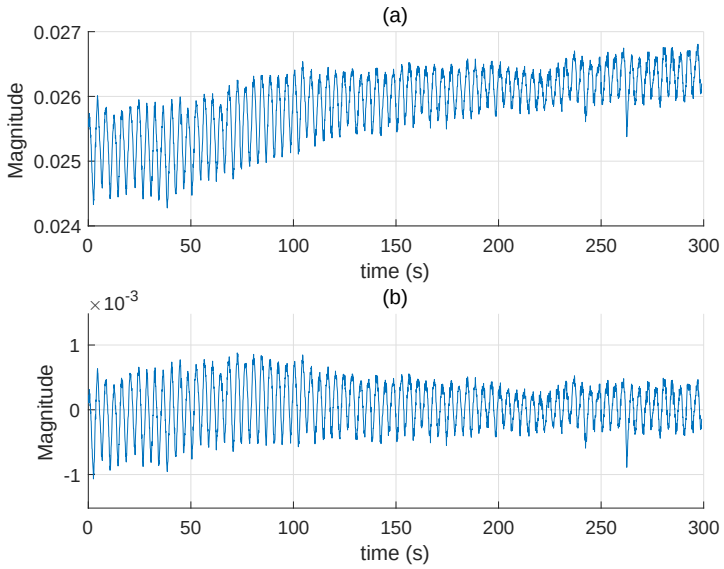

Figure 3.6: (a) RF signals before passing through the DC blocking filter (b) RF signals after passing through the DC blocking filter.

of DC component, unwanted noise components are also eliminated due to the cascaded differentiator/integrator structure [124]. In our case, this filtering improves signal-to-noise ratio (SNR) of the measurements and it also decreases the model and measurement errors of UKF and preventing stochastic stability and divergence problems.

3.4.2. Outlier Removal

In some cases, deviations that are not induced by respiratory movements are observed on the received signal. This deviations are called as outliers. In Fig. 3.7, the outliers can be seen that near 8, 10, 38, 46, 55 and 59 sec. If this signal is used as input to the respiration rate estimation system, the results will be incorrect. So, the outliers must be eliminated. For this purpose, the well known Hampel identifier is used [126]. Hampel identifier calculates the median (μ) and standard deviation (σ) of the samples in the measurement window. Then, it determines an upper and lower bound using μ and σ. Upper and lower bounds are set to $\mu + 3\sigma$ and $\mu - 3\sigma$, respectively. A new sample which is out of these bounds is qualified as outlier. The outliers are detected and removed from the original signal as seen from the Fig. 3.7.

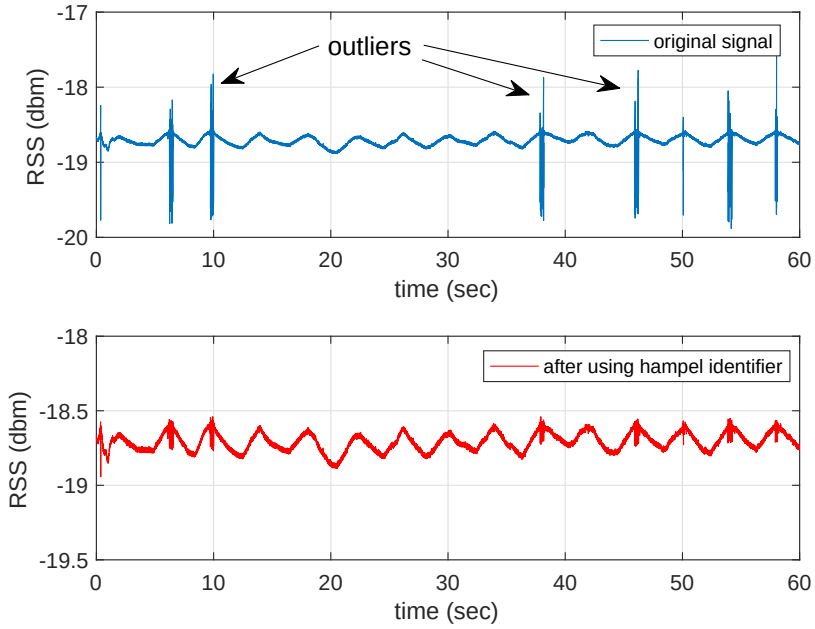

Figure 3.7: (*Top*) The original signal with outliers. (*Bottom*) The signal whose outliers are removed using Hampel identifier.

3.4.3. Downsampling

The received signal is sampled by the USRP at 1200 Hz. Since the respiration rate of a healthy adult is below 1 Hz, high sampling rate makes difficult to distinguish the respiration signal in the frequency spectrum. Downsampling is required to increase the frequency resolution with the aim of resolve the low-frequency respiratory rate. Moreover, high sampling rate increases the computational cost. Due to these reasons, the received signal is downsampled without distorting its waveform and periodic form.

3.5. Materials and Methods

The organizations of the presented three RF-based RR estimation system are shown in Fig. 3.1, Fig. 3.2, and Fig. 3.3, respectively. We assume that the monitoring area is between the propagation path of the radio transmitter and receiver.

3.5.1. Subjects

In experiments, 10 healthy nonsmoking subjects with no history of respiratory disease are used. The measurements are taken while the subjects are lying and sitting using

the setups shown in Fig. 3.8. The subjects consist of the staff and the students of the Anadolu University. The relevant Institutional Review Board approval for this study is obtained from the Anadolu University Scientific Research and Ethics of Publication Board of Health Sciences. Each volunteer agreed to be a subject and signed the study protocol.

3.5.2. Experimental Setup

The real measurements are taken using the two experimental setups in the laboratory as shown in Fig. 3.8. The scaled graphical representations of these setups are also illustrated in Fig. 3.9. The low-cost SDRs which are developed by Ettus Research [127] are used as the radio transmitter and the receiver. The SDR modules which ensure flexibility to the users are re-configurable devices. Two Universal Software Radio Peripheral (USRP) B210 modules which are deployed two sides of a bed (or a chair) are used as the radio transmitter and the receiver. The radio transmitter emits a continuous wave signal at 900 MHz. The transmit power of signal is adjusted as zero decibel-milliwatt (dBm) so that it does not exceed the limit specified by the Federal Communications Commission (FCC) regulations [128]. The receiver module down-samples and digitizes the RF signal to baseband for processing. After down-sampling, the sampling rate is specified as 10 Hz which ensures the Nyquist rate criterion for obtaining the respiratory frequency. Omni-directional antennas are used in both transmitter and receiver.

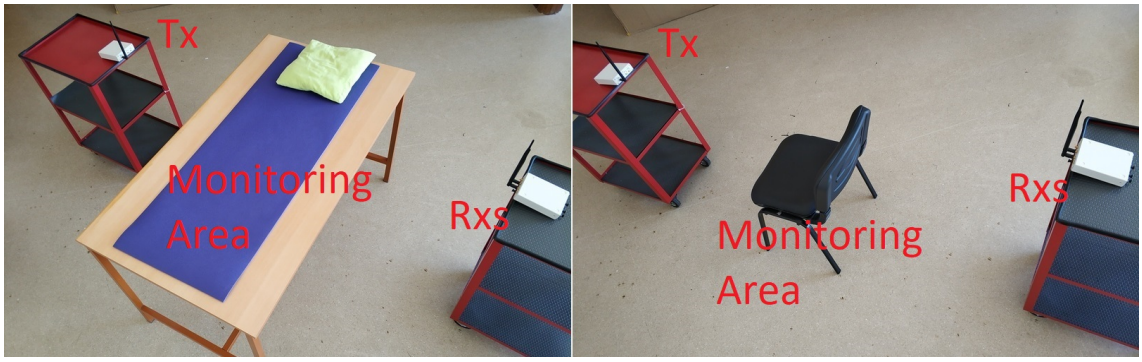

Figure 3.8: The measurements are collected when lying and sitting using the experimental setups.

3.5.3. Problem Definition

The problem is to accurately estimate and track the RR, namely the frequency of sinusoidal (f_R) in noisy breathing signal y_k. The breathing signals are collected as the mag-

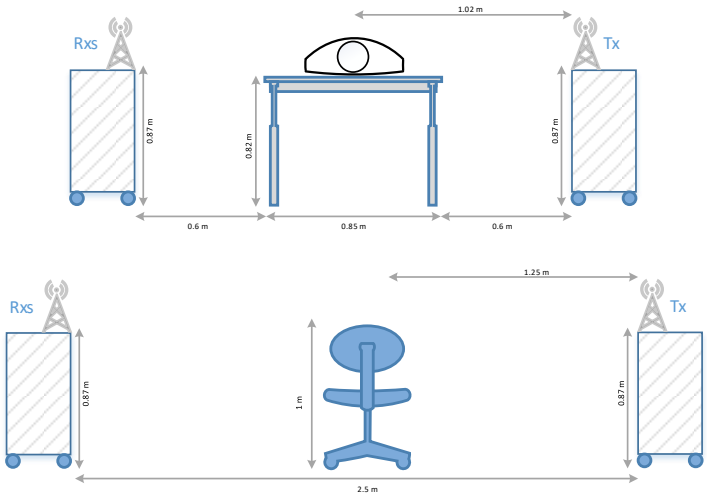

Figure 3.9: The graphical representations of the experimental setups for lying and sitting positions, respectively.

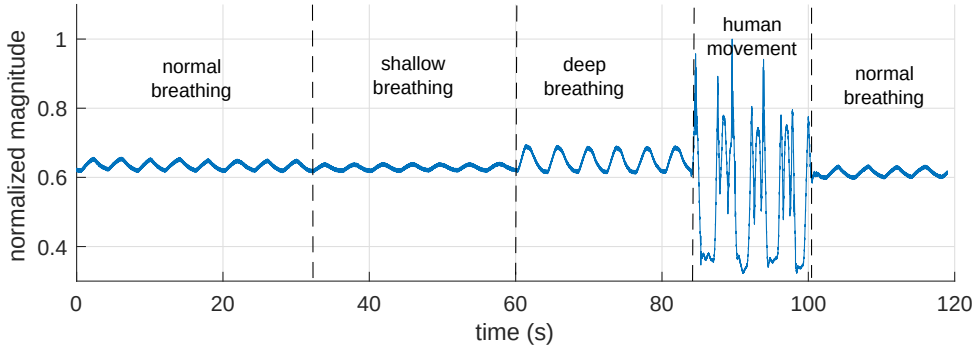

Figure 3.10: The normalized magnitude of the breathing signal, $y(t)$ in the cases of normal, shallow and deep breathing and during large-scale body movements in the monitoring area.

nitude of the received sensor signal which can be seen in Fig. 3.10. In this figure, the magnitude of the received signal in cases of the normal, shallow and deep breathing and large-scale body movements are shown. Figure shows that the mean, powers of signal and noise levels are changing with time even with these limited stationary measurements. Thus, it is a big challenge to track accurately the RR. Another challenge is to accurately detect the presence of the movement of subjects in the monitoring area. In the following sections, event detection and RR estimation methods are presented for the best solutions of these challenges.

3.5.4. Event Detection

This section discusses the presented event detection methods to eliminate some situations that prevent the RR from being estimated during monitoring.

3.5.4.1. *Motion Detection With Adaptive Threshold*

It is critically important to preciously detect the motion of a human body or a moving object in the monitoring area. Fig. 3.10 shows the real normalized magnitude of received signal, $y(t)$. In this example, an adult steadily breathes until 32^{nd} second. Then, he takes shallow breaths and deep breaths, along 30 seconds and 24 seconds, respectively. Afterwards he makes some large-scale body movements such as head and limb motions between the 84^{th} and 100^{th} seconds. Soon after, he continues breathing without any motion until the end. It can be seen that the body motions of an adult cause big fluctuations on the received RF signal. If the RR estimation algorithm is executed in these time intervals, the system may result in a false alarm (result). To avoid this, all the other motions except breathing should be detected and the RR estimation algorithms should not be executed in these time intervals.

The motions cause wild fluctuations such as outliers on these non-stationary breathing signal. In literature, there are outlier detection methods such as the Hampel identifier [126]. But Hampel identifier is a non-causal structure which is not suitable for these kind of real time applications. In [68] and [38], the body movements during breathing is detected by comparing the received signal variance with a pre-defined threshold. Pre-defined threshold-based methods can fail to detect motions when the received signals are nonlinear and non-stationary. Besides, the signal variance that is easily affected by outliers is not a suitable parameter for the motion detection.

In this work, to detect the body motions except breathing, we propose an adaptive algorithm whose thresholds are updated by using the median and median absolute deviation of newly collected data. The proposed approach consists of three stages. The first is the **calibration** stage where N_{th} samples length data, $\mathbf{Y}_{cl}$, are initially recorded. It is assumed that there is no motion except the breathing in the monitoring area. The second is the **update** stage where the median ($\tilde{x}$) and median absolute deviation (Ψ) of collected data, upper (γ_{upp}) and lower (γ_{low}) thresholds are calculated as $\gamma_{upp,low} = \tilde{x} \pm n_\sigma * \Psi$ like

the Hampel identifier [126]. n_σ is a scaling factor and is set to a constant as a result of empirical observations. The last stage is the **detection** where if the median value of the current data $\tilde{x}_d$ is out of threshold bounds, the motion is detected. Otherwise, no motion is detected as,

$$\begin{aligned} H_1: &\quad \tilde{x}_d < \gamma_{low} \ \ or \ \ \tilde{x}_d > \gamma_{upp} \\ H_0: &\quad otherwise, \end{aligned} \tag{3.18}$$

where H_1 and H_0 denote the motion and no motion cases, respectively. We use dynamic thresholds rather than pre-defined fixed thresholds for adapting the motion detection algorithm to dynamic environments. The proposed procedure is summarized in Algorithm 1.

Algorithm 1 Motion detection with adaptive thresholding

calibration: $\mathbf{Y}_{cl} = \mathbf{y}(1 : N_{th})$
for $t_i = N_{th} + 1 : step : N$ **do**
update: calculate $\tilde{x}$ and Ψ from $\mathbf{Y}_{cl}$
    $\gamma_{upp} = \tilde{x} + n_\sigma * \Psi$
    $\gamma_{low} = \tilde{x} - n_\sigma * \Psi$
    $\tilde{x}_d = median(\mathbf{y}(t_i : t_i + step - 1))$
detection:
    if $\tilde{x}_d < \gamma_{low}$ *or* $\tilde{x}_d > \gamma_{upp}$ **then**
        motion detected
    else update $\mathbf{Y}_{cl}$
    end if
end for

3.5.4.2. *Sleep Event Detection*

Fig. 3.11 shows the change of received RF signal with time for an example scenario. During this real measurement of 90 seconds, an adult lies on the bed between the transmitter and the receiver which are shown in Fig. 3.8(a). In this example, the person breathes normally during the first 12 seconds. The person then makes turn movements in bed. It is seen that the amplitude of RF signal changes significantly during these movements. It is clear that these body movements affect the RF signal excessively. It is not possible to estimate the respiratory rate during this time interval. In addition, the breathing of a person stops when sleep apnea occurs. To observe the changes of the RF signal during

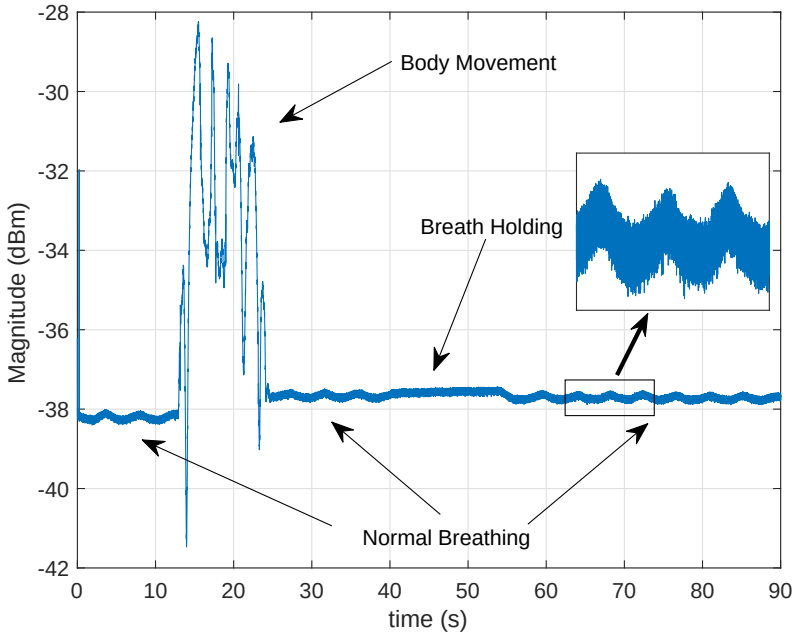

Figure 3.11: An example of real measurement. Received RF signal includes the normal breathing, body movement, and breath holding cases.

a sleep apnea scenario, the person holds him/her breath between 40^{th} and 55^{th} seconds. It is observed that the RF signal is stationary in this time interval. Afterward, the person continues to normal breathing until the end. Therefore, before estimating a person's respiratory rate, there is a need for a method that eliminates these cases during sleep. It is clear that the variances of the amplitude of the RF signal are different in all three cases. Hence, it is possible to distinguish the normal breathing, body movements, and breath-holding cases by using the variance of the amplitude of the RF signal. For this purpose, we use the signal variance as a feature for the sleep event detection. The variance is widely used in literature to separate dynamic and static cases such as in this study [68, 38]. It can be seen in Fig. 3.12 that the variance of the same received signal in Fig. 3.11 is a distinctive feature to separate the normal breathing, body movements, and breath-holding cases. In this method, the variance of the received signal in the sliding window is calculated and compared with the threshold value as the following,

$$\begin{aligned} Body\ \ movement\ (turnover) &: \sigma_y^2 > Thr_1 \\ Breath-holding\ (apnea) &: \sigma_y^2 < Thr_2 \\ Breathing\quad\ \ &: otherwise \end{aligned} \tag{3.19}$$

where σ_y is the variance of the received signal in the sliding window. Thr_1 and Thr_2 are the threshold values which are determined according to the empirical results.

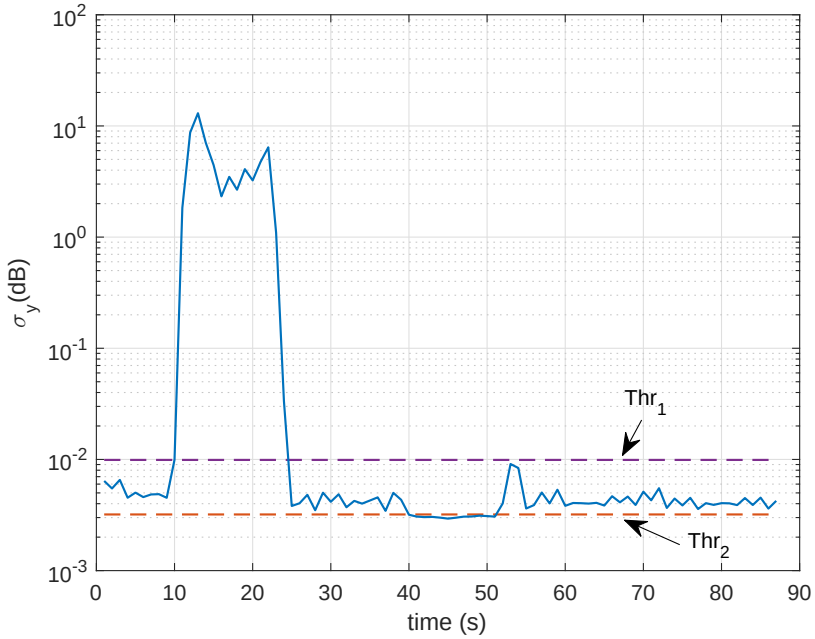

Figure 3.12: The variance (σ_y) of the received signal. Threshold values are also shown.

Before estimating the respiratory rate, w_R, the DC component of the received signal is removed simply by subtracting the mean of the signal from itself in every sliding window as a preprocessing step.

3.5.5. RR Estimation with High-Resolution Subspace Techniques

Noncontact RF-based RR estimation problem is similar to estimating the periodicities in a batch of noisy signal. Spectrum estimation techniques are widely used for RR estimation such as in [19, 66, 37, 68, 18, 38, 69, 43, 44]. These methods are known as nonparametric spectrum estimation techniques. The frequency resolution and accuracy of these methods are limited by the size of the collected data (windows). Since the periodicity (RR) in these signals varies by time, it is necessary to reduce the window size to precisely track sudden changes in the breathing signal. Because of this trade off, in this study we apply the high resolution spectrum estimation techniques for the RR estimation. These methods are known as parametric spectral estimation methods and their estimation performances completely depend on the assumed signal model. If the assumed model fits with the real data, the parametric methods provide superior performance with the limited number of

data according to the nonparametric methods. In this study, the subspace-based ESPRIT [78] and MUSIC [79] algorithms are applied for the RR estimation. Both ESPRIT and MUSIC methods are called high-resolution techniques due to their ability to resolve the closely spaced frequencies [122]. These methods are based on the eigen analysis of the covariance matrix data model. With the eigen analysis, the signal and the noise subspaces can be separated from each other, hence they are known as subspace techniques. According to our knowledge, the ESPRIT algorithm is firstly used for the RR estimation and compared with the MUSIC algorithm.

The proposed RR estimation methods use the covariance matrix data model of the received breathing signal (y_k) that is defined in (3.2).

3.5.5.1. *Search-Based MUSIC Algorithm*

This algorithm requires that the signal and noise subspaces be separated from each other. Then, it makes a spectral search to find the true respiratory frequencies. Using received signal $\{y_k\}_{k=1}^{N}$, sample covariance matrix, $\hat{\mathbf{R}} = \frac{1}{N}\sum_{k=m}^{N} \mathbf{y}_k \mathbf{y}_k^H$, is computed and its eigendecomposition is performed. $\hat{\mathbf{S}}$ and $\hat{\mathbf{G}}$ which denote the estimates of $\mathbf{S}$ and $\mathbf{G}$ in (3.7), respectively, are obtained by using $\hat{\mathbf{R}}$. The respiratory frequency estimates are determined as the locations of the n highest peaks of the estimation function as follows,

$$\hat{\mathbf{P}}_{music}(f) = \frac{1}{\mathbf{a}^H(f)\hat{\mathbf{G}}\hat{\mathbf{G}}^H\mathbf{a}(f)} \tag{3.20}$$

where, $\mathbf{a}(f)$ is a function of the frequencies $\{f_k\}_{k=1}^{n}$. Since the signal subspace is orthogonal to noise subspace, the true respiratory frequencies $\{f_k\}_{k=1}^{n}$ are the only solutions of the equation $\mathbf{a}^H(f)\mathbf{G}\mathbf{G}^H\mathbf{a}(f) = 0$ for any $m > n$.

3.5.5.2. *Search-Free ESPRIT Algorithm*

This algorithm which is computationally efficient does not require to search parameter space to find the true frequency. The true respiratory frequencies are obtained by solving linear system equations. ESPRIT algorithm also exploits the covariance matrix model in (3.6). The $\mathbf{A}$ matrix in (3.5) is divided into two parts as follows,

$$\begin{aligned} \mathbf{A_1} &= [\mathbf{I}_{m-1} \;\; \mathbf{0}]\mathbf{A} \qquad (m-1)\times n \\ \mathbf{A_2} &= [\mathbf{0} \;\; \mathbf{I}_{m-1}]\mathbf{A} \qquad (m-1)\times n \end{aligned} \tag{3.21}$$

where $\mathbf{I}_{m-1}$ is the identity matrix with the dimension of $m-1 \times m-1$. The relation between $\mathbf{A_1}$ and $\mathbf{A_2}$ can be defined as follows,

$$\mathbf{A_2} = \mathbf{A_1}\mathbf{D} \tag{3.22}$$

where

$$\mathbf{D} = \begin{bmatrix} e^{-j2\pi f_1} & & 0 \\ & \ddots & \\ 0 & & e^{-j2\pi f_n} \end{bmatrix} \tag{3.23}$$

As $\mathbf{D}$ is a unitary matrix, the transformation in (3.22) can be stated as a rotation. Similarly with the relation between the $\mathbf{A_1}$ and $\mathbf{A_2}$, the signal subspace $\mathbf{S}$ can be divided into two parts as follows,

$$\mathbf{S_1} = [\mathbf{I}_{m-1} \;\; \mathbf{0}]\mathbf{S}, \qquad \mathbf{S_2} = [\mathbf{0} \;\; \mathbf{I}_{m-1}]\mathbf{S}. \tag{3.24}$$

We have that

$$\mathbf{S} = \mathbf{A}\mathbf{C} \tag{3.25}$$

where $\mathbf{C}$ is a nonsingular matrix with the dimension of $n \times n$. By using (3.22) and (3.25), we can write,

$$\mathbf{S_2} = \mathbf{A_2}\mathbf{C} = \mathbf{A_1}\mathbf{D}\mathbf{C} = \mathbf{S_1}\mathbf{C}^{-1}\mathbf{D}\mathbf{C} = \mathbf{S_1}\mathbf{\Phi} \tag{3.26}$$

where

$$\mathbf{\Phi} \triangleq \mathbf{C}^{-1}\mathbf{D}\mathbf{C}. \tag{3.27}$$

$\mathbf{A_1}$ and $\mathbf{A_2}$ are full column rank due to the Vandermonde structure of $\mathbf{A}$. $\mathbf{S_1}$ and $\mathbf{S_2}$ must also have full column rank according to (3.25). Then, $\mathbf{\Phi}$ is obtained by (3.26) as the following,

$$\mathbf{\Phi} = (\mathbf{S_1}^H\mathbf{S_1})^{-1}\mathbf{S_1}^H\mathbf{S_2} \tag{3.28}$$

As $\mathbf{C}$ is any nonsingular matrix, $\mathbf{\Phi}$ and $\mathbf{D}$ have the same eigenvalues. $\mathbf{\Phi}$ is said to be related to $\mathbf{D}$ by a similarity transformation. The estimate of $\mathbf{\Phi}$ is obtained by solving the linear equation $\hat{\mathbf{S}}_{\mathbf{2}} = \hat{\mathbf{S}}_{\mathbf{1}}\hat{\mathbf{\Phi}}$ as the following,

$$\hat{\mathbf{\Phi}} = (\hat{\mathbf{S}}_{\mathbf{1}}^{H}\hat{\mathbf{S}}_{\mathbf{1}})^{-1}\hat{\mathbf{S}}_{\mathbf{1}}^{H}\hat{\mathbf{S}}_{\mathbf{2}} \tag{3.29}$$

ESPRIT approach estimates the respiratory frequencies $\{f_k\}_{k=1}^{n}$ as $-arg(\hat{v}_k)$, where $\{\hat{v}_k\}_{k=1}^{n}$ are the eigenvalues of the estimated matrix $\hat{\mathbf{\Phi}}$ in (3.29).

3.5.6. RR Estimation Using Quinn & Fernandes Method

In this study, Quinn and Fernandes method in [80, 129] is applied to the respiratory rate estimation. The organization of this RR estimation system is shown in Fig. 3.2. The QF method was first used for the estimation of the frequency of a sinusoidal component in the presence of noise. The QF method which is based on the ARMA model acts as a second-order filter which annihilates the sinusoid at the respiratory frequency (rate). Eq. (3.9) can be re-written as follows,

$$y_k - \beta y_{k-1} + y_{k-2} = v_k - \alpha v_{k-1} + v_{k-2} \tag{3.30}$$

The aim is to estimate the unknown parameters α and β from the ARMA (2,2) equation in (3.30) under the constraint $\alpha = \beta$. If v_k are independent and identically distributed, then β can be estimated by maximum likelihood (ML) by minimizing the cost function J as the following,

$$J(\beta) = \sum_{k=1}^{n} v_k^2 = \sum_{k=1}^{n} \{\varepsilon_k - \beta\varepsilon_{k-1} + \varepsilon_{k-2}\}^2 \tag{3.31}$$

where $\varepsilon_k = 0, kT_s < 1$ and ε_k is written as,

$$\varepsilon_k = y_k + \alpha\varepsilon_{k-1} - \varepsilon_{k-2} \tag{3.32}$$

β which minimizes the cost function J can be obtained as,

$$\alpha + \frac{\sum_{k=1}^{n} y_k\varepsilon_{k-1}}{\sum_{k=1}^{n} \varepsilon_{k-1}^2} \tag{3.33}$$

The value obtained from (3.33) is put the new value of α and then β is re-estimated. This iterative procedure continues until α and β are sufficiently close. When the convergence is ensured, finally, the respiratory rate (w_R) is estimated from the equation $w_R = \frac{\cos^{-1}(\alpha/2)}{T_s}$. The algorithm steps are given as follows,

- Step-1: Put $\alpha_1 = 2\cos(\hat{w}_{R_1} T_s)$, where $\hat{w}_{R_1}$ is the initial estimate of the respiratory rate.
- Step-2: For j ≤ 1, compute $\varepsilon_k = y_k + \alpha_j \varepsilon_{k-1} - \varepsilon_{k-2}, \quad k = 1, .., n$ where $\varepsilon_k = 0, kT_s < 1$.
- Step-3: Compute
$$\beta_j = \alpha_j + \zeta \frac{\sum_{k=1}^{n} y_k \varepsilon_{k-1}}{\sum_{k=1}^{n} \varepsilon_{k-1}^2}$$
- Step-4: If $|\beta_j - \alpha_j|$ is small enough, put $\hat{w}_R = \frac{\cos^{-1}(\beta_j/2)}{T_s}$. Otherwise, let $\alpha_{j+1} = \beta_j$ and go to Step-2.

where ζ is the acceleration factor. If $\zeta = 1$ chosen, the estimation is called as the "simple QF" method. Simple QF method requires more iterations for the convergence to true parameter. In the accelerated version of QF method, the acceleration factor, ζ, which ensures the fast convergence is chosen as $\zeta = 2$. In the accelerated version, two iterations are sufficient for the convergence [129]. The performances of simple and accelerated versions of the QF method are compared with the real measurements in the next section. The QF method requires an initial estimate as seen in Step-1 and the periodogram method is used as the initial estimator as in [80].

3.5.7. RR Estimation Using ModJUKF

It is reported in [130, 114, 131] that there are two main types of parameter estimation approaches using family of KFs, these are dual and joint filtering. In joint filtering, the parameters are concatenated to state vector and they are estimated by just one filter, whereas in dual filtering, two filters are separately used for the state and parameter estimation. In a joint scheme, since states and parameters are concatenated in an augmented matrix, a cross–covariance between states and parameters are calculated. Nevertheless, in dual

filtering such calculation of cross–covariance is missing, [130]. As indicated previously, first modification to JUKF is to create an initial sigma point vector for parameters

$$\boldsymbol{\chi}_\theta = \begin{bmatrix} \hat{\boldsymbol{\theta}}_1 & \hat{\boldsymbol{\theta}}_2 & \dots & \hat{\boldsymbol{\theta}}_n \end{bmatrix}^T, \qquad n = 2L+1 \tag{3.34}$$

where parameters are *initially* distributed as

$$\hat{\boldsymbol{\theta}}_i = \left(\hat{\boldsymbol{\theta}}_0 - \mathbf{p}_\theta \left(L+1\right)\right) + \mathbf{p}_\theta i, \qquad i = 1, \dots, 2L+1 \tag{3.35}$$

where $\hat{\boldsymbol{\theta}}_0$ is the initial parameter estimate vector, $\mathbf{p}_\theta$ contains the initial error covariances of parameters. i is the index of the sigma point of corresponding parameter and L denotes the number of states. In ModJUKF, just like the concatenation of states and parameters into a vector, the corresponding sigma point vectors are also concatenated. Suppose a system has L states and L_θ parameters, the system generates $2(L+L_\theta)+1$ sigma points for JUKF, whereas for ModJUKF it generates $2L+1$ and it corresponds to the standard state filter (UKF). Clearly, the number of generated sigma points is reduced by $2L_\theta$ and in $\frac{(2L_\theta)}{(2(L+L_\theta)+1)} \times 100\%$, if ModJUKF is used for parameter estimation. Nevertheless, computational complexity reduction is less than this percentage due to the separate parameter update rules given in (3.36) and (3.37).

The major modification for the JUKF is in the measurement update section, the parameter estimate and sigma point vector update is carried out as

$$\boldsymbol{\chi}_{\theta_i} = \hat{\boldsymbol{\theta}}_k^- - \xi T \tanh\left(\xi\left(\mathbf{y}_k ./ \boldsymbol{\Upsilon}^*_{i,k|k-1} - 1\right)\right) \qquad i = 1, \dots, 2L+1 \tag{3.36}$$

$$\hat{\boldsymbol{\theta}}_k = \frac{1}{2L+1} \sum_{i=0}^{2L} \boldsymbol{\chi}_{\theta_i}, \qquad i = 1, \dots, 2L+1 \tag{3.37}$$

where $\hat{\boldsymbol{\theta}}_k$ is the parameter estimate at k^{th} index, ξ is a scaling parameter, T is the transformation matrix with the size of $L_\theta \times L_m$ which transforms measurement errors of measurement sigma point vector to parameter errors, where L_θ is the number of parameters and L_m is the number of measurements. Selection of T is simple and it includes one for

each of its element. Scaling parameter ξ is determined based on simulations of the considered system. In RR estimation, there is only one measurement and parameter, so both L_θ and L_m are one. Thus, T is considered as one and the parameter ξ selected as 0.025 based on simulations of the system. The selection of T and ξ are the important points of the proposed modification for RR estimation. For the further details of the modification and the selection of T and ξ please refer to [114]. As indicated previously, parameter update rule is changed and a hyperbolic tangent function is considered in this study to include non-linearity between measurements and parameters. Algorithm for the ModJUKF is provided in Algorithm 2. The organization of RR tracking system using ModJUKF is shown in Fig. 3.3.

In ModJUKF, the estimated parameters may have some undesired fluctuations around the true rate, which reduces overall accuracy. These fluctuations can be reduced by smoothing methods such as the α-trimmed mean filter, the moving average filter, and the standard median filter [37] but they all require batch-processing as they use the estimates in a time window. Instead, for the smoothing of the RR estimates, we use the exponential filter which does not require batch-processing as it uses only one past output value. Thus, it is able to be applied to real-time applications. In the simple moving average filtering, the past output values are equally weighted, while the exponential filter uses the exponentially changing weights for the outputs. The exponential filter is as,

$$s_k = \gamma e_k + (1-\gamma)s_{k-1}, \quad k > 0 \tag{3.38}$$

where e_k denotes the respiratory rate estimates, s_k is the smoothed data. γ is smoothing factor where $0 < \gamma < 1$. This smoothing process causes a small latency due to the cumulative structure of the filter, which increases the convergence time. To accelerate convergence, the smoothing process begins at 15^{th} seconds. The values of the smoothed data before 15^{th} seconds are selected the same as the estimates.

Algorithm 2 ModJUKF Algorithm for Additive Noise Case

DefineFilter Parameters
  L, L_m, L_θ ▷ Size of state,measurement and parameter vector, respectively
  $\alpha \leftarrow 1$ ▷ $(10^{-4} \leq \alpha \leq 1)$
  $\kappa \leftarrow 2$ ▷ (generally $\kappa = 3 - L$)
  $\beta \leftarrow 2$
  $\lambda \leftarrow \alpha^2(L + \kappa) - L$
  $W_0^{(m)} \leftarrow \frac{\lambda}{L+\lambda}$
  $W_0^{(c)} \leftarrow \frac{\lambda}{L+\lambda} + 1 - \alpha^2 + \beta$
  for $i \leftarrow \{1, \ldots, 2L\}$ **do**
    $W_i^{(m)} \leftarrow W_i^{(c)} := \frac{1}{2(L+\lambda)}$
  end for
End
function UKF($\hat{\mathbf{x}}$,$\mathbf{P}_x$, $\mathbf{p}_\theta$)
  Initialize
    $\hat{\mathbf{x}}_\mathbf{0} \leftarrow \mathbb{E}[\mathbf{x_0}]$
    $\mathbf{P}_0 \leftarrow \mathbb{E}\left[(\mathbf{x_0} - \hat{\mathbf{x}}_\mathbf{0})(\mathbf{x_0} - \hat{\mathbf{x}}_\mathbf{0})^T\right]$
    $\hat{\boldsymbol{\theta}}_\mathbf{0} \leftarrow \mathbb{E}[\boldsymbol{\theta_0}]$
    $\mathbf{p}_\theta \leftarrow \mathbb{E}\left[(\boldsymbol{\theta_0} - \hat{\boldsymbol{\theta}}_\mathbf{0})(\boldsymbol{\theta_0} - \hat{\boldsymbol{\theta}}_\mathbf{0})^T\right]$
    for $i \in \{1, \ldots, n = 2L + 1\}$ **do**
      $\hat{\boldsymbol{\theta}}_i \leftarrow \left(\hat{\boldsymbol{\theta}}_0 - \mathbf{p}_\theta\,(L + 1)\right) + \mathbf{p}_\theta i,$
    end for
    $\boldsymbol{\chi}_\theta \leftarrow \left[\hat{\boldsymbol{\theta}}_1 \quad \hat{\boldsymbol{\theta}}_2 \quad \ldots \quad \hat{\boldsymbol{\theta}}_n\right]^T$
  End
  for $k \in \{1, \ldots, \infty\}$ **do**
    function SIGMA POINTS($\hat{\mathbf{x}}$, $\mathbf{P}_x$)
      $\boldsymbol{\chi}_{k-1} \leftarrow [\hat{\mathbf{x}}_{k-1}, \hat{\mathbf{x}}_{k-1} + \sqrt{(L + \lambda)\,\mathbf{P}_x},$
        $\hat{\mathbf{x}}_{k-1} - \sqrt{(L + \lambda)\,\mathbf{P}_x}]$
    end function
    function TIME UPDATE($\boldsymbol{\chi}_{k-1}$, $\mathbf{P}$, $\mathbf{Q}$, $\boldsymbol{\chi}_\theta$)
      $\boldsymbol{\chi}^\dagger_{k-1} \leftarrow [\boldsymbol{\chi}_{k-1}|\boldsymbol{\chi}_\theta]$
      $\boldsymbol{\chi}^*_{k|k-1} \leftarrow f(\boldsymbol{\chi}^\dagger_{k-1})$
      $\hat{\mathbf{x}}_k^- \leftarrow \sum_{i=0}^{2L} W_i^{(m)} \chi^*_{i,k|k-1}$
      $\mathbf{P}_k^- \leftarrow \sum_{i=0}^{2L} W_i^{(c)} (\chi^*_{i,k|k-1} - \hat{\mathbf{x}}_k^-) \times$
        $(\chi^*_{i,k|k-1} - \hat{\mathbf{x}}_k^-)^T + \mathbf{Q}$
    end function
    function MEASUREMENT AND PARAMETER UPDATE $\left(\boldsymbol{\chi}^*_{k|k-1}, \mathbf{R}\right)$
      $\boldsymbol{\Upsilon}^*_{k|k-1} \leftarrow g(\boldsymbol{\chi}^*_{k|k-1})$
      $\hat{\mathbf{y}}_k^- \leftarrow \sum_{i=0}^{2L} W_i^{(m)} \boldsymbol{\Upsilon}^*_{i,k|k-1}$
      $\mathbf{P}_{\tilde{\mathbf{y}}_k \tilde{\mathbf{y}}_k} \leftarrow \sum_{i=0}^{2L} W_i^{(c)} (\boldsymbol{\Upsilon}^*_{i,k|k-1} - \hat{\mathbf{y}}_k^-) \times$
        $(\boldsymbol{\Upsilon}^*_{i,k|k-1} - \hat{\mathbf{y}}_k^-)^T + \mathbf{R}$
      $\mathbf{P}_{\mathbf{x}_k \mathbf{y}_k} \leftarrow \sum_{i=0}^{2L} W_i^{(c)} (\chi^*_{i,k|k-1} - \hat{\mathbf{x}}_k^-) \times$
        $(\boldsymbol{\Upsilon}^*_{i,k|k-1} - \hat{\mathbf{y}}_k^-)^T$
      $\mathbf{K}_k \leftarrow \mathbf{P}_{\mathbf{x}_k \mathbf{y}_k} \mathbf{P}^{-1}_{\tilde{\mathbf{y}}_k \tilde{\mathbf{y}}_k}$
      $\hat{\mathbf{x}}_k \leftarrow \hat{\mathbf{x}}_k^- + \mathbf{K}_k(\mathbf{y}_k - \hat{\mathbf{y}}_k^-)$
      $\mathbf{P}_k \leftarrow \mathbf{P}_k^- - \mathbf{K}_k \mathbf{P}_{\tilde{\mathbf{y}}_k \tilde{\mathbf{y}}_k} K_k^T$
      $\boldsymbol{\chi}_{\theta_i} \leftarrow \hat{\boldsymbol{\theta}}_k^- - \xi T \tanh\left(\xi\left(\mathbf{y}_{k\cdot} / \boldsymbol{\Upsilon}^*_{i,k|k-1} - 1\right)\right)$
      $\hat{\boldsymbol{\theta}}_k = \frac{1}{2L+1} \sum_{i=0}^{2L} \boldsymbol{\chi}_{\theta_i}$
    end function
  end for
end function

3.6. Experimental Results

3.6.1. Evaluation of Model 1

In this section, we consider the real performances of the proposed high resolution subspace techniques, ESPRIT and MUSIC, derived from the covariance matrix model (Model 1) for the respiratory rate (RR) estimation. The results are compared with the periodogram, which is a nonparametric benchmark method in literature for various cases.

We test the features of the proposed method with various experiments conducted in realistic scenarios. In experiments, ten healthy nonsmoking subjects with no history of respiratory disease are used. The main anthropometric characteristics of the subjects are given in Table 3.2. The subjects steadily breathe at different rates (range 12 bpm to 20 bpm) during the experiments and a metronome which acts as the ground-truth is used to keep subjects' respiratory rate constant. In all the experiments that show the estimation performance, we consider one subject case which corresponds to the number of the sinusoidal source in (3.3). The parameters of the adaptive thresholding method which are the number of calibration sample (N_{th}) and the scaling factor (n_σ) are selected 10 and 7, respectively. In addition, the model order of the covariance matrix (m) in (3.5) is selected as 10. The performances are obtained by using the mean of the 90 records, each record is 120 seconds long. The different length sliding window is shifted along the signal and the respiratory rate is estimated from each measurement window. The mean absolute error (MAE) is used as a performance metric, which measures the accuracy of the system in terms of bpm. MAE is calculated as $\frac{60}{n}\sum_{t=1}^{n}|\hat{f}_R(t) - f_R(t)|$, where $\hat{f}_R$ is the estimated value in bpm and f_R is the ground-truth value at time t. For the performance evaluation, we run the algorithms on a Desktop computer which has Intel Core(TM) i7-3770K CPU @ 4.60 GHz Processor and 16 GB RAM.

Table 3.2: The anthropometric characteristics of the subjects.

	Range	**Mean**	**Median**	**St. Dev.**
Age	23 - 39	31.3	32	4
Weight (kg)	70 - 120	79.3	75.5	17
Height (cm)	165 - 190	175.6	174.5	7.8

Fig. 3.13 shows the overall RR estimation performances of ESPRIT, MUSIC and

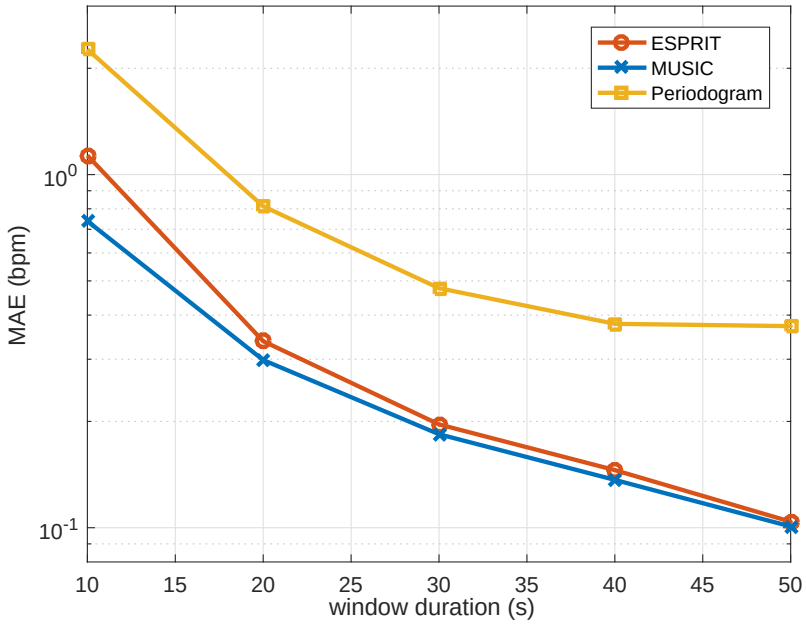

Figure 3.13: The RR estimation performances of ESPRIT, MUSIC and periodogram methods for different window durations.

Table 3.3: The execution times of ESPRIT and MUSIC algorithms.

Algorithm	**Average Execution Time**
MUSIC	$8.4\ ms$
ESPRIT	$0.17\ ms$

periodogram methods for different window durations. The ESPRIT and MUSIC algorithms have superior performance than the benchmark method periodogram for all window durations as shown in the figure. As the window duration increases, the RR estimation error decreases to the level of 0.1 bpm. We also observe that the MUSIC and ESPRIT's performances are close to each other and overall error rates are below 0.6 bpm even with only 15 seconds data. Table 3.3 shows the average execution times of ESPRIT and MUSIC algorithms for the given data set. As shown in the table, since the ESPRIT is a search-free method unlike the MUSIC, it is computationally efficient and works approximately 49 times faster than the MUSIC algorithm on the given configuration. While the performances of ESPRIT and MUSIC are similar, the ESPRIT algorithm shines out with the advantage of computational burden especially for real time noncontact RR monitoring applications. It seems that increasing the window duration improves the accuracy in RR estimation, but it also increases the latency of the system which can be an undesirable

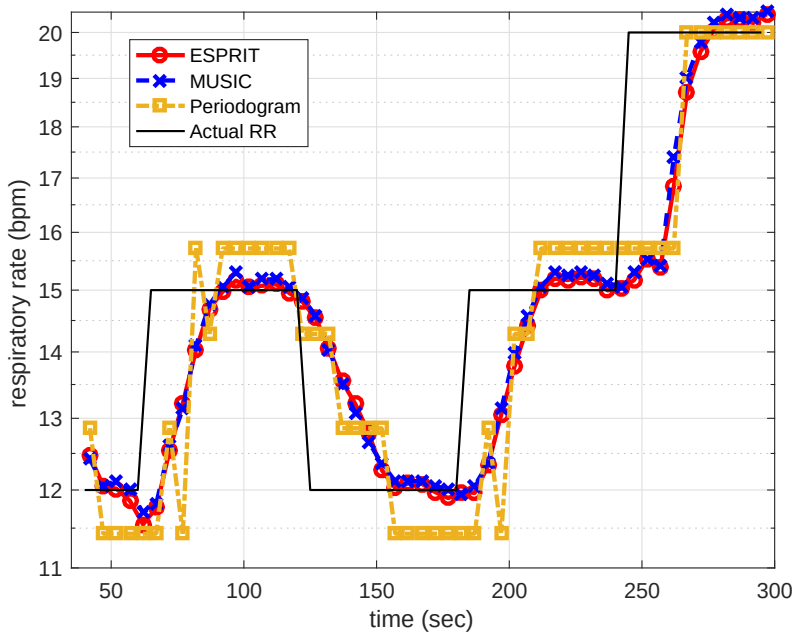

Figure 3.14: RR tracking behavior of the algorithms when sudden changing on RRs with long (42 samples) window duration.

situation due leading to miss abrupt changes in RR.

Fig. 3.14 shows the tracking performances of the algorithms for 5 minutes of recording (300 s) which includes sudden RR changes between 12 and 20 bpm. In this experiment, the RR is changing in a controlled manner at one-minute intervals. The duration of the measurement window is selected as 42 samples which is slightly longer than the previous values to observe the latency. As expected, the algorithms' latency is in the same level as the selected window duration. Figure shows that the ESPRIT and MUSIC follow the actual respiratory rate with a latency. but periodogram estimates have both latency and significant deviations due to its limited resolution capabilities.

Fig. 3.15 shows the performance results of the case where two subjects sitting on the chairs between the transmitter and the receiver sensors. One subject is asked to breathe at a rate of 15 bpm (0.25 Hz) and the other to breathe at a rate of 20 bpm (0.33 Hz). They try to keep their RR constant with the help of two metronomes. Fig. 3.15 (a) shows the results of ESPRIT and MUSIC spectrum estimates which successfully separate the two actual RRs. Fig. 3.15 (b) shows the result of the periodogram which cannot separate the two actual RRs. The main lobe width of the periodogram spectrum is $1/W$ where W is the window duration and selected as 16 samples in this experiment to test the algorithms in

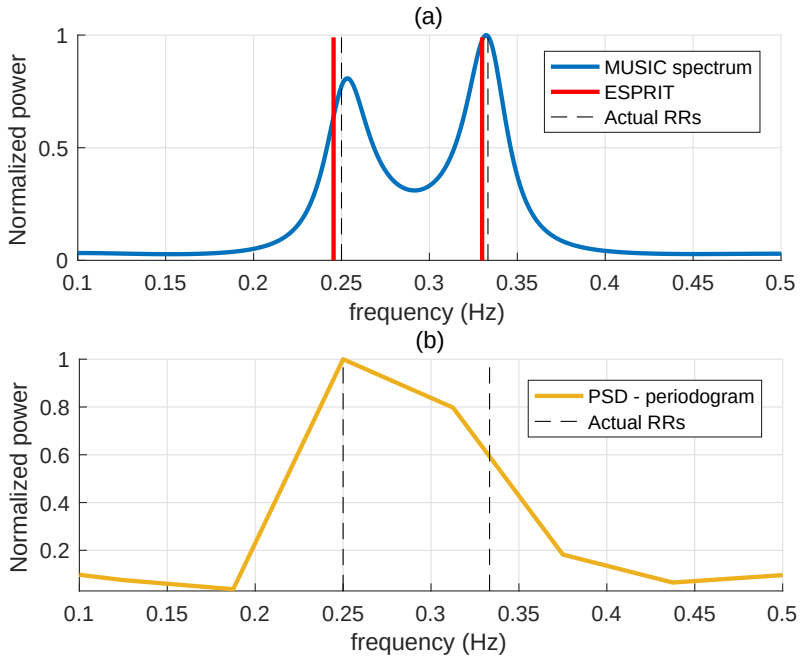

Figure 3.15: There are two subjects breathing with actual rates of f_{R1} = 0.25 Hz (15 bpm) and f_{R2} = 0.33 Hz (20 bpm). (a) The normalized MUSIC spectrum and ESPRIT estimates with actual RRs (b) The normalized power spectrum of periodogram.

low latency case. So the periodogram cannot separate the multiple frequencies separated by a space less than $1/W$. On the other hand, the high resolution subspace techniques, ESPRIT and MUSIC, offer superior resolution with limited window duration which also minimizes the latency.

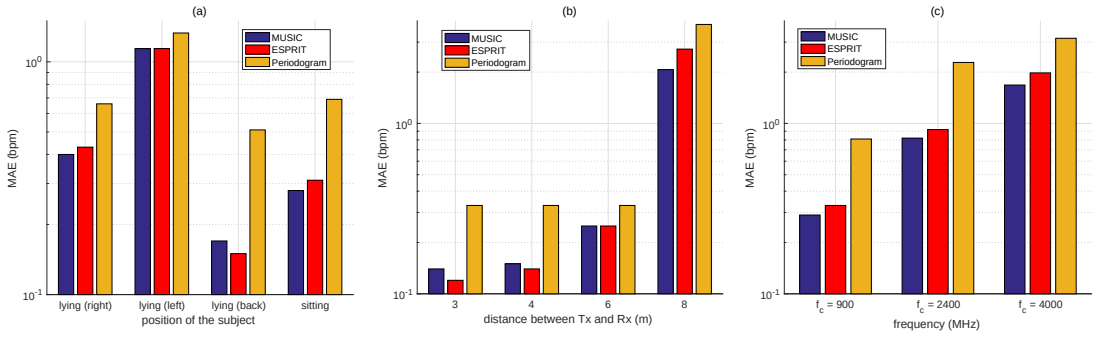

Figure 3.16: MAE (bpm) values of the methods according to the (a) position of the subjects, (b) distances between transmitter (Tx) and receiver (Rx), (c) carrier frequency (f_c) of the transmitted RF signal.

Fig. 3.16(a) presents the RR estimation performances of the proposed methods for different positions of the subjects. In real-life conditions, it is unlikely that the person being monitored will always be lying or sitting in a fixed position. Therefore, this experiment is designed to investigate the effect of the position of the subjects to the RR

estimation performance. The window size is fixed as 20 s and the given performances are obtained by using 40 minutes length data. The measurements are taken in four different positions: 1) the subject is lying towards his right side (facing the transmitter sensor), 2) the subject is lying on his left side (facing the receiver sensor), 3) the subject is lying on his back, and 4) the subject is sitting on the chair between the transmitter and the receiver sensors. During breathing, the chest displacement on the front side is larger than the mediolateral side, so it produces bigger variations on the signal. Therefore, when the subject is lying on his back, the breathing waveform can be well extracted from the received signal, and the best accuracy is obtained. Otherwise, when the subject is lying on one side, since the chest displacement is small, the signal varies less and the accuracy reduces correspondingly. The experimental results also show that the high resolution ESPRIT and MUSIC methods outperform the periodogram for all different positions of the subject.

Fig. 3.16(b) shows the error rates (in terms of MAE) of the proposed methods according to the distances between the transmitter and the receiver sensors for a fixed window duration of 20 s with 24 minutes length data. In this experiment, a subject lies on a bed as shown in Fig. 3.8 and the distances between the transmitter and the receiver sensors placed on both sides of the bed are chosen as $3m$, $4m$, $6m$, and $8m$ in each step. The output power of the transmitter is the same for each distance. For each distance, three measurements in which the subject steadily breathes at 12 bpm, 15 bpm, and 20 bpm are taken. As the distance between the transmitter and the receiver sensors increases, the strength of the signal reaching the receiver sensor decreases depending on the environmental noise. As is seen, the proposed subspace-based methods can estimate the RR of an adult less than 0.3 bpm error rate even when the distance between the transmitter and the receiver sensors is $6m$.

Fig. 3.16(c) shows the effect of the carrier frequency of the transmitted signal to the RR estimation performance. In this experiment, the carrier frequencies are chosen 900 MHz, 2400 MHz and 4000 MHz. The output power of the transmitter and the distance between the transmitter and the receiver are the same for each frequency. The performances are obtained using a sliding window with a length of 20 s. The total length of used data is 30 minutes. The purpose of this experiment is to determine carrier frequency that provides better accuracy. As is shown in the figure, the best accuracy is obtained when the carrier frequency is chosen as 900 MHz. The strength of a RF signal is directly

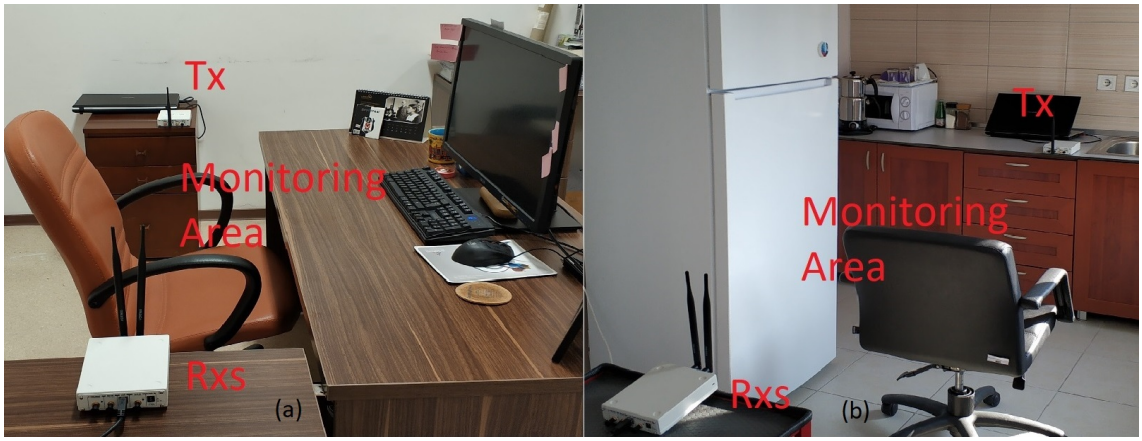

Figure 3.17: For the investigation of the effect of the environments on the RR estimation, we tested our system in two different rooms: (a) office room, (b) kitchen.

Table 3.4: RR estimation performances (in terms of MAE (bpm)) of the methods under the different environments.

Method	Lab.	Office	Kitchen
MUSIC	0.17	0.15	0.16
ESPRIT	0.15	0.13	0.14
Periodogram	0.51	0.5	0.5

related with the frequency. With the increase of the carrier frequency, the received signal strength decreases, so a RF signal with lower SNR is obtained. It should also be noted that the proposed high resolution methods perform better than the periodogram method for all carrier frequencies.

The proposed system is also tested outside the laboratory in two different fully furnished environments such as an office room and a kitchen. In both environments there were more than one Wi-Fi signals available as the interfering signal. The setups for these environments are presented in Fig. 3.17 (a) & (b), respectively. The performances are obtained by using 20 minutes of measurements for a fixed window duration, $W = 20$ s. Then, the RR estimation performances are compared with the results in laboratory (Fig. 3.8). Table 3.4 shows the RR estimation results of the methods for different environments. As seen, the proposed methods which can handle different environments offer high accuracy independently of the environment and are superior to the periodogram method.

We finally present the performance of the proposed motion detection algorithm for real measurements in Table 3.5. In this experiment, the monitored subject makes random limb and body movements for a certain period of time. Then, he/she continues to breathe

Table 3.5: Confusion Matrix of Motion Detection Results.

	Motion (H_1)	**No Motion (H_0)**
Motion (H_1)	0.883	0.117
No Motion(H_0)	0.107	0.893

properly. Table 3.5 shows the confusion matrix of the motion detection results, which are obtained by using 51 minutes length data. The true positive rate (TPR) or *sensitivity* indicates the percentage of cases where a motion of the human body is correctly detected. The true negative rate (TNR) or *specificity* indicates the percentage of cases where no motion presence is correctly detected. As is shown, the proposed system achieves TPR and TNR of 88.3% and 89.3%, respectively. The TPR and TNR values are close to 90% and they are obtained when there are distortions in the signal and continuous transitions between two states (with and without motion). Most of the false detections are recorded at the time of transitions between states. In literature one of the best results are close to 95% in [38], which utilize the amplitude and phase of CSI for multiple subcarriers. But in our case, considering that only a single channel measurement are used without pre-processing, results seem to be sufficient.

3.6.2. Evaluation of Model 2

In this section, experimental results of the proposed Quinn and Fernandes (QF) method derived from the ARMA model (Model 2) are given for various cases. The QF method is tested for the different distances between the transmitter and the receiver and for different sleeping postures of the monitored person. In addition, the performances of the some benchmark methods such as maximum likelihood estimation (MLE), the periodogram are compared with the simple and accelerated versions of the QF method. The mean absolute error (MAE) is used as a performance metric, which measures the accuracy in terms of breaths per minute (bpm). MAE is calculated as follows,

$$MAE(bpm) = 60\frac{1}{n}\sum_{t=1}^{n}|\frac{\hat{w}_R(t) - w_R(t)}{2\pi}| \tag{3.39}$$

where $\hat{w}_R$ is the estimated value in radian and w_R is the ground-truth value at time t. The result is multiplied by 60 to obtain the number of breaths per minute. The ground-truth data are obtained by means of the metronome application on the smartphone of the

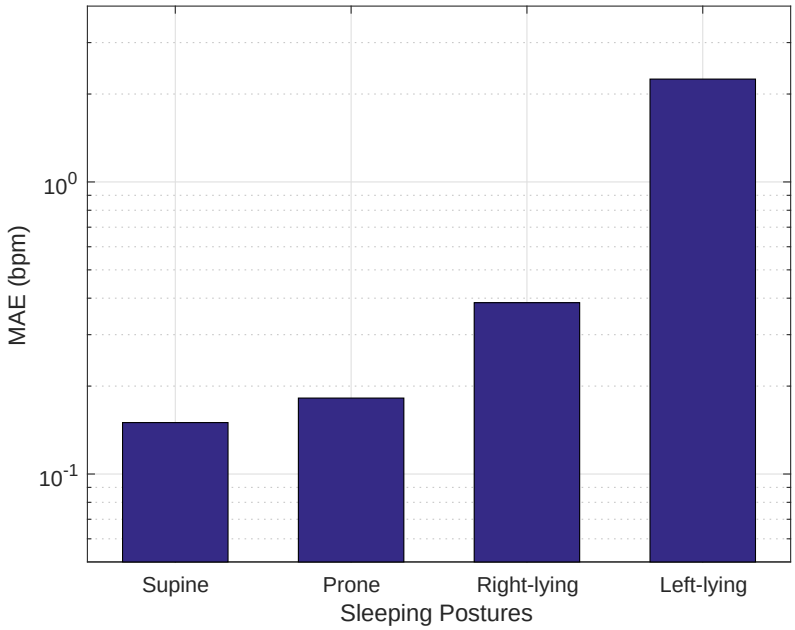

Figure 3.18: RR estimation performances of the QF method according to the sleeping postures.

person. The person listens to the metronome and adjusts him/her breath according to the metronome beat rate. To obtain estimation results, the sliding window is shifted in steps along the entire signal and a respiratory rate is estimated at each step. In the experiments, the sliding window duration is chosen especially short to show that the proposed method performs well even with limited data.

Fig. 3.18 shows the effect of the sleeping postures to the respiratory rate estimation. The person lies on the bed as shown in Fig. 3.8(a) during the experiments in four different positions such as supine, prone, right-lying, and left-lying and breathes with 14 bpm and 15 bpm rates in different measurements. The window duration is chosen as 20 seconds which corresponds to limited data. The effective path is defined as the path through which the signal propagates directly between the transmitter and the receiver [67]. The number of effective paths is a significative factor for the accuracy of the respiratory rate estimation system. In supine and prone positions, the number of effective paths is more than the one-side lying positions. Therefore, the better performances are obtained in these positions as seen in Fig. 3.18. In left-lying position, the person is lying on his left side and facing the receiver. In this position, the effect of chest movements is less felt according to the other positions. Therefore, the error rate is relatively high in this position.

Fig. 3.19 shows the performances according to the distances between the transmitter

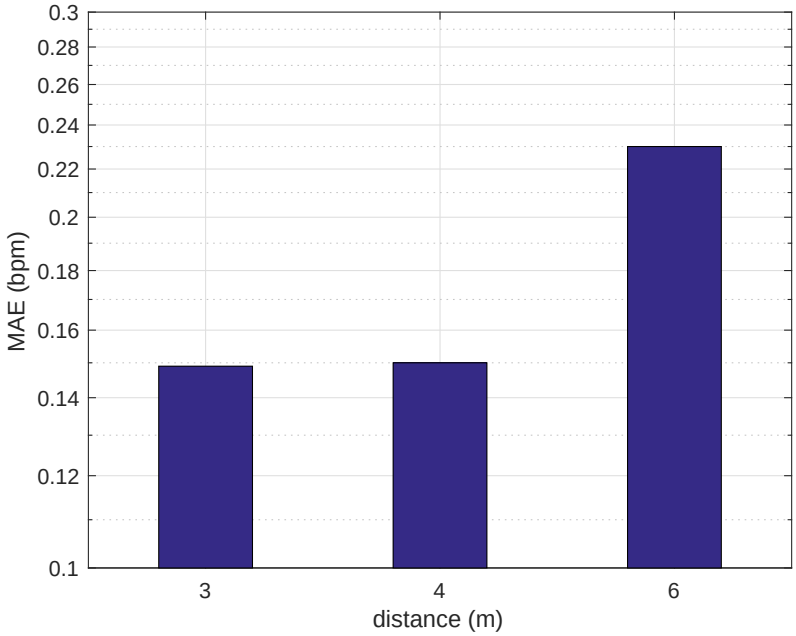

Figure 3.19: RR estimation performances of the QF method according to the distance between the transmitter and the receiver.

and the receiver. The window duration is also chosen as 20 seconds. To investigate the effect of the distance to the performance, the distance is determined as 3 m, 4 m, and 6 m and the performances are extracted for each distance. In the measurements, the person breathes in a controlled manner with the rates 12 bpm, 15 bpm, and 20 bpm. As expected, it can be seen that error rates increase as the distances increase. When the results obtained are analyzed, it is seen that the proposed method provides a very good accuracy with limited data even if the distance is 6 m which is a sufficient distance for the two sides of a bed in a real environment.

Fig. 3.20 shows the performance of the respiratory rate estimation methods for different window duration. The performances of the MLE, the periodogram, the QF (simple) and the QF (accelerated) methods are given for the comparison. The results are obtained from total of 67 measurements, each 120 seconds long. It is seen that the proposed QF method (accelerated) is superior to its simple version for the same number of iteration. The performance of the simple QF method will improve with the increasing of the number of iteration, however, it will extend the convergence time of the method. Although the initial estimates of the QF method are provided by the low-accuracy periodogram method, the results of the proposed method are quite satisfactory. It is seen that the proposed QF

method also outperforms the MLE and the periodogram methods for different window duration and it achieves 0.07 bpm error rate with increased window duration.

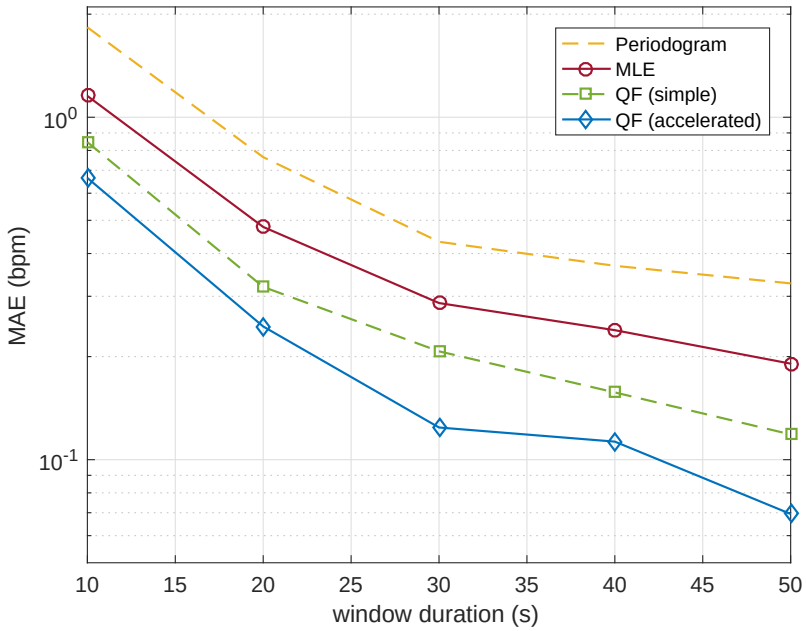

Figure 3.20: Performance comparison of the RR estimation methods for different window duration.

3.6.3. Evaluation of Model 3

We design some experiments to obtain the real-time performances of the proposed ModJUKF method derived from the third-order state-space model (Model 3). The respiratory rate tracking performances of the ModJUKF method for time-varying and constant respiratory rate scenarios are given and compared with the standard JUKF method and high resolution ESPRIT and MUSIC approaches and the periodogram method. The real measurements are taken from eight healthy participants. The participants breathe with rates in the range of 12 bpm (breath per minute) to 20 bpm in different experiments and they synchronize their respiratory rates with the help of a metronome which acts as a ground-truth. The absolute estimation errors of the ModJUKF and the JUKF for the constant RR scenario are also shown. The absolute error equals to $|e(n)| = 60 \times |\hat{f}_R(n) - f_R(n)|$ in terms of bpm, where $\hat{f}_R$ and f_R are the estimated and the actual respiratory rates in terms of Hz, respectively, and n is the estimation index. The underlying reason for multiplying by 60 is to convert the frequency unit from Hz to breath per minute (bpm). The parame-

ters p in (3.16) and γ in (3.38) are selected 0.9995 and 0.0093, respectively. These values are obtained empirically. In addition, state covariance matrix used in the experiments is taken as,

$$\mathbf{Q} = \text{diag}\,[10^{-10} \quad 10^{-10}] \tag{3.40}$$

and measurement noise covariance, R, is selected as 0.1. $\mathbf{Q}$ and R are determined by physical intuition and empirically. We use MAE as an error metric for the experiments.

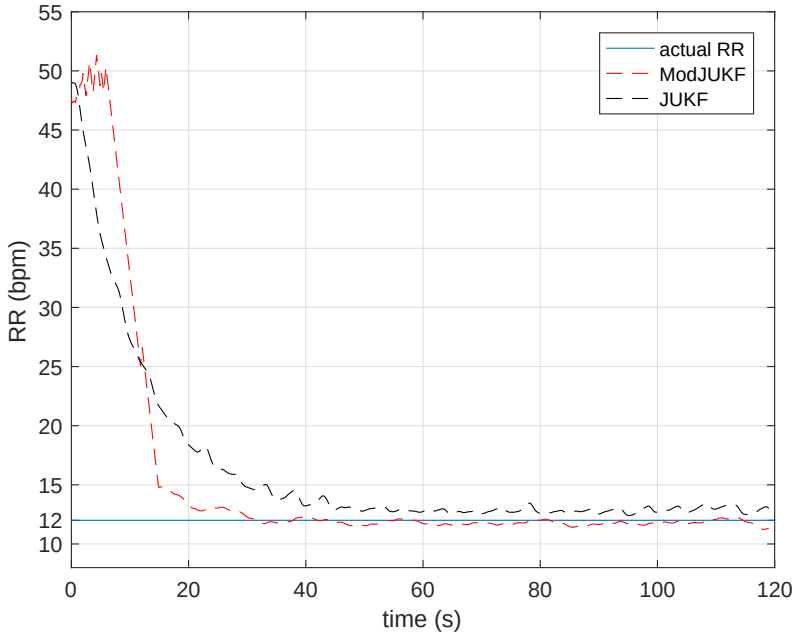

Figure 3.21: Respiratory rate (RR) tracking performances of the ModJUKF and JUKF methods in the constant RR scenario.

1) Constant RR Scenario: In the first experiment, the behaviors of the Kalman Filter approaches in the constant respiratory rate scenario are investigated. In this scenario, the participant keeps his/her respiratory rate constant with the help of a metronome and does not change the rate during the measurements. Fig. 3.21 shows the RR tracking performance of the ModJUKF and the JUKF methods when the participant breathes at a rate of 12 bpm. As is seen, both methods converge to the actual rate, while the proposed ModJUKF method has less oscillation than the JUKF method, which increases accuracy. The absolute estimation errors of the methods for this measurement are shown in Fig. 3.22. It is also seen that the steady-state errors of the proposed method are less than 0.5 bpm. The error rate of the JUKF method, which has bias estimates, is around 1 bpm. In addition, the proposed ModJUKF method converges faster than the JUKF method as

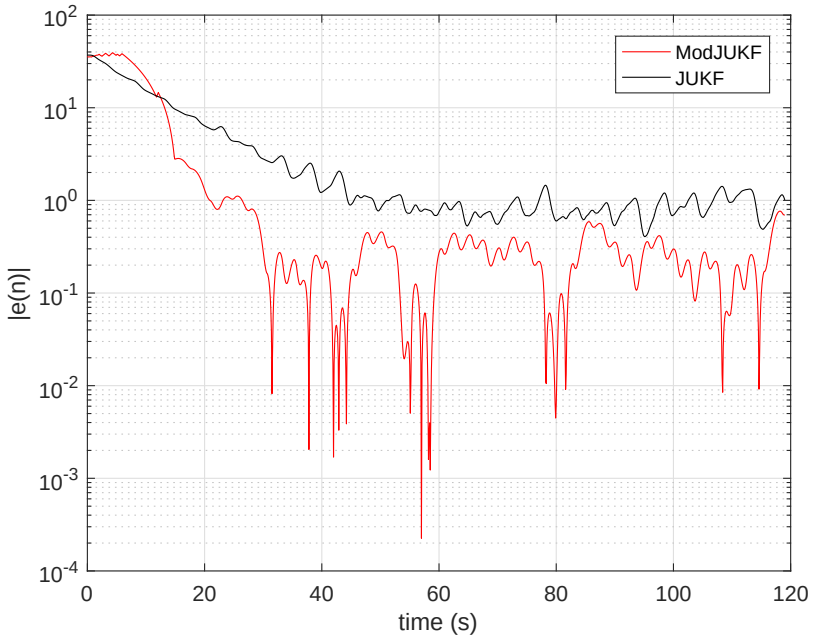

Figure 3.22: Absolute estimation errors of ModJUKF and JUKF methods in the constant RR scenario.

shown in the figure. ξ parameter, which is a scaling parameter, is chosen as 0.025 in (3.36).

Fig. 3.23 shows the cumulative density function (CDF) of the respiratory rate estimation error for the proposed ModJUKF and the standard JUKF methods. The results are obtained by using a data set, which includes a total of 25 measurements, each 2 minutes long, collected from 8 healthy participants who breathe in a controlled manner for different respiratory rates in a range between 12 bpm and 18 bpm. As shown in the figure, over 90% estimation errors of the proposed ModJUKF method are less than 0.6 bpm which is a reasonable value for the real-time RR tracking. It can clearly be stated that the proposed ModJUKF method has superior performance than the standard JUKF.

2) Time-Varying RR Scenario: In the second experiment, the case of time-varying respiratory rates is investigated. In the experiment, the participant changes his/her respiratory rate from 12 bpm to 15 bpm at 114^{th} seconds and from 15 bpm to 12 bpm at 234^{th} seconds in a controlled manner to observe the response of the methods to the sudden changes of the respiratory rates. The proposed ModJUKF method is tested according to this scenario and the standard JUKF method is also given for the comparison. The results for a 6-minutes recording are shown in Fig. 3.24. Although the proposed ModJUKF

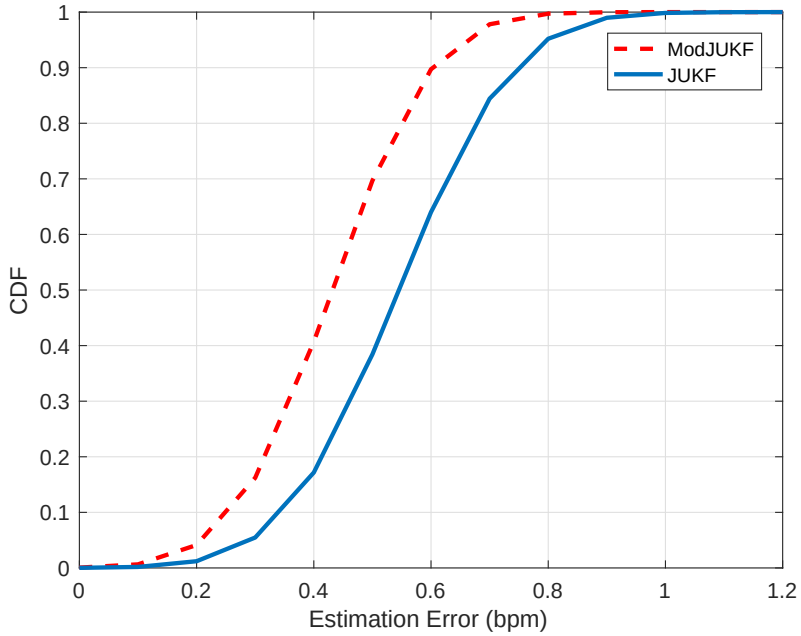

Figure 3.23: The CDF of the respiratory rate estimation error.

method has more oscillations according to the constant RR scenario, the proposed method can track the respiratory rate without missing the sudden changes after the convergence as seen in the figure. However, the standard JUKF method has considerable oscillations on the actual rate, which decreases accuracy. In addition, the RR tracking performances of the windowing-based methods such as high resolution ESPRIT and MUSIC methods and the periodogram method are given. As seen in the figure, these methods track the changing RR with latency due to the windowing approach. The window duration is selected as 30 s for these methods. The periodogram also has deviations, especially when the respiratory rate is 15 bpm, depending on the limited frequency resolution. The MAE values of all the methods for this experiment are shown in Fig. 3.25. The proposed ModJUKF method has the lowest error among the other methods. High-resolution ESPRIT and MUSIC methods are expected to achieve very high accuracy in a constant RR scenario, while their accuracies decrease depending on the latency in the time-varying scenario. The JUKF shows the worst performance since it has many oscillations around the actual rate.

3) Impact of Distance Between Transmitter and Receiver: In the third experiment, the effect of changing the distance between the transmitter and the receiver on the performance is investigated. Measurements are taken for distances in the range of 3 to 8 meters. Fig. 3.26 shows the received signal magnitudes for these different distances. As

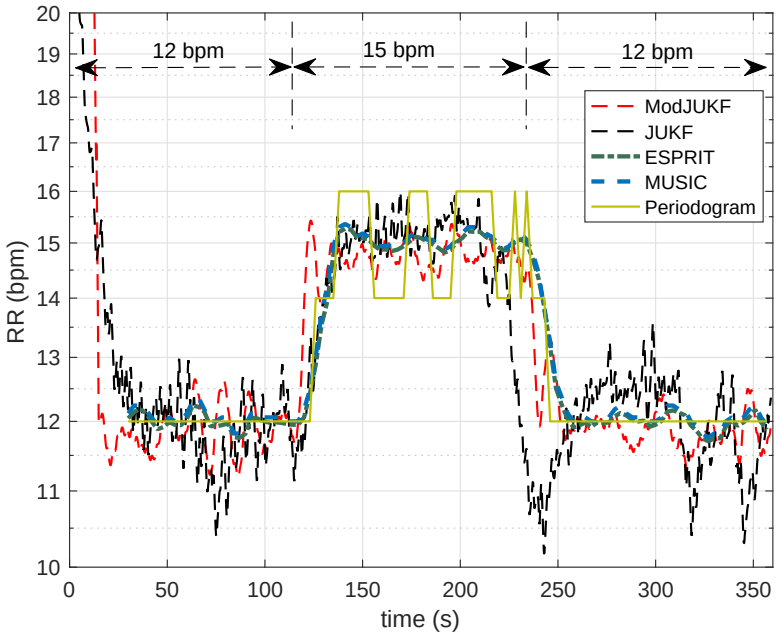

Figure 3.24: RR tracking performances of the methods in the time-varying RR scenario.

seen in the figure, the effect of the chest movements caused by breathing on the received signal magnitude decreases with the increase of the distance between the transmitter and the receiver. When the distance reaches 8 meters, the effect on the signal disappears completely as shown in Fig. 3.26(d). Fig. 3.27 shows the respiratory rate estimation error values of the proposed method according to the distance. A decrease in performance is seen with the increase of the distance as shown in the figure. The strength of the radio signals that propagate in the air changes inversely with the distance. Therefore, the radio signals attenuate as they travel in free space. While error values are low both in 3 and 4 meters of distance, error increases when the distance is increased to 6 meters, but it is still in an acceptable range. When the distance reaches to 8 meters, the attenuation in the signal increases a lot and the signal drops below the noise level. Therefore, it can be said that it is hard to extract the breathing signal to estimate the respiratory rate in 8 meters.

4) Impact of Human Orientation: Fig. 3.28 shows the effect of the orientation of the human to the RR estimation performance. The purpose of this experiment is to reveal how human orientation affects RR estimation. To test this case, five different human positions are taken into account, four of which are lying positions and one is sitting position. In lying positions, the participants lie on the bed in the experimental setup shown in Fig. 3.8(a) in the supine, prone, and right and left side positions. Better performances are

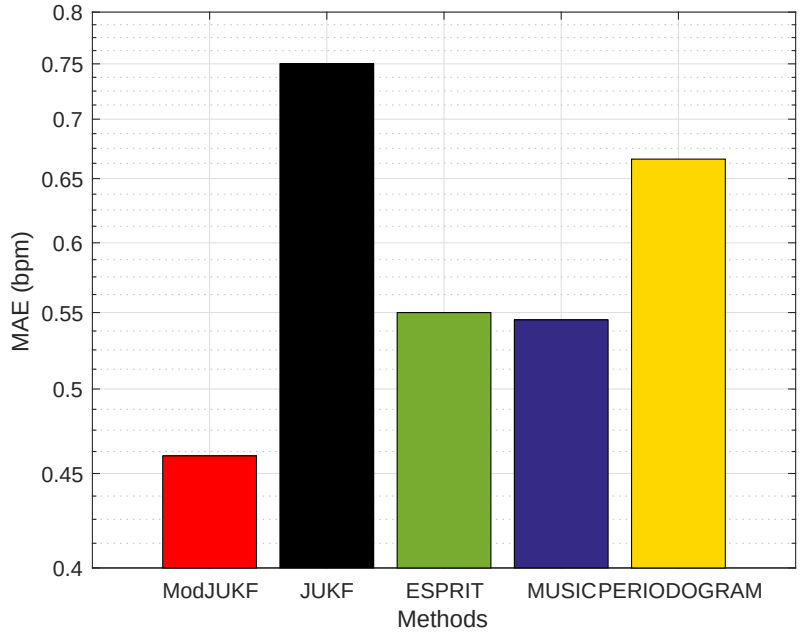

Figure 3.25: The MAE values of the methods for the time-varying RR scenario.

obtained in prone and supine positions since the number of active paths in these positions is more than the paths in the one-side lying positions. The active path is defined as the one that is more affected by human breathing than other paths [18]. In addition, the participants sit on the chair as shown in Fig. 3.8(b) for testing the sitting position. It can be seen that the proposed method attains 0.45 bpm error rate in this position. It is clearly seen that our proposed system can accurately estimate RR without being affected by human orientation.

5) Impact of Different Environments: In this experiment, we applied the proposed RR estimation method for the RF signals which are collected in different places to see the effects of the environments. RF signals are easily affected by the environmental conditions. Especially indoors, the amplitude of the RF signal can change due to some effects such as reflection, scattering, etc. The size of the room, the furniture in the room, even the number of WiFi signals as the interference source are different in each environment. Hence, the purpose of setting up experiments in different places is to illustrate that the proposed RR monitoring system is minimally affected by these changing factors. The proposed method is tested in two different places in addition to the laboratory with this goal. Environment-1 is the laboratory shown in Fig. 3.8, where all other experiments are carried out. Environment-2 is an office room in the university and Environment-3 is a liv-

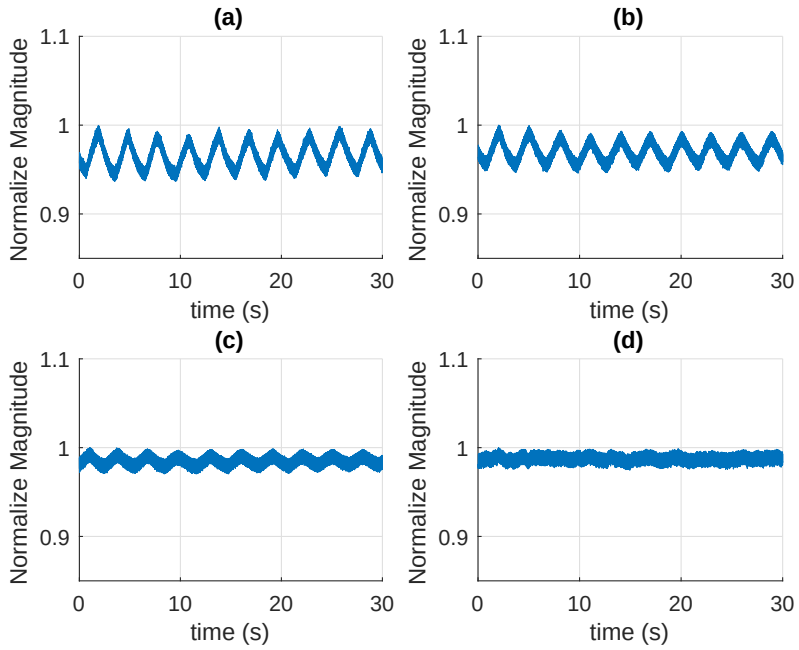

Figure 3.26: Received signal magnitudes according to distance between Tx and Rx: (a) 3m, (b) 4m, (c) 6m, (d) 8m.

ing area with a kitchen inside, which are shown in Fig. 3.17. RR estimation performances of the proposed method for these environments are shown in Fig. 3.29. Performances are obtained using 45 minutes of measurements. The proposed method can accurately estimate RR in all three environments according to the performances in the figure. It is demonstrated by this experiment that the proposed method can estimate RR regardless of the environmental changes and achieve high accuracy in different environments.

6) Impact of Breathing Forms: Even the respiratory rate is same, breathing forms can vary from person to person. A robust RR estimation method should not be affected by these variations. In this experiment, the proposed method is tested for different breathing forms. Fig. 3.30(a) shows the received signal magnitude for different breathing forms. The participant who lies on the bed breathes normally during the first 30 seconds. Then, he takes breaths shallowly in the next 30 seconds, and finally, he takes deep breaths until the experiment lasts. As seen, peak-to-peak values of received signal change according to the breathing form. While chest displacement is minimal in shadow breathing, the person draws more air into the lungs in deep breathing form. Fig.3.30(b) shows the RR estimation performance of the proposed method for this scenario. As seen in the figure, the proposed method can track RR accurately after convergence regardless of breathing

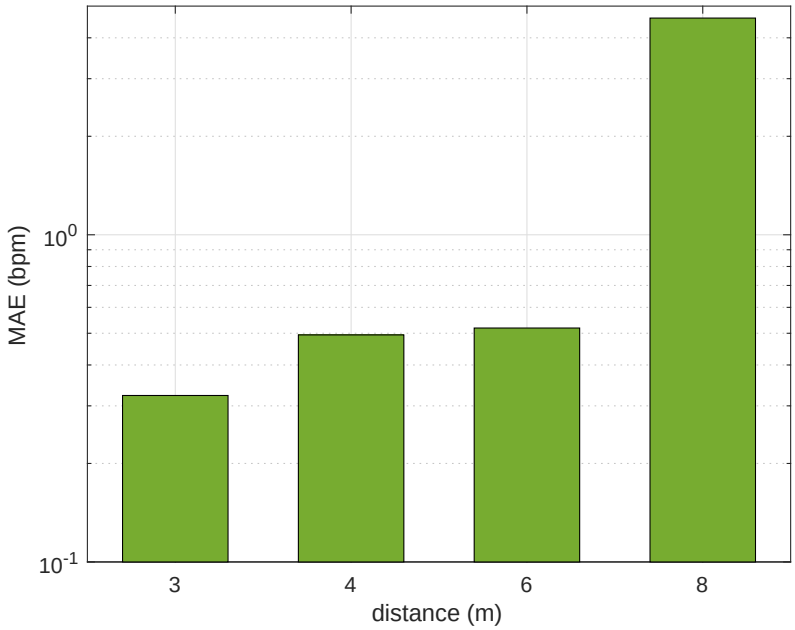

Figure 3.27: RR estimation errors (in terms of MAE) of ModJUKF according to distance.

forms.

7) Computational Complexity Comparison: Lastly, computational complexities of JUKF and ModJUKF are compared. Stopwatch timer in MATLAB® 2016a software is considered for comparison. Same coding style is used for both JUKF and ModJUKF, and codes are run on a ASUS ROG CG8580 desktop computer with a 4.60 GHz Intel Core™ i7-3770K processor and 24 GB RAM. 6 minutes of recording, for which the results are illustrated in Fig. 3.24, is used for comparison. Time step considered in the realization of mathematical models is same for both JUKF and ModJUKF, and it is 0.1 s. Codes are run 10^3 times for both JUKF and ModJUKF, and the average elapsed times are recorded. Average elapsed time for JUKF is found as 0.3905 s, whereas it is 0.3594 s for ModJUKF. It can be seen that ModJUKF reduces the computational complexity approximately 8.54% with respect to the JUKF. In this parameter estimation case, actually the number of states is 2 in ModJUKF and 3 for JUKF as provided in (3.10) and (3.11), but the last state is used for parameter estimation in JUKF. As previously stated, the number of reduction in sigma points for ModJUKF is $\frac{(2L_\theta)}{(2(L+L_\theta)+1)} \times 100 = \frac{2\times1}{(2(2+1)+1)} \times 100 = 28.5\%$. However, due to the separate parameter update rule given in (3.36) and (3.37), which include the calculation of a unary function $\tanh$ and a mean operation, the real reduction in computational complexity is found as $\approx 8.54\%$. Clearly, ModJUKF is a

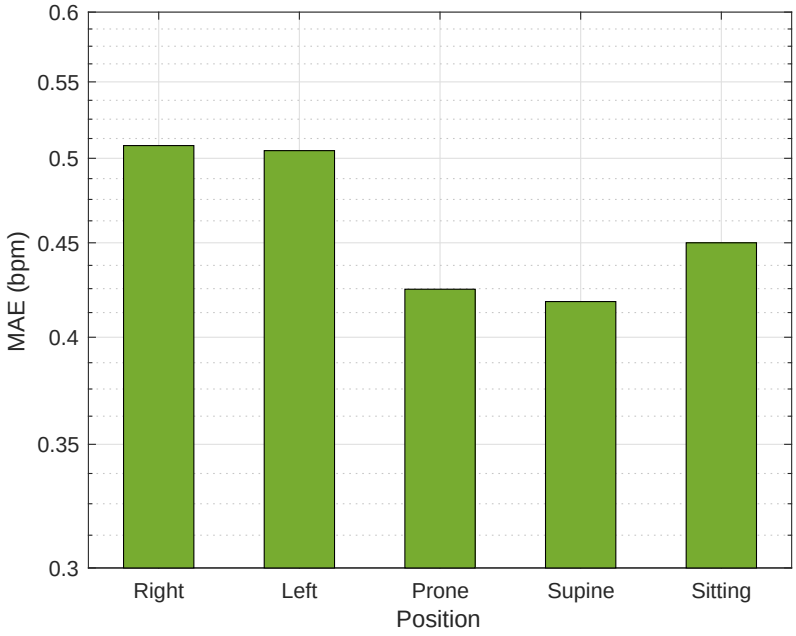

Figure 3.28: RR estimation errors (in terms of MAE) of ModJUKF according to human orientation.

promising alternative to JUKF for respiratory rate estimation with respect to its accuracy and computational complexity.

3.7. Conclusion

In this chapter, the noncontact RR estimation problem is investigated. We present three RR estimation methods derived from three different signal models. The unmodulated continuous wave signals which are used as the monitoring signal are transmitted and captured by the SDR modules. The presented systems use changes in the amplitude of the received RF signal caused by the breathing. First, high resolution subspace techniques, ESPRIT and MUSIC, which are derived from covariance matrix model are used for the RR estimation. It is shown that ESPRIT is computationally efficient and works approximately 49 times faster than the MUSIC algorithm. In addition, we propose a new motion detection algorithm based on adaptive thresholding to eliminate the effects of the large-scale body movements before the RR estimation. In the experiments, the body movements are detected with 88.3% accuracy and eliminated from the breathing signal. The proposed system is validated by real measurements using ten participants, and several different cases in various environments (kitchen, office room and laboratory) appropriate to real-

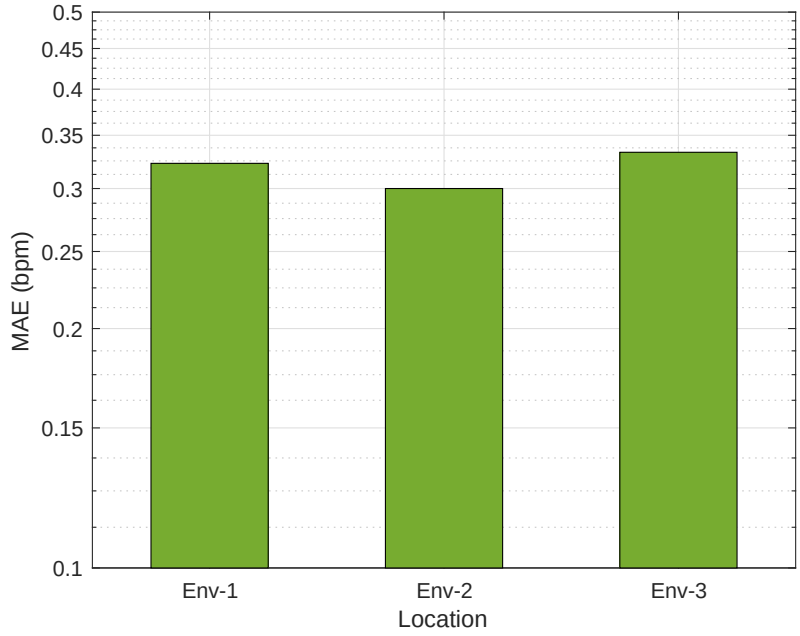

Figure 3.29: RR estimation errors (in terms of MAE) of ModJUKF according to environments (Env-1: Laboratory, Env-2: Office, Env-3: Living Area).

istic scenarios are examined to demonstrate the practical factors affecting RR estimation performance. It is shown that the high resolution ESPRIT technique achieves 0.13 bpm error rate with the limited number of data and significantly improve the RR estimation accuracy according to the benchmark (periodogram) method in literature. In addition, it is shown that high resolution techniques can be able to estimate the closely spaced RRs of two subjects, which is a challenging task, while the periodogram fails due to its inherent resolution potential. Then, the ARMA (2,2) model-based QF method is firstly adapted and used for the noncontact RR monitoring during sleep. The QF method treats as a filter which iteratively annihilates the RR. In addition, this system includes a simple separation of three sleep events such as body movements (turnovers), breath-holding (sleep apnea), and breathing cases. It is shown in various real experiments that the proposed QF method achieves 0.15 bpm error rate with 20 seconds of measurement and is also effective for different distances and sleeping postures. In the end, a new real-time noncontact RR estimation and tracking algorithm which is derived from the third-order stat-space model is proposed. Briefly, the standard joint unscented Kalman filter method is modified for the transformation of the measurement error into parameter error by using the hyperbolic tangent function. The proposed method is validated by the various ex-

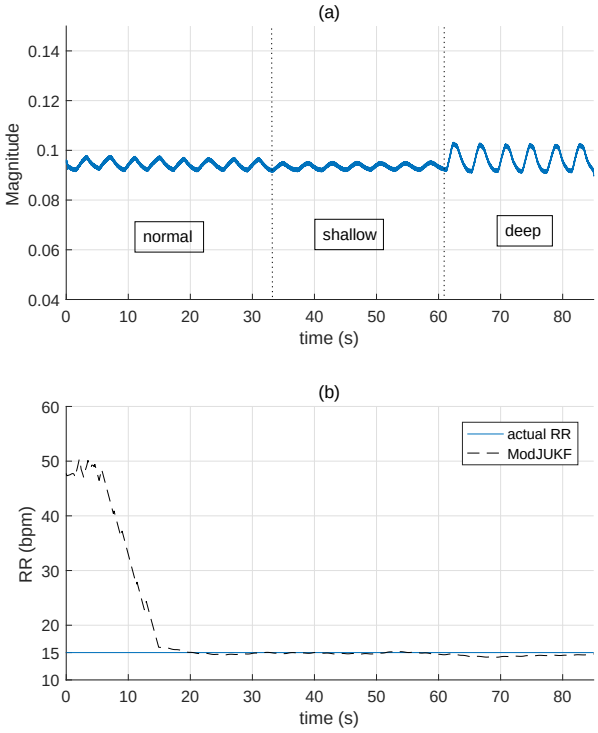

Figure 3.30: (a) Received signal magnitude during different breathing forms. (b) RR tracking performance of ModJUKF for different breathing forms.

periments compatible with realistic scenarios to show the practical factors affecting RR estimation performance. It is shown in the experiments conducted with real measurements that the proposed ModJUKF method offers both a decrease in computational complexity of 8.54% and an increase in accuracy of 36.7% according to the JUKF method. It is also shown that the proposed ModJUKF method outperforms the windowing-based methods in the time-varying RR scenario.

4. RECOGNITION OF MOVING OBJECTS WITH RF SIGNALS USING MACHINE LEARNING TECHNIQUES

Machine learning is to learn how to solve a task using the data collected for a defined problem. Learning problems can be formulated as a mapping between input and output for a model. It is basically classified as supervised learning, unsupervised learning, semi-supervised learning, and reinforcement learning. Supervised learning methods consist of the following two stages: offline training stage and online classification stage. In the offline training stage, we can train the machine learning model and determine the parameters of the model using the labeled training data that consists of features and corresponding classes. In the online classification stage, the machine learning model classifies inputs using the extracted features. The advantage of the machine learning approach is that it is suitable for classification as long as the effect of different classes is different. The disadvantage is that it needs offline training, which is time consuming and labor-intensive [132]. Machine learning has made great progress in the last two decades. This technique is used in many different fields such as speech processing [133, 134], computer vision [135, 136], and robotics [137], etc. These application fields use the image, video, and sound, etc. technologies.

In recent years, there has been an increasing interest in machine learning-based human sensing using RF signals. In this context, studies using radio propagation characteristics as features are increasing. RF-based human sensing techniques aim to recognize information about humans such as presence, location, moving trajectory, activity, gesture, identity, and vital sign, etc. using radio waves. To build an RF-based human sensing system, a link must be established between variations in the signal and human movements. If RF signal patterns are associated with human movements, it can be possible to accurately recognize human movements from signal patterns using a learning-based method [36]. In this section, machine learning approaches for the recognition of moving objects are considered. In this scope, detection of static/moving human presence through the wall and air-writing recognition which is the one of the applications of human-machine interactions are performed.

4.1. Through The Wall Human Detection

4.1.1. Introduction

In recent years, TTW human detection (sensing) systems have been widely used for applications such as hostage rescue, home healthcare, and life detection in post-disaster scenarios [138]. Unlike optical, thermal, and infrared systems, using RF signals that have the ability to penetrate obstructions like walls, trees, and smoke to detect the presence of noncooperative people and identify the objects behind a wall is advantageous. Traditional methods, ultra-wideband (UWB) radars, have the ability to distinguish people from other objects since they use very short pulses. UWB is used not only for human detection behind the wall but also to determine the building layouts or to identify materials that exist underground [139, 140]. Despite these advantages, UWB radars also have some disadvantages. UWB radars are high-cost equipment and require big, specific antennas. In addition, these systems are susceptible to interference signals from other spectral bands since they occupy very high bandwidth. In recent years, the developed systems for TTW sensing purposes have begun to use WiFi technology [141, 138]. Since WiFi signals are ubiquitous, they are preferred in many different TTW sensing applications such as activity recognition [142], indoor localization [143], gesture recognition [144], and human detection [145]. The vast majority of WiFi-based systems use fine-grained channel state information (CSI) for TTW sensing. However, CSI is provided by only specific network interface cards (NIC) such as Intel 5300, Atheros 9580, which are available for a limited number of PC models.

Existing RF-based human detection systems leverage the mobility of the people to be sensed. The movement of a person can affect RF signals and cause changes that can be observed from the received signals. Static human detection is always a more challenging problem than moving human detection, because the presence of static human does not cause obvious signal changes on the received signal, especially in the through-the-wall scenarios. One of the commonly used static human detection methods is to use the signal strength attenuation caused by the presence of the human [146]. In this method, signal strength measurements are collected in the empty environment as reference data. Signal strength measurements in the static human state are compared with reference data for the

presence detection of the human. However, this method requires sensor networks with dense-deployment and can be easily affected by environmental changes and multipath effects [147].

In this section, a novel system for TTW presence detection of both static and moving humans is proposed. The software defined radios (SDR) are utilized as the radio transmitter (TX) and receiver (RX). The proposed system presents human breathing as a distinctive indicator for static human detection in the double TTW scenario; this is a more challenging scenario where both TX and RX are placed outside the room because the signal reflected from the target must pass through the wall twice. The chest/abdomen of the person moves rhythmically during breathing. Since these rhythmic movements affect the received signal in the same manner, they can be used to separate the presence of the static human from the human-free state. In [38], the authors use the human breathing for the detection of moving and static human. There are other studies using human vital signs for human detection [67, 68]. However, all these studies are designed according to the LOS scenario, these methods remain functionless in the through-the-wall scenario, as the signal passing through the wall is significantly weakened. Subsequently, the detection of human presence is carried out by a classification process applied to the extracted RR-based features. It is shown in the various experimental results that the proposed method achieves an accuracy over 99% for both static, moving human state, and human-free state. In addition, it is demonstrated that the proposed method can be applied in different environments without requiring a specific re-training.

4.1.2. Related Work

In this section, we summarize the previous works related to our through the wall human presence detection system based on human breathing in three categories: human detection, through-the wall sensing and breathing rate estimation using RF signals.

4.1.2.1. *Human Detection via RF Signals*

In recent years, the RF-based human detection systems that use the reflection of low-cost RF signals from the target have drawn much attention. These systems can detect both static and moving humans using the basic principles of RF signals. The first works in this

concept use the received signal strength (RSS) parameter that is easily accessible from any kind of wireless device [148, 146]. In [148], RASID method constructs a silence profile from RSS measurements collected in a short offline phase when there is no human in the environment. Then, in a monitoring phase, the system decides whether a human is present or not by comparing the RSS measurements with the silence profile's measurements. In [146], the authors develop a radio tomographic imaging method based on imaging of attenuation of physical objects using RSS measurements to detect human presence. However, RSS can not stable especially in dynamic indoor environments that have many multipath reflections. Since RSS is easily affected by environmental changes, it is not a reliable measurement parameter for this kind of application. In the following years, the main direction in the works that detect human presence using wireless signals has shifted to channel state information (CSI) which is more sensitive than RSS [149, 150, 38, 151]. FIMD [149] is the first study that shows CSI provides better motion detection performance than RSS. They demonstrate that the maximum and second maximum eigenvalues of the CSI-based correlation matrix differ in static and dynamic environments. In PADS [150], the authors integrate the phase of CSI to the system alongside the amplitude. Thus, they achieve higher accuracy than other CSI-based systems for the detection of moving targets. The basic requirement in all these studies is that the people whose presence to be detected are mobile. However, especially in search and rescue operations, the detectability of stationary people is very important. Therefore, methods that require mobility are inadequate for the detection of stationary persons. In DeMan [38], both the amplitude and phase of CSI are extracted for the detection of both moving and stationary humans without requiring scenario-specific calibration. They show that the maximum eigenvalues of amplitude and phase correlation matrices are used for the presence detection of moving human. In [151], they utilize phase difference of CSI between antenna pairs to deal with the randomness of raw phase for the detection of a static human.

4.1.2.2. *Through-The-Wall Sensing via RF Signals*

There are some various applications that investigate the through-the-wall scenario such as crowd counting [152], human presence detection [143, 138, 145], gesture recognition [17, 42], and activity recognition [142], etc. In [152], the authors propose a method that counts the number of people behind the walls using RSS measurements of WiFi signals.

Table 4.1: RF attenuation for a through-the-wall scenario.

Frequency (MHz)	TTW	Double TTW
900	7 dB	15 dB
2450	11 dB	23 dB

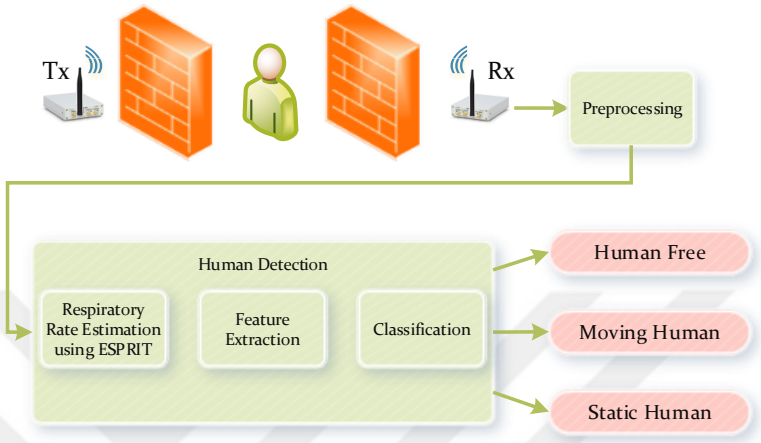

Figure 4.1: The organization scheme of the proposed double TTW human detection system.

In [143], they propose a variance-based radio tomographic imaging method for tracking a moving object through the wall using RSS. In [138], the authors present a TTW presence detection method for both stationary and moving humans. They extract Doppler spectrum based features and test the system for double-TTW scenario. In [145], the authors propose a method that detects presence of a moving human with WiFi signals in a TTW scenario. Although they use the first order difference of eigenvector of CSI as the distinctive feature for human detection, their system cannot distinguish the stationary and moving human cases. In [17], the authors propose a hand gesture recognition system that controls the devices with WiFi connection in the home environment. In [142], the authors propose a human activity recognition system using CSI of WiFi signals. They aim to obtain a correlation between human activity and CSI values using an opposite robust principal component analysis approach.

4.1.3. Static and Moving Human Detection System

4.1.3.1. *System Overview*

The architecture of the proposed system is given in Fig. 4.1. All measurements are collected according to the double TTW scenario, i.e the RF transmitter and receiver are placed in different rooms outside the monitored room as shown in the figure. In our experiments, the distance between the transmitter and the receiver is 4.2 m. The SDR platforms are used as RF transmitter and receiver. The wall penetration attenuates the RF signal. For example, while a concrete wall with 30 cm width attenuates a 900 MHz RF signal by 7 dB, two concrete walls attenuate the same signal by 15 dB. These signal power measurements are done with Keysight FieldFox Handheld Microwave Spectrum Analyzer. Table 4.1 shows the RF signal attenuations in TTW and double-TTW scenarios for different frequencies. The wall penetration loss at 900 MHz is less than the loss at 2450 MHz as shown in the table. It is clear that to detect the presence of static and moving humans in the double-TTW scenario is more challenging problem than the one through wall scenario.

As the signal attenuation increases, the signal-to-noise-ratio (SNR) decreases, which may cause signals to be distorted. We apply a low-pass filter to increase the signal level relative to the noise level. After denoising, features based on human breathing are extracted from the data in a sliding window. The proposed through the wall human detection system builds a training model using the extracted features and distinguishes the static and moving human, and human-free cases using a decision tree (DT) classifier.

4.1.3.2. *Preprocessing*

Sampling rates of SDR modules are quite high. As our proposed system is based on human breathing rate which typically has a low-frequency range, high sampling rates are not required. Since it is not possible to reduce the sampling rate to low values using existing hardware while capturing the signal, the sampling rate is reduced by downsampling, which is a signal processing technique. However, downsampling causes aliasing which corresponds overlapping the replica signals in the frequency domain. We should use an anti-aliasing filter to avoid overlap. Therefore, the signal is passed through a low-pass

filter with 40 Hz which works as an anti-aliasing filter. The signal is then downsampled to a maximum of 20 Hz. Thus, the computational complexity is greatly reduced. However, since the signal penetrates behind the wall, it weakens greatly and the noise over the signal becomes dominant. There is again a need for low-pass filtering to reduce the effect of the noise over the signal. Since the meaningful frequency components (breathing rate) for our system which uses human breathing-based features are below 0.5 Hz, it is preferred a low-pass filter with 2 Hz cutoff frequency. Noisy and denoised signals for the static human, moving human, and human-free cases are shown in Fig. 4.2.

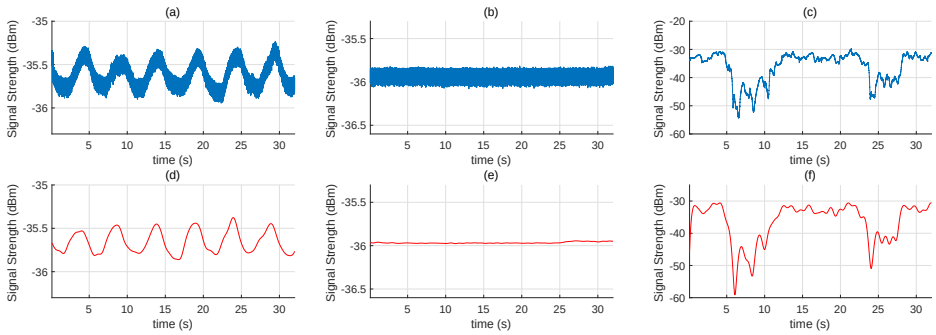

Figure 4.2: Received signal strength values before and after denoising when the experimental setup in Room A is used. (a) Before denoising (static human). (b) Before denoising (human-free). (c) Before denoising (moving human). (d) After low-pass filtering (static human). (e) After low-pass filtering (human-free). (f) After low-pass filtering (moving human).

4.1.3.3. *Human Detection*

In this study, the following states are considered: 1) *Human-Free*, 2) *Moving Human*, 3) *Static Human*. In the human-free state, the room is empty, any moving human or object does not exist in the environment. The received signal's amplitude remains nearly constant in this case as shown in Fig. 4.2(b). In the state of the moving human, a person walks randomly in the environment. The speed or style of walking is not specified priorly. The movements in the monitoring environment cause significant variations and fluctuations on the received signal as shown Fig. 4.2(c). In the state of static human, a person is present in the room, but, the person sits/stands/lies motionlessly.

Feature Extraction: We get two main observations with our experiments. First, as seen in Fig.4.2(c), the variance of the signal, which is widely used for the separation of dynamic and static conditions, has a great potential to distinguish moving human from other states. Second, breathing-induced movements are the main difference between the state of the

presence of a static human and the human-free state. Therefore, the RR estimates can be used to distinguish the presence of a static human from a human-free environment.

It is reported in the previous chapter that it is not possible to estimate the RR of the moving person. In this situation, the RR estimates consist of random results and do not contain meaningful information about the presence of a human. The same is true for the empty environment. Random RR estimates are obtained as shown in Fig. 4.3. It can be seen that the RR estimates can be the same in both moving human and human-free states. On the other hand, it is insufficient to use only a single RR estimate to distinguish the static human from other cases since random RR estimates of these two cases can be overlap with the true RR estimate in the static human state. Therefore, instead of a single RR estimate, multiple RR estimates obtained over a period of time are used as the system features. Under normal circumstances, a person's respiratory rate does not fluctuate much, it continues on a certain course. Therefore, there is no significant differences between successive RR estimates. However, high differences can be obtained in the other two cases (moving human and human-free) since their RR estimates are random results. The variance of RR estimates obtained from the successive overlapping blocks can be used as distinctive feature for static human detection. Based on these observations, the variance of RR estimates are calculated as,

$$var(\mathbf{R}) = \sum_{i=1}^{N} \left(f_{Ri} - \frac{1}{N} \sum_{k=1}^{N} f_{Rk} \right)^2 \tag{4.1}$$

where $\mathbf{R}$ consists of RR estimates ($[f_{R1}, f_{R2}, \ldots, f_{RN}]$) in a measurement data block. f_R is the RR estimate, N denotes the number of RR estimates in the data block. f_Rs are estimated by using ESPRIT method presented in Chapter 3. The scatter plots of the features of the three states for two different environments are shown in Fig. 4.4. As seen, there is a clear gap between the features that correspond to the related states. The variance of RR estimates for the static human state does not suffer from environmental changes as shown in Fig. 4.4. Although the variance of the signal changes for all three states when the environment changes, the clear gap between the states does not close much.

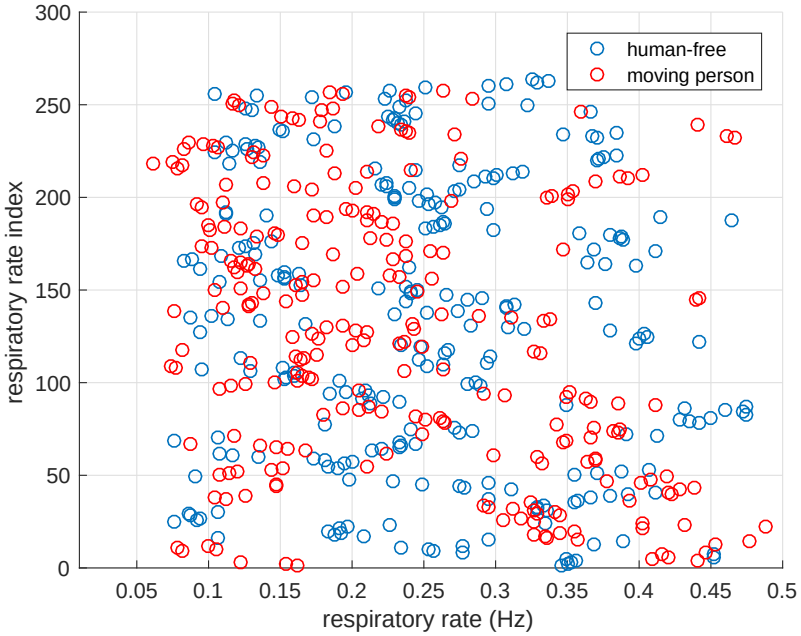

Figure 4.3: Distribution of RR estimates for human-free and moving human states.

4.1.3.4. *Classification*

In this stage, we use a decision-tree (DT) classifier to detect the presence of static or moving human. The decision tree algorithm is a classification procedure that partitions the input space into smaller regions and fits a simple separate model to predict the target in each region [153]. A decision tree structure includes a root node, decision nodes, and leaf nodes. Decision trees have some advantages. First, they are nonparametric methods that do not require an assumption about the distribution of input data. Second, the decision tree figures out the nonlinearities between the features and classes. In addition, one of the main advantages of decision trees is that they can be easily interpreted by humans since they predict the targets using a simple model. In this study, we focus on one of the tree-based models called classification and regression trees (CART) [154]. While dependent values are categorical in classification trees, they are continuous in regression trees [155]. CART uses Gini index as the splitting criteria. Gini index is a measure of impurity used in the decision trees to do binary splits is given as,

$$Gini(T) = \sum_{k=1}^{K} p_{\tau k}\,(1 - p_{\tau k}) \tag{4.2}$$

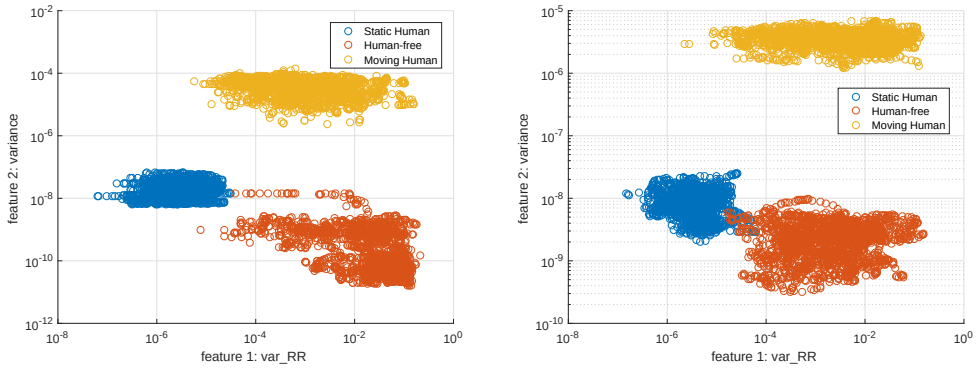

(a) Room A **(b)** Room B

Figure 4.4: Scatter plots of the features for samples obtained from different environments. (a) Room A. (b) Room B.

where T is the total number of leaf nodes, K is the number of classes, $p_{\tau k}$ denotes the ratio of data points in the corresponding region assigned to the class k.

4.1.4. Experimental Results and Discussion

4.1.4.1. *Experimental Setup*

Experiments are conducted in two different environments. First environment is a 2.8 m $\times$ 3.8 m office room in the EEE department, which is shown in Fig. 4.5(a). The second test environment is a 6.1 m $\times$ 9 m classroom in the EEE department, which is shown in Fig. 4.5(b). The layouts of the environments are shown in Fig. 4.6. As seen from the layouts, both setups are compatible with the double TTW scenario, where the transmitter and the receiver are located in two different rooms, and the monitored person is in a separate room. In each test environment, there are tables, desks, cabinets, and other furniture that create multipath reflection. Both environments are surrounded by 30 cm thick concrete walls. The proposed TTW human detection system uses SDR modules as the radio transmitter and the receiver. A unmodulated CW signal is transmitted at 900 MHz with the power of 0 dBm. Omni-directional vertical polarized dipole antennas are used in both transmitter and receiver.

Experimental Methodology: In the experiments, we collect data for three states: 1) Human-free: The test environments are empty during the experiments. 2) Moving Human: There is one subject in the environment walking randomly without tracking a certain trajectory. 3) Static Human: There is one human in the environment sitting or lying in different po-

(a) Room A **(b)** Room B

Figure 4.5: Experimental environments. (a) Office room. (b) Classroom.

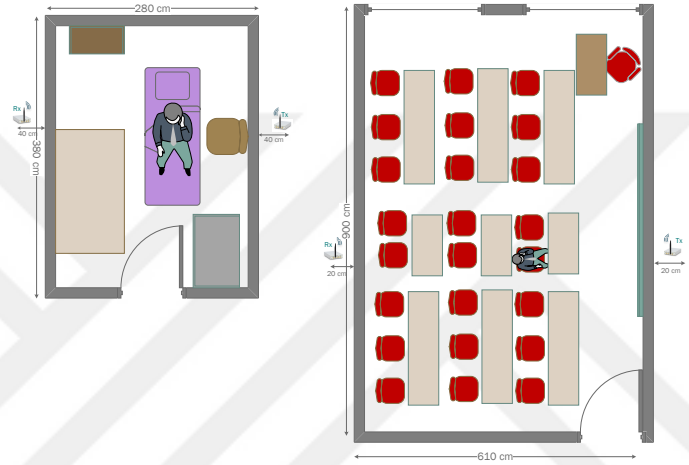

Figure 4.6: Comm Lab and Classroom Layouts

sitions, breathing naturally. The experiments are conducted in five different working days to evaluate the robustness of the proposed system. A different number of measurements are taken each day, which are shown in Table 4.2. As seen from the table, in total, the number of measurements collected in the first environment is 2058, while the number of measurements in the second environment is 1993, for each state. For each experiment, we use the training data and test data collected from different places to show the generality of the method.

4.1.4.2. *Results*

The first experiment is designed to show the effect of the sampling rate to the system accuracy. The performances are obtained for three different groups of experiments to reveal the relationship between the sampling rate and accuracy. The sampling rate is selected 2 Hz, 10 Hz and 20 Hz. The normalized accuracies of each state obtained using

Table 4.2: Number of measurements taken in different days and environments

Environment		Static	Human-free	Moving
Room A	Day-1	458	458	458
	Day-2	310	310	310
	Day-3	386	386	386
	Day-4	428	428	428
	Day-5	476	476	476
	Total	2058	2058	2058
Room B		1993	1993	1993

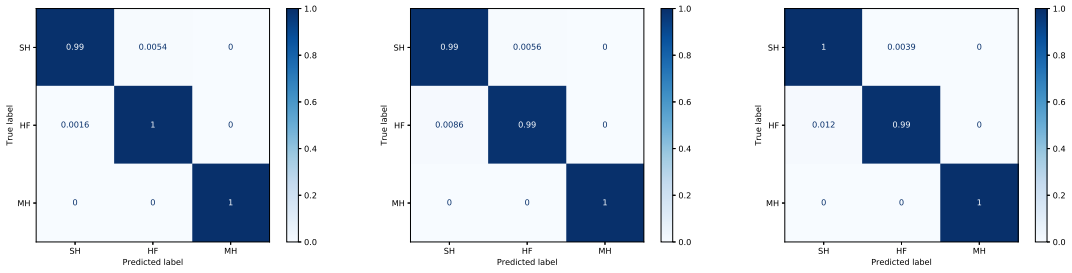

(a) $f_s = 2$ **(b)** $f_s = 10$ **(c)** $f_s = 20$

Figure 4.7: System accuracy according to the sampling rate (f_s). (a) $f_s = 2$. (b) $f_s = 10$. (c) $f_s = 20$.

Decision Tree classifier according to the sampling rates are shown in Fig. 4.7. In this experiment, training and test samples are collected in Room A. The results are obtained used 10-fold cross validation. For each value of the sampling rate, the accuracies of the Static Human, Human-Free and Moving Human states are higher than 99%. The overall accuracies for each sampling rate are 99.76%, 99.52%, and 99.48%, respectively. As seen from the figure, changing the sampling rate has little effect on system accuracy. Changing the sampling rate as long as the signal's periodicity is maintained does not affect the RR estimation performance. However, as mentioned previously, RR estimates can be equal to any frequency up to half the sampling rate for moving human and human-free states. Although changing the sampling rate affects the variance of RR estimates, which is the second feature of the system, in the cases of the moving human and human-free, it is seen as not concretely affecting system accuracy.

To evaluate the robustness of the proposed system, a different strategy which is called leave-one day-out cross validation is applied while taking measurements. Leave-one day-out technique is a specific version of cross-validation. For this purpose, the experiments are conducted in five different working days. In this technique, samples of

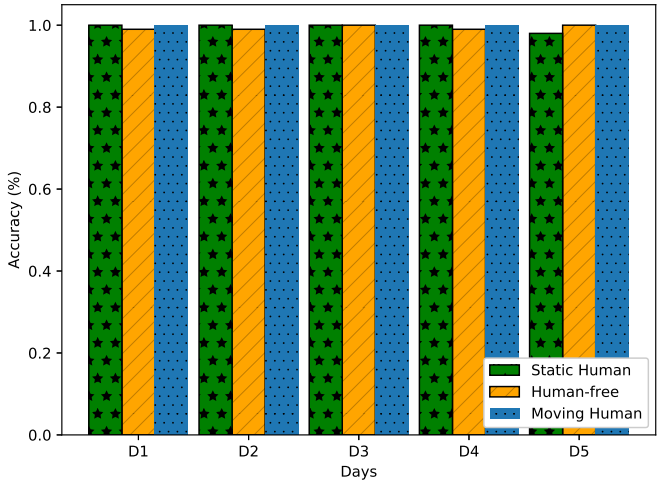

Figure 4.8: Overall accuracies for different measurement days.

one day are separated from the whole set and the remains are used to train the model. Then, the trained model is tested with the separated samples. This process is repeated for samples of each day, thus leave-one day-out cross validation results are obtained. The results are shown in Fig. 4.8. It can be seen in the figure that the proposed method can detect the moving human faultless for each day. For other situations, the system accuracy does not drop below 98%. As the experiments are done on working days, there may be students in the corridors. This can affect system performance negatively. Therefore, the decrease in performance these days may arise depending on more movements in the environment.

The system accuracy under different training sample sizes are shown in Fig. 4.9. The figure also shows the system accuracies in the cases that training data and test data are obtained from the same environment and different environments. First, the situation in which training and test samples are collected in Room A is explored. The results are obtained with 10-fold cross validation. First, 70% of the whole dataset is taken for training the model. In each step, the number of samples is decreased from 70% to 30%, 20%, 10% and 5%, respectively. The model is built for each state. The overall accuracy for all states for 70% of samples is 99.90%. As the number of samples decreases, the overall accuracy slightly decreases. When 5% of samples are used, the overall accuracy reaches 99.56%. It is clear that the training sample size has little effect on the overall accuracy when training and test samples are obtained from the same environment. In the second situation, the samples collected in Room B are tested with the model trained with samples collected in

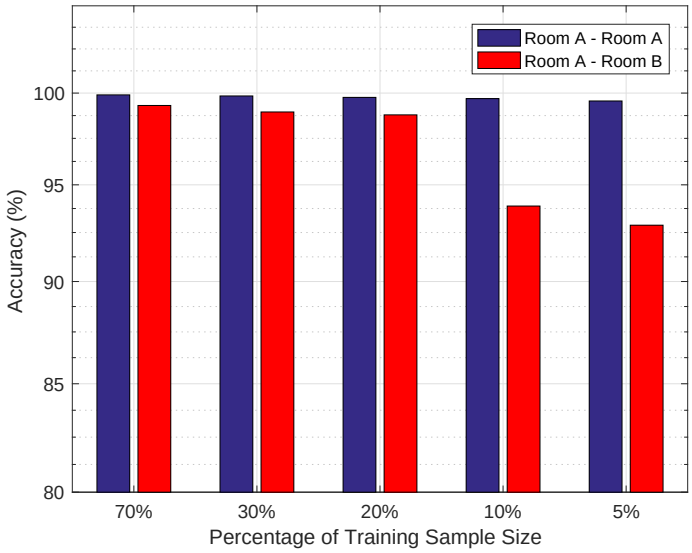

Figure 4.9: Overall accuracies according to the training sample size.

Room A. The overall accuracy is 99.31% when 70% of training samples are used. As the number of samples decreases, the overall accuracy slightly decreases, similar to the first case, until the number of samples reaches 20%. As seen in the figure, after this stage there is a faster decrease in the overall accuracy. When using 10% of the training samples, the overall accuracy is 93.88%, while using 5% of the samples, the accuracy drops to 92.88%. The reason for this decrease in the overall accuracy is that the impact of diversity in the data collected from different environments is felt more with the decrease in the number of samples. However, even if only 5% of the samples are used, it is evaluated that a general model that fits different locations is found.

We design an experiment in which training and test data are collected from different environments to evaluate the generalization of the presented system. Fig. 4.10 shows the accuracies of the system in match and mismatch situations. While match means that the training and test data are collected from the same environment, mismatch means that the training and test data are collected from different environments. As seen in Fig. 4.10, the proposed system achieves very high accuracy in both match and mismatch situations for Room A and Room B. This indicates that the proposed method can be used in a new environment without the need for retraining. This is because all three states locate separately in the feature space in a compact form as shown in Fig. 4.4. Even if the environment changes, it is possible to achieve the same performances since this compact

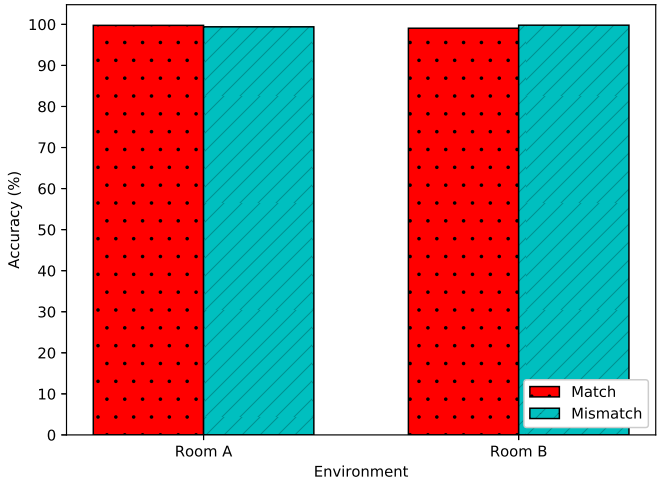

Figure 4.10: Comparison of accuracy in training and test locations. Match means that training and test data are collected from the same environment, and mismatch means that they are collected from different environments.

structure is not damaged.

Fig. 4.11 shows the detection performance of the proposed system according to the used features. In this experiment, the training data are collected in Room A and test data are collected in Room B. Fig. 4.11(a) shows the confusion matrix when the variance of RR estimates is used as a single feature. In this situation, as seen, although the presence of a static human is successfully detected, the moving human state cannot be separated from the empty environment. This is because there is no breathing activity in the empty environment and an accurate RR estimation cannot be made when the person is moving. It is insufficient using a single RR-based feature for separating these three classes. Second, system performance is shown in Fig. 4.11(b) when the variance of the signal is used as a single feature. Surprisingly, the system cannot separate the empty environment and the static human state and determines them as a single class. Variance is a very effective feature to distinguish the presence of moving humans from an empty state. However, this does not apply in the case of motionless humans. Micro-level chest movements, caused by the breathing, of a static person in the environment are not sufficient to detect the presence of the person, using the only variance. Third, the system accuracy are shown in Fig. 4.11(c) when two features are used. It can be seen that the combination of these two features allows the three classes to be separated from each other with high accuracy. The overall accuracy of the proposed system is obtained as 99.40%.

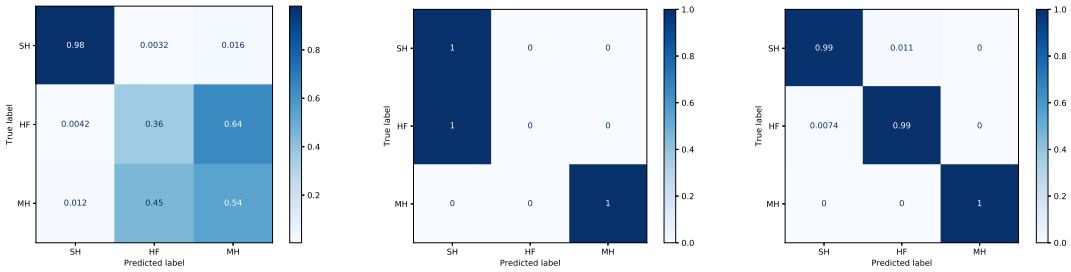

(a) feature 1 **(b)** feature 2 **(c)** feature 1 & feature 2

Figure 4.11: System accuracy according the used features. (a) System uses only $var(\mathbf{R})$. (b) System uses only $variance$. (c) System uses the combination of $var(\mathbf{R})$ & $variance$.

4.1.5. Conclusion

In this work, we propose a double TTW (DTTW) presence detection system for both static and moving humans using RF signals. The proposed method is tested for the DTTW scenario which is a more challenging scenario where both transmitter and receiver are placed in different rooms from the one in which the human exist. The low-cost and easy to use SDR modules are used as RF transmitter and receiver. In the proposed system, the periodic pattern caused by human breathing on the RF signals is used as an indicator of a static human presence behind the wall. In addition, variance of the signal is used as the second feature. The extracted features are classified by Decision Tree classifier. We collect measurement data in two different environments. Experiments are carried out for five days, taking into account environmental changes, various walking speeds, people around, etc. Experimental results show that these two features are very effective to separate the three states: 1) Static Human, 2) Human-free, 3) Moving Human. To show the robustness of the proposed method, the model trained with the data collected in one environment is tested with the data collected from the second environment. The proposed system achieves an overall accuracy of more than 99% without the need for retraining in a different environment.

4.2. Air-Writing Recognition

4.2.1. Introduction

In recent years, the requirements of the human-machine interactions are increasing, especially for smart home, and industry applications, gaming and virtual reality world, etc. [156]. Conventional methods such as keyboard and touch screen are not preferred in some of the above applications. Contactless techniques such as air-writing [157, 158], gesture recognition [42], speech recognition [159] are becoming more popular. These noncontact techniques are widely using visual and acoustic technologies. But nowadays, the ambient RF waves are successfully used for the applications such as sleep monitoring [160], fall detection [161], etc. The potentials of RF waves for human-machine interactions such as air-writing, which is defined as the user writing letters or words in the air, should be investigated. Air-writing recognition using RF waves is a very challenging problem since the RF waveforms of the same letter are never identical even if the letters are written by the same person. In literature, air-writing recognition systems can be categorized as device-free and device-based. Device-based methods require the user to wear a special sensor such as Data Glove [162] or to hold a controller such as Wiimote [163] for air-writing.

Device-free systems, which do not require any sensor/device to be held, enable people to interact with smart devices in different environments. Data acquisition in device-free systems is mainly performed using vision-based methods which use a camera to capture the writing of the user [164]. These methods are completely dependent on daylight and can also violate users' privacy. The other possibility is the use of radio signals [157, 158, 165, 166] to capture the motions. Wireless signals propagating from the transmitter to the receiver can be affected by finger-wrist movements on the propagation path. In [157], the authors proposed a hand motion tracking system using WiFi signals. They utilize the angle-of-arrival (AOA) information to track the user's hand trajectory, however, they take these estimated trajectories into a commercial application and use its handwriting recognition functionality. In [158], they proposed an air-writing recognition system based on WiFi signals using commercial WiFi devices. However, in [157] and [158], the size of required writing area for the air-written letter is quite large and inconvenient for some applications. In [165], the authors proposed a fine-grained WiFi-based writ-

ing recognition system for 26 capital letters. They use Dynamic Time Warping (DTW) that has a heavy computational burden to match test samples with the training models. In addition, they use a context-based error correction algorithm to improve the accuracy. In [166], the authors proposed a handwriting recognition system both for uppercase and lowercase letters using WiFi signals. In [165] and [166], the size of writing region is reasonable, but the users write with a pencil on a sheet or a tablet, which is incompatible with the concept of the device-free air-writing. In this study, unlike the above methods, a new air-writing recognition system with high accuracy and with a reasonable size writing area is proposed which does not require a sheet or tablet for writing, and not require any assistant application to improve the accuracy. Table 4.3 shows the comparison of some of the existing works that use RF signals for device-free air-writing recognition.

In this thesis, we propose a device-free air-writing recognition system that classifies 26 capital letters using wireless signals. In the proposed system, the oppositely polarized antennas are used in the two-channel receiver to provide polarization diversity that is exploited to improve the classification accuracy. The proposed system uses discrete cosine transform (DCT) coefficients as features that are fed into the machine learning algorithm to generate a model. The DCT coefficients constitute a new feature vector for representing the RF signal waveform. These discriminative spectral coefficients are much more efficient than conventional time-domain features. DCT is mainly used for 2D signals in image compression [167] and face recognition [168]. It is also preferred for one-dimensional time series [169, 170]. The proposed system does not require any wearable sensor or hand-held controller for writing the letters in the air. Software defined radios (SDR) are used as the radio transmitter and the receiver. It is observed that the finger and wrist gestures of the user can affect the received signal's amplitude differently for each letter and, thus unique patterns for each letter are obtained in each channel of the receiver.

4.2.2. Related Work

In this section, we discuss some works on hand gesture recognition and handwriting recognition, which have a similar concept with air-writing recognition.

Table 4.3: Related Works of Using RF Signal for Device-free Air-Writing Recognition. ✗: advantage, ✔: disadvantage

Method	Letter Size (cm)	Required Writing Tools	Required Ass. App.	Accuracy (%)
Wi-Wri [165]	10	tablet	✔	82.7
Wri-Fi [158]	25	✗	✗	86.75
WiDraw [157]	30	✗	✔	89
Mcsm-Wri [166]	5	pencil/paper	✗	96.68
Proposed Method	15	✗	✗	95.15

4.2.2.1. *Hand Gesture Recognition*

Hand gesture recognition (HGR) is one of the components that provide human-computer interactions. HGR is used in areas such as smart-home systems, gaming consoles, sign language recognition, etc. HGR methods can be categorized as vision-based, sensor-based and RF-based. In [171], the authors propose a hand gesture recognition method using Kinect depth camera. In [172], the Leap Motion data is combined with the Kinect data to improve the hand gesture recognition accuracy. In [173], the authors present a sound-based gesture sensing method that exploits Doppler shifts. An inertial sensor-based system in [174] recognizes the hand poses of the user using a wrist-worn sensor. Vision-based methods have a high incidence of dependency on daylight and line-of-sight (LOS) conditions. Sensor-based systems require users to wear a device/sensor, which limits the mobility and comfort of the users. In recent years, RF-based gesture recognition systems gain increasing popularity due to the ubiquitous and pervasive characteristics of wireless signals. RF-based methods do not need daylight or wearing any device. These methods utilize the effect of the hand gestures to the RF signals. In [17], WiFi-based hand gesture recognition system is presented. Their system recognizes the hand gestures to contactless control the media-player application. They utilize multiple access points for majority voting in the hand motion detection. They create pre-defined hand gestures used for controlling the applications to be different from each other. Thus, it is easier to recognize hand gestures defined by the user than to recognize letters with certain shapes. In [42], a whole-home gesture recognition system that leverages Doppler shifts on WiFi signals is presented. In [175], the authors used WiFi signals to recognize four hand gestures of the users. In [176], the authors presented a hand gesture recognition system using WiFi signals. Their system can recognize seven hand gestures both in LOS and through-wall

scenarios. While these RF-based gesture recognition methods provide high accuracy, they can only recognize pre-defined simple gestures and large scale motion.

4.2.2.2. *Handwriting Recognition*

Handwriting recognition (HWR) is the recognition of the letters, numbers or signs written by hand, by the computer systems. When talking about handwriting recognition, the first thing that comes to mind is the recognition of the text written on a paper, tablet or on any surface with a pen or a stylus. However, since it is in accordance with the concept, recognition of the letters and characters written in the air will be discussed here. Similar with HGR systems, HWR (air-writing) methods can be categorized as vision-based, sensor-based and RF-based. A vision-based method in [164] recognizes the words or characters written in mid-air. They can track the 3D hand trajectory of the users who are instructed to write large letters. In [177], the authors presented an air-writing recognition system, where the gestures are acquired by Kinect. In [162], the authors presented a wearable input system for handwriting recognition. The accelerometer and gyroscope sensors are attached to the back of the hand using a glove. A hybrid framework is presented in [163] which combines optical infrared tracker and a handheld Wiimote device's data. In [178], the authors presented a finger motion tracking system using WiFi signals. Their system can recognize the trajectories of 10 digits written in the air. A handwriting recognition system using wireless backscattering technology was presented in [179]. They use a passive tag to backscatter the signal to the receiver. They utilize the phase domain features besides conventional statistical features for letter and word classification.

4.2.3. System Overview

In the proposed air-writing recognition system, RF signal that is emitted from a transmitter is captured by a two-channel receiver as shown in Fig. 4.12. The antennas of receiving channels are placed as orthogonal to each other for providing polarization diversity. The user writes characters (letters) in the air-writing area which is over the line-of-sight (LOS) path between the transmitter and the receiver. When a user writes letters in the air, the signal amplitude can be affected by blockage of the LOS and multipath effect. The user's wrist and finger gestures create a unique effect on the signal amplitude for each letter.

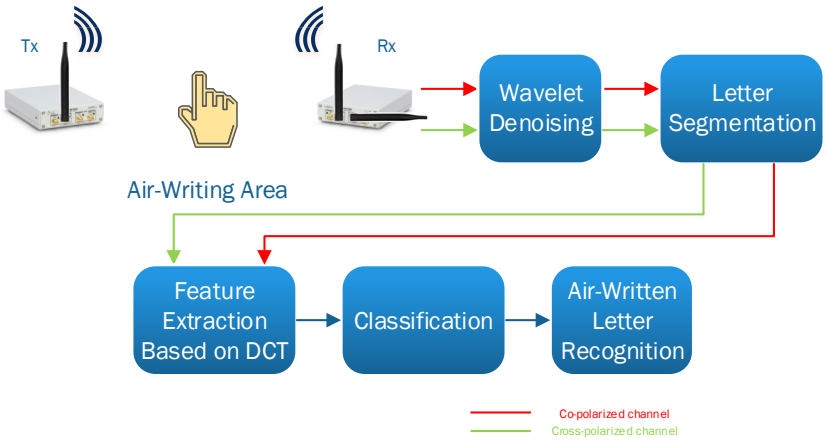

Figure 4.12: The general organization of the proposed air-writing recognition system.

Our system recognizes the letter written in the air based on these variations on the signal amplitude. The proposed system consists of the main blocks including data collection, denoising, letter segmentation, feature extraction based on DCT and classification. The general flow chart of the proposed air-writing recognition system is given in Fig. 4.12.

In the data collection step, the user writes letters in the air with the stroke-by-stroke and overlapped style, and the measurements are recorded. The received signal involves the noise due to various environmental factors. In denoising step, the Discrete Wavelet Transform (DWT) is performed to remove the noise from the received signal. The letter segmentation stage uses a thresholding-based method to identify the data segments which contain air-writing. In the feature extraction stage, DCT of the opposite polarized two channels of the received signal is performed, and the proposed system uses the extracted DCT coefficients as the features. Finally, SVM classifier is used to classify 26 capital air-written letters in the English alphabet.

4.2.3.1. *Signal Model*

In indoor environments, there are many signal paths between the transmitter and the receiver. The path in which signal arrives directly to the receiver from the transmitter is defined as direct path or line-of-sight (LOS) path. In addition, the signal reflected or scattered from various static or dynamic objects (or the human body) arrives the receiver in many different paths which are called multipath. Indoor environments are rich in multipath reflections due to many objects are close to each other. In our system, the received

signal has two channels. These channels are called vertical and horizontal channels depending on antenna polarization. The two-channel received baseband signal is defined as,

$$y^{\ell}(t) = \underbrace{\alpha_1^{\ell} s_1(t)}_{\text{direct path}} + \underbrace{\sum_{m=2}^{M} \alpha_m^{\ell} s_m(t) e^{-j\phi_m^{\ell}}}_{\text{multipath}} + w^{\ell}(t), \quad \ell = 1, 2 \tag{4.3}$$

where ℓ is channel index. $s_m(t)$ represents propagated signal along many paths. M is the number of paths signal arrives the receiver from the transmitter. First path is defined as direct path (LOS path), remaining $M-1$ is the number of multipaths. m is path index. The second term of the summation in (4.3) is the multipath due to static objects and human arm or finger movements. α_m^{ℓ} denotes attenuation in path m in channel ℓ. α_1 is the attenuation in the direct path. ϕ is phase of the signal in path m for channel ℓ. We assume that $w(t)$ is a white Gaussian measurement noise.

4.2.4. Air-Writing Recognition Using Polarization Diversity

4.2.4.1. *Writing Style*

During the air-writing process, various writing styles create different patterns for each letter as expected. The speed of writing also changing the patterns. When various writing styles are allowed, it is required to train the model for each possibility. In this study, the air-writing style which is determined as a standard consists of two components as stroke-by-stroke and overlapped styles. In the stroke-by-stroke style, the user completes a letter using multiple strokes instead of one continuous stroke. In Fig. 4.13, 'B', 'E', and 'W' letters written in the stroke-by-stroke style are shown. The stroke orders are also shown in the figure with numbers. As seen that the stroke numbers and orders are different for each letter. Therefore, these differences lead to unique patterns for each letter. The second component of the writing style is that the user writes the letters in an overlapped manner in an imaginary region which is an air-writing box with the size of 15 cm $\times$ 15 cm. Otherwise, if the letters are written from the left to right manner instead of overlapped style, the unique pattern of the letter is distorted since arm movements along with finger movements become a part of the activity. In addition, when writing from left to right, changes in the signal amplitude that damage the shape of the waveform appear

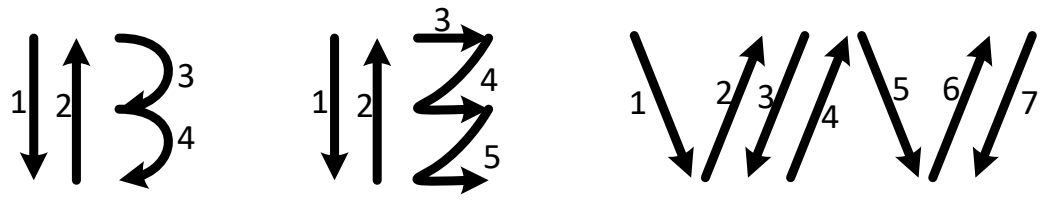

Figure 4.13: Letter formations for B, E, and W letters. Stroke orders are also shown.

as the user's hand comes close to the receiver (or transmitter).

4.2.4.2. *Basics of Antenna Polarization*

An electromagnetic wave consists of an electric field and a magnetic field. Both of them are perpendicular to each other and also perpendicular to the direction of propagation. Polarization is one of the characteristics of the antenna and refers to the orientation of the electric field component of the radio waves, which are emitted or received by the antenna, relative to the earth [180]. The polarization can be classified into three types as linear, circular and elliptical polarization [181]. In this study, we considered linear polarization, so other types of polarization are out of scope. In linear polarization, the electric field is always directed along a line. It can be either vertical or horizontal as shown in Fig. 4.14. In general case, there should be a polarization matching between transmitting and receiving antennas. If the receiving antenna is in different polarization with the transmitting antenna, it cannot receive the signal emitted by the transmitter. However, in short-range communication, this is somewhat different, that is, the receiving antenna can receive the signal emitted from a transmitting antenna with different polarization by some attenuation [180]. The case that the receiving and the transmitting antennas have opposite polarization is called *cross-polarization*. On the other hand, the fact that the receiver and transmitter have the same polarization is called *co-polarization*. Using these two polarization structures together in a system provides polarization diversity. In our system, a signal is emitted from a transmitter using a vertically polarized antenna and is captured by a two-channel receiver using two antennas with orthogonal polarization (e.g. vertical and horizontal) each other. The antenna layout of the proposed system using polarization diversity is shown in Fig. 4.15. Using polarization diversity at the receiver end provides different correlated signals that describe the same class (letter), which provides more fea-

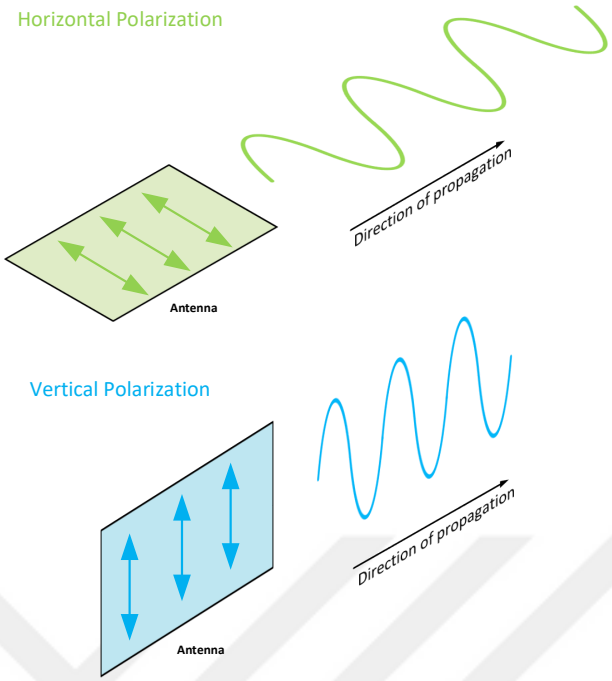

Figure 4.14: The polarization scheme of horizontal and vertical antennas.

tures to be extracted to improve classification accuracy. How polarization diversity affects the amplitude of received signal will be given in the next section.

4.2.4.3. *The Effect of Finger/Wrist Gestures on Received Waveform and the Role of Polarization Diversity*

The finger or wrist gestures of the user while writing letters in the air affect the amplitude of the RF signal. In the proposed air-writing system, we distinguish the effect of the user's finger/wrist gestures to the RF signal similar to the effect of the walking people to the occupancy estimation system in [34] into two ways: 1) blocking the LOS, 2) multipath effect. Since the imaginary air box where the letters are written is on the LOS path between the transmitter and the receiver, the finger or wrist of the user blocks the LOS, causing a drop in the signal amplitude. The effect of blocking the LOS occurs in different positions in two receiver channels due to the polarization diversity. For instance, when the finger is at the bottom region of the imaginary air box, it blocks the LOS of the cross-polarized channel, when it moves up, it blocks the LOS of the co-polarized channel. Thus, the finger's bottom-to-top movement increases the amplitude of the cross-polarized channel signal, while it decreases the amplitude of the co-polarized channel signal, as

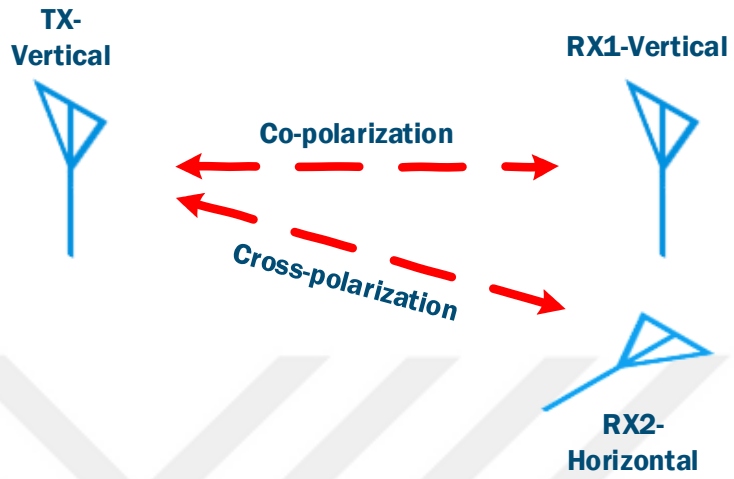

Figure 4.15: The antenna layout of the proposed system using polarization diversity.

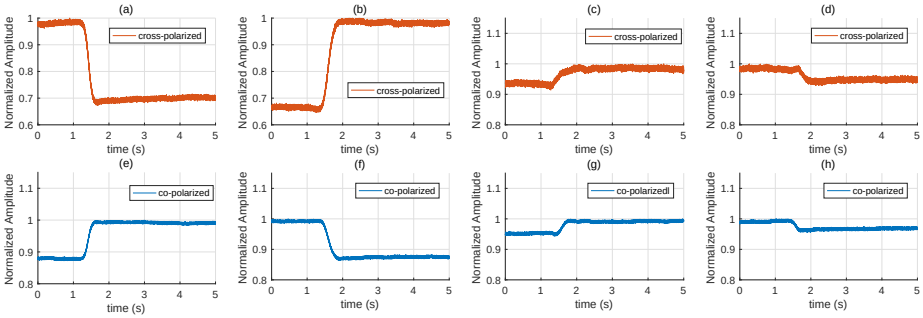

Figure 4.16: The amplitudes of the received two-channel signal when sample movements are made: (a)top-to-bottom, (b) bottom-to-top, (c) left-to-right, (d) right-to-left, in the cross-polarized channel; (e) top-to-bottom, (f) bottom-to-top, (g) left-to-right, (h) right-to-left, in the co-polarized channel.

shown in Fig. 4.16 (b) and (f). The opposite of the effect of this movement is observed when the finger moves top-to-bottom as seen in Fig. 4.16 (a) and (e). In addition, it is seen that the change in the amplitude of cross-polarized channel signal is more than the change in the amplitude of co-polarized channel signal for these two movements. In the co-polarized channel, only the user's finger blocks the LOS path, while in the cross-polarized channel, along with the finger, the arm also blocks the LOS path. The second component that affects the signal amplitude is the multipath effect. If there exists a strong LOS component, the multipath reflections are superimposed on a LOS signal. Otherwise, the received signal consists of many randomly distributed reflections [180]. Unlike perpendicular movements, the effects of left-to-right and right-to-left movements to receiver channels are in the same direction as seen in Fig. 4.16 (c)-(g) and Fig. 4.16 (d)-(h). Since the position of the finger does not change perpendicularly in parallel movements, the LOS state remains the same. In this situation, the signal amplitude changes only due to the multipath effect. Therefore, fewer changes are seen on the signal amplitude compared to the perpendicular movements.

Fig. 4.17 shows the received RF signals' amplitude for two-channels when different letters are written in the air. Fig. 4.17 (a), 4.17 (b) and 4.17 (c) show the waveform of the letters 'B', 'E' and 'W', respectively. It can be seen that the waveforms of different letters have quite different patterns and the number of strokes. In the cross-polarized channel, from top to bottom strokes that are perpendicular to the LOS path cause drops in signal amplitude. The strokes 1, 3, and 4 in the letter 'B', and the stroke 1 in the letter 'E', and the strokes 1, 3, 5, and 7 in the letter 'W' are the examples for this case. In the co-polarized channel, from bottom to top strokes that are perpendicular to the LOS path cause drops in signal amplitude. The stroke 2 in the letter 'B', the stroke 2 in the letter 'E', and the strokes 2, 4, and 6 in the letter 'W' are the examples. On the other hand, the strokes that are parallel to the LOS path (for e.g. the strokes 3, 4, and 5 in the letter 'E') do not cause much change in the signal amplitude. As discussed earlier, the amplitudes of the signal in the channels, which have polarization diversity, are affected in the opposite direction by the perpendicular movements, while in the same direction by the parallel movements. It is validated with the real measurements as shown in Fig. 4.17. Additionally, the number of strokes are different for the sample letters as seen in the figure. For instance, the letter 'B' is written in the air with four strokes. On the other hand, the letter 'E' has five strokes.

The letter 'W' has the most complicated waveform among them since it consists of seven strokes. The numbers of strokes for different letters seen in the received RF signal in Fig. 4.17 are compatible with the number of strokes that came into existence when writing the letters shown in Fig. 4.13.

4.2.4.4. *Noise Removal Based on Discrete Wavelet Transform*

Wireless signals are exposed to various noise effects such as thermal noise, internal device noise, and external ambient/interference signals, etc. in indoors and can also have many outliers/peaks. It is crucial to remove some of the unwanted signals to make the air-written recognition system operable. It is reported in [182] that the frequency range of human gestures is between 0.3 Hz and 4.5 Hz. Therefore, the considered signal is low frequency signal and high frequency components can be removed but on the other hand, lower cut-off frequency causes loss of some characteristic information related to the gestures. The Discrete Wavelet Transform (DWT) is preferred in this study to remove noise without loss of useful information. DWT which is a powerful tool, is used in wide range applications such as signal processing, image compression, pattern recognition [183]. The main idea in DWT is that decompose the signal to sub-bands in different frequencies. The common wavelets are daubechies, symlets, coiflets, etc. [184]. Denoising based on wavelet transform consists of three steps: decomposition of the signal, thresholding and reconstruction of the signal. In wavelet analysis, the signal is decomposed to approximation coefficients and detail coefficients in each decomposition level. In order to remove the noise on the wavelet coefficients, the thresholding method is used. After the decomposition, the detail coefficients below the threshold are assumed as noise and they are shrunk to zero. In each decomposition level, this process is repeated. Thus, in the reconstruction stage, the signal purified from the noise is obtained. In this study, Daubechies-4 (db4) is chosen as the basis wavelet function and 7 is selected as the decomposition level by analysing the recorded data set. The example received noisy signal and the wavelet filtered signal for writing the letter 'K' is shown in Fig. 4.18. Since the shape of the waveform is distorted, the need for noise removal is seen from the figure.

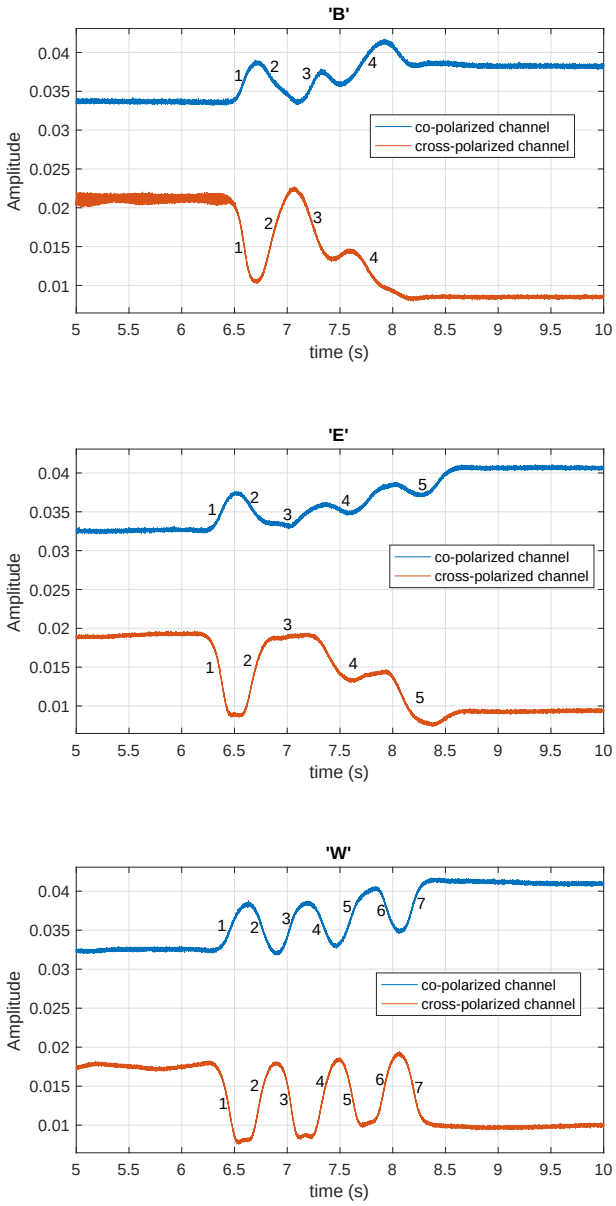

Figure 4.17: RF signal waveforms in the vertical and horizontal channels for letters ’B’, ’E’, and ’W’.

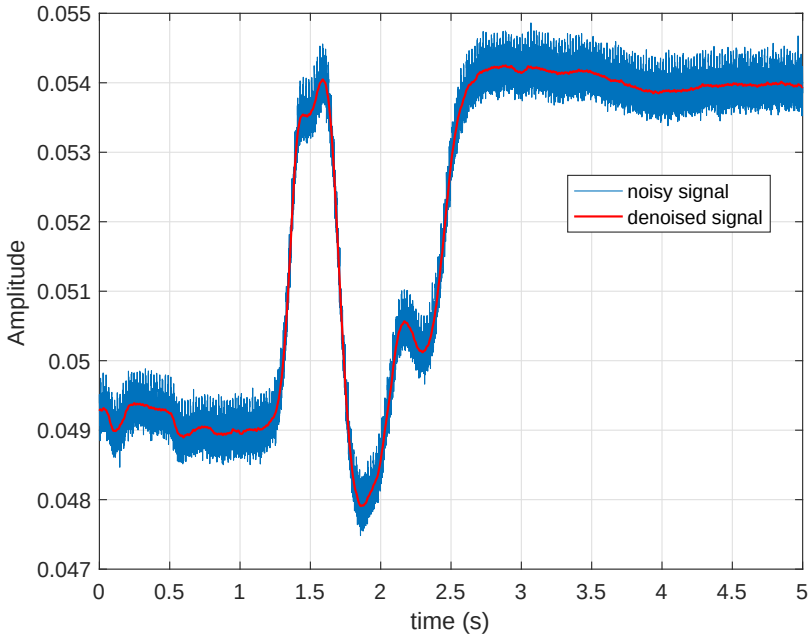

Figure 4.18: The received noisy signal and the denoised signal for writing the letter 'K'.

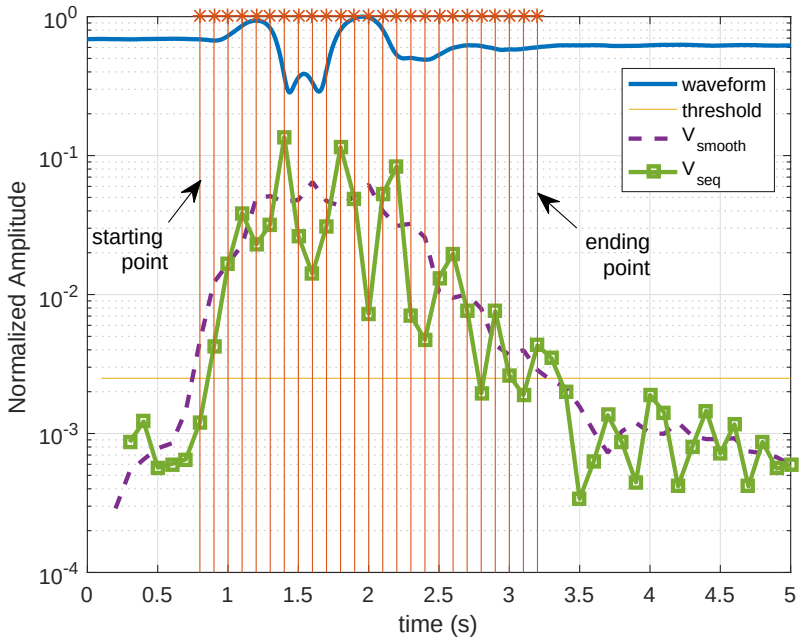

Figure 4.19: Segmentation of writing activity.

4.2.4.5. *Letter Segmentation*

To capture the signal waveform of a letter, the time periods when the letters are written need to be identified and distinguished. Therefore, a letter segmentation that corresponds to distinguish a segment of data in which writing a letter has occurred is done. For the letter segmentation, the aim is to detect the starting and ending points of the writing activity. It is seen in Fig. 4.19 that the amplitude of the RF signal is almost stable in the absence of writing activity and significantly change while writing the letters. Therefore, it is expected that data segments which contain air-writing activity have higher variance.

In this thesis, we use a simple and efficient method based on variance-thresholding for the detection of starting and ending points. In this method, we use a sliding window approach in both two channels synchronously for the segmentation. First, the denoised signal is divided into windows of 100 ms. A sliding window is used to calculate the variance, thereby obtaining a variance sequence that is called V_{seq}. Then, we apply the moving average smoothing to the V_{seq} for reducing the variations shown in Fig. 4.19. We denote this smoothed version as V_{smooth}. If the value of V_{smooth} is greater than a dynamically calculated threshold, it is decided that there is a writing activity in the corresponding window. We compute the threshold once for each letter to be segmented and use it for all windows belonging to that letter. The threshold is determined as 9 times the variance of the first window of 200 ms. This value is set based on physical intuition and empirical observations. We assume that the user waits steadily for 200 ms without moving at the beginning. These procedures are applied to each channel individually. Then, we combine the results by simply taking the logical AND of the two channels to obtain the starting and ending points of the letter. In other words, in order to determine the presence of the writing activity in the corresponding window, it must be sensed in both channels. The reason is to prevent the outliers that may occur at different times in the two channels from damaging the segmentation. The first and the last of the points detected jointly in both channels are determined as the starting and ending points, respectively. Time durations between the starting and ending points are determined as the letter segment. In order to perform the segmentation properly, there must be a certain time gap between the writing of the letters. In the measurements, the letters are written in the air by users every 5 seconds. Therefore, at least 2 seconds of the gap is provided between the writings.

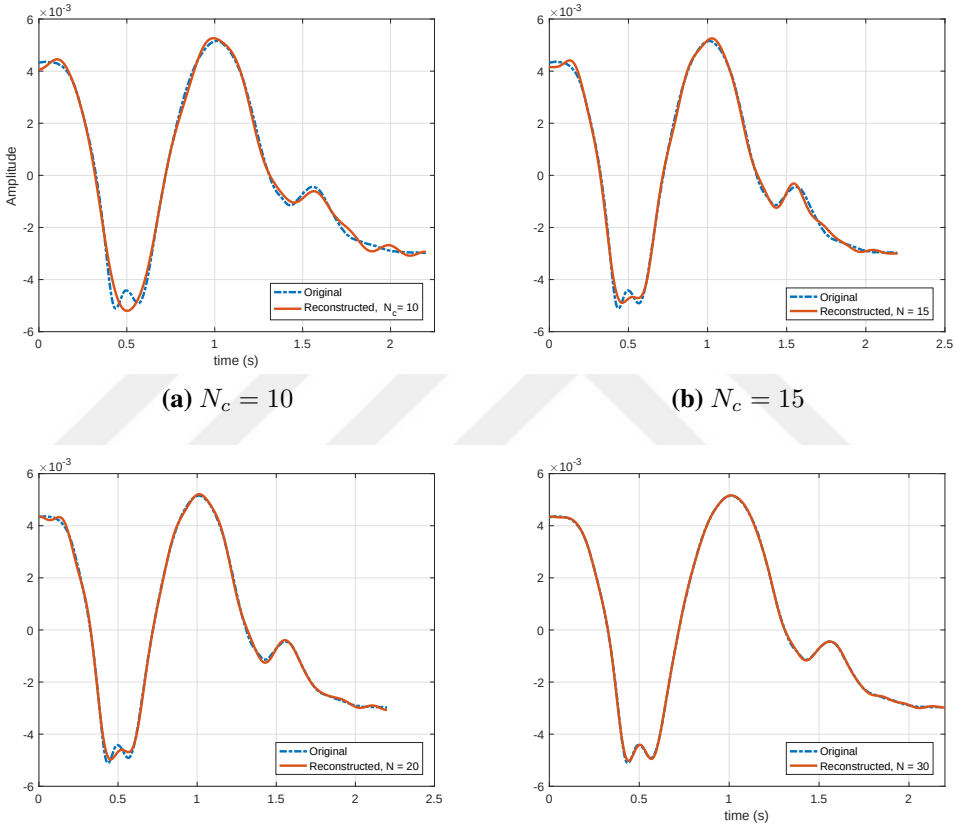

(a) $N_c = 10$ **(b)** $N_c = 15$

(c) $N_c = 20$ **(d)** $N_c = 30$

Figure 4.20: Original waveform of the letter 'R' and its reconstruction using different low-frequency DCT coefficients.

4.2.4.6. *Feature Extraction Using DCT*

Discrete Cosine Transform (DCT) is one of the transformation methods that transform the input signals from time-domain to frequency domain [185]. Unlike Discrete Fourier Transform (DFT), DCT uses only real-valued cosine functions instead of complex exponential functions. DCT of a discrete signal, $x(n)$, in time domain is defined as,

$$X(0) = \frac{1}{\sqrt{N}} \sum_{n=0}^{N-1} x(n) \tag{4.4}$$

$$X(k) = \frac{2}{\sqrt{N}} \sum_{n=0}^{N-1} x(n) \cos(\frac{(2n+1)k\pi}{2N}) \qquad k = 1, \ldots, N-1 \tag{4.5}$$

where N is the length of the input signal. X denotes the DCT coefficients, which are always real, and k is the coefficient index. Low-frequency DCT coefficients have high energy [169]. To set the remaining coefficients to zero does not significantly affect the total energy of the signal. This is the reason why DCT is widely preferred in compression algorithms. Thus, by using several DCT coefficients, it is largely possible to preserve the waveforms of letters written in the air without distortion. Fig. 4.20 shows the original waveform of the letter 'R' after segmentation and its reconstruction using different number of low-frequency DCT coefficients. The remaining coefficients are set to zero. Then, the signal is reconstructed using the DCT coefficients. As seen, with the increase of the number of DCT coefficients, the reconstructed signals are more similar to the original signal. However, only 10 coefficients with the highest energy are sufficient to reconstruct the original signal without shape deformation. These 10 DCT coefficients represent 99.75% of the energy of the original signal. In this study, the first 10 magnitudes of DCT coefficients are extracted as the features for air-writing recognition. Similarly, 10 features (DCT coefficients) are obtained from the second channel of the receiver, and we get a feature set of 20 features in total.

The speed and magnitude of gestures can affect the RF waveform of the letters. Even if the letters are written by the same user, their RF patterns are never identical. Fig. 4.21 shows an example for this situation that can be encountered in practical scenarios and needs to be solved. When the letter 'A' is written at different speeds by the same person, the obtained RF waveforms are shown in Fig. 4.21(a). The letter 'A' is written in two

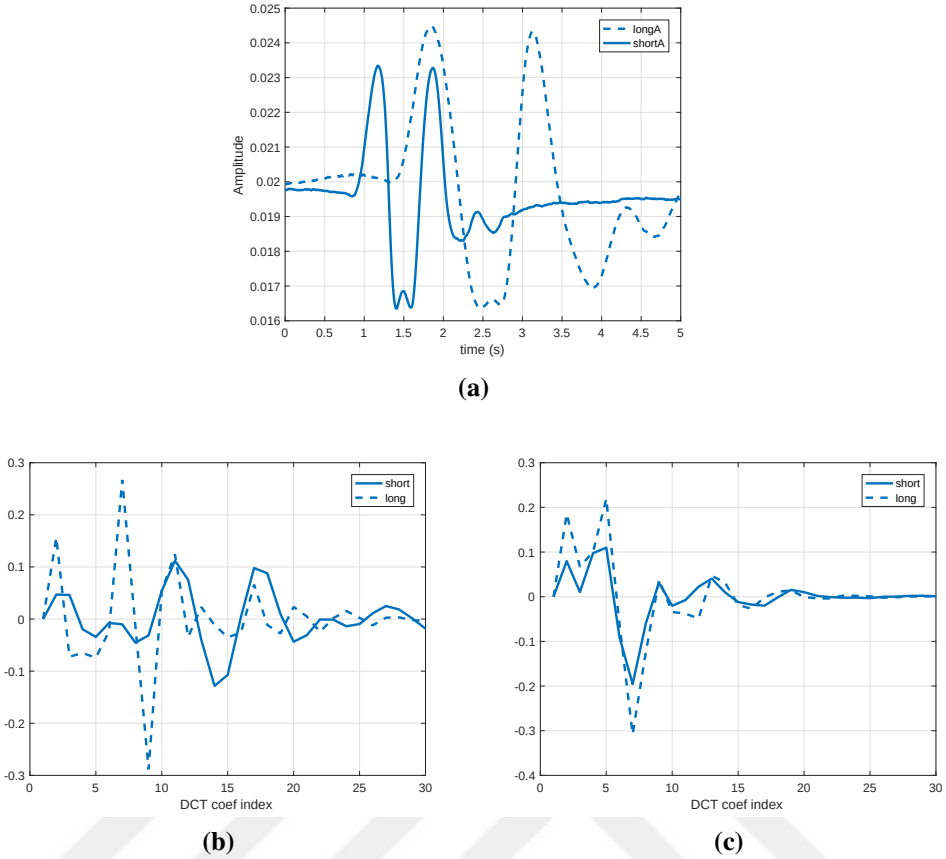

Figure 4.21: (a) RF signal waveforms of the short 'A' and long 'A'. (b) DCT coefficients before segmentation. (c) DCT coefficients after segmentation.

styles: slow and fast. It can be seen that although the waveforms of the two styles are the same, they are different in time and magnitude-scale. When we apply DCT to the entire 5-second signal, the DCT coefficients of two styles are shown in Fig. 4.21(b). As seen in the figure, DCT coefficients seem to belong to different letters in this case, which is a problem for the air-writing system. However, there is a solution to this problem: segmentation. Fig. 4.21(c) shows the DCT coefficients of the two styles after segmentation. By using segmentation, it can be seen that waveforms of the same letter even they are written at different speeds are obtained very similarly as they should be. Thus, it is verified that the proposed method can recognize the air-written letters regardless of the speed and magnitude of writing. In addition, we apply L2 normalization to the feature space. L2-normalization which rescales the samples in the feature space to have a unit form does not change the distribution of the samples. It is aimed to improve the classification accuracy by normalization which reduces the in-class variations. The normalization is applied to test data alongside the training data.

4.2.4.7. *Classification*

In the classification stage, we applied support vector machines (SVM) to recognize 26 air-written letters using the extracted DCT-based features. SVM which is a supervised learning approach is originally developed for the binary classification using a maximized margin mechanism. To adapt SVM to the multi-class problem, some strategies that decompose the multi-class problem into several two-class problems are developed. For this purpose, we used the one-versus-rest (ovr) strategy in this study. Linear SVM aims to find a hyperplane that separates two classes of data. For non-separable data linearly, kernel functions are developed. Using kernel functions, input samples are projected into a higher dimensional feature space to find a linear decision boundary (ie, a hyperplane) with the aim of classifying the data [186]. We choose the polynomial kernel function defined as,

$$K\left(\mathbf{x}_i, \mathbf{x}_j\right) = \left(\mathbf{x}_i^T \mathbf{x}_j + r\right)^d \tag{4.6}$$

where K is kernel function, $\mathbf{x}_i, \mathbf{x}_j$ are the feature vectors, d is the degree of polynomial function, r is a coefficient used in inhomogeneous polynomial kernel functions. In addition, C is the regularization parameter, which provides trade-off between the minimizing training error and maximizing the margin [187]. We set the parameters C to be 10, d to be 3, r to be 0 using hyperparameter tuning process.

4.2.5. Experimental Evaluations

4.2.5.1. *Data Collection*

The experiments are conducted using the setup shown in Fig. 4.22(a) in an office room with a size of 3 m $\times$ 5 m whose layout is shown Fig. 4.22(b). The generality of the proposed system is tested with a different environment, a laboratory, with a size of 8.6 m $\times$ 10.8 m whose layout is shown Fig. 4.22(c). For this early (concept validation) stage, we extract the single user recognition performance. The distance between the transmitter and the receiver which are placed on the desk is 1 m and they are placed 1 m above the ground. The user sits in front of the desk and all letters are written using the same predefined stroke order and with an index finger into an imaginary air box of 15 cm $\times$ 15 cm on the LOS between the transmitter and receiver. For each letter, 7 measurements

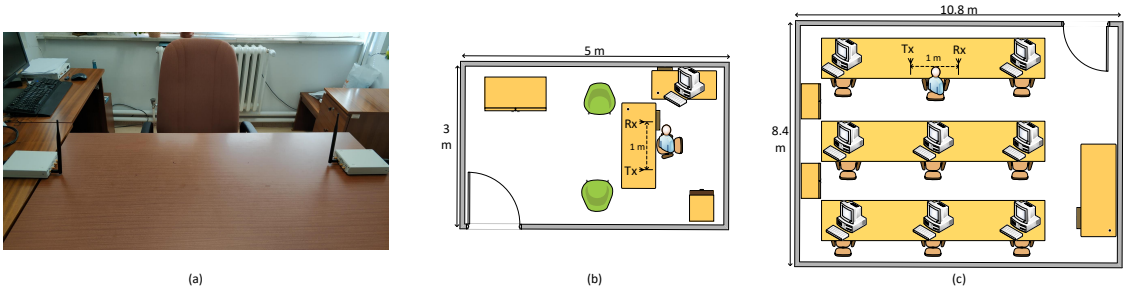

Figure 4.22: (a) The experimental setup in the office room, (b) Layout of the office room, (c) Layout of the laboratory

were taken per day. The measurements were completed on 18 different days. Thus, a total of 3276 measurements ($7 \times 26 \times 18$) were taken for 26 letters, and each of them lasted 5 seconds. The training set consists of 126 measurements per letter.

4.2.5.2. *Experimental Setup*

The SDR modules are used as the radio transmitter and the receiver. In this study, we used the Universal Software Radio Peripheral (USRP)- B210 radios. As a radio waveform, the unmodulated continuous wave (CW) signal at 825 MHz is used. The transmitter RF output power is adjusted to give -10 dBm (the maximal allowed received signal power of WiFi networks). In our system, a transmitter and a two-channel receiver exist. The transmitter has a vertically polarized antenna and the two-channel receiver has two antennas with orthogonal polarization (vertical and horizontal) to provide polarization diversity. The sampling rate of the SDR module is adjusted as 10 kS/s. The machine learning model described here is implemented by Scikit-learn in Python, and we run its training and testing on a Desktop computer which has Intel Core(TM) i7-3770K CPU @ 4.60 GHz Processor and 32 GB RAM.

4.2.5.3. *Results*

Firstly, we introduce our evaluation metrics used in the classification. We use four metrics for the evaluation of the performance of the proposed method as precision, recall, f1-score and overall accuracy. Precision (P) is $\frac{TP}{TP+FP}$, where TP (true positive) and FP (false positive) represent the correctly classified and incorrectly classified, respectively. Recall (R) is calculated as $\frac{TP}{TP+FN}$, where FN (false negative) represent the incorrectly rejected.

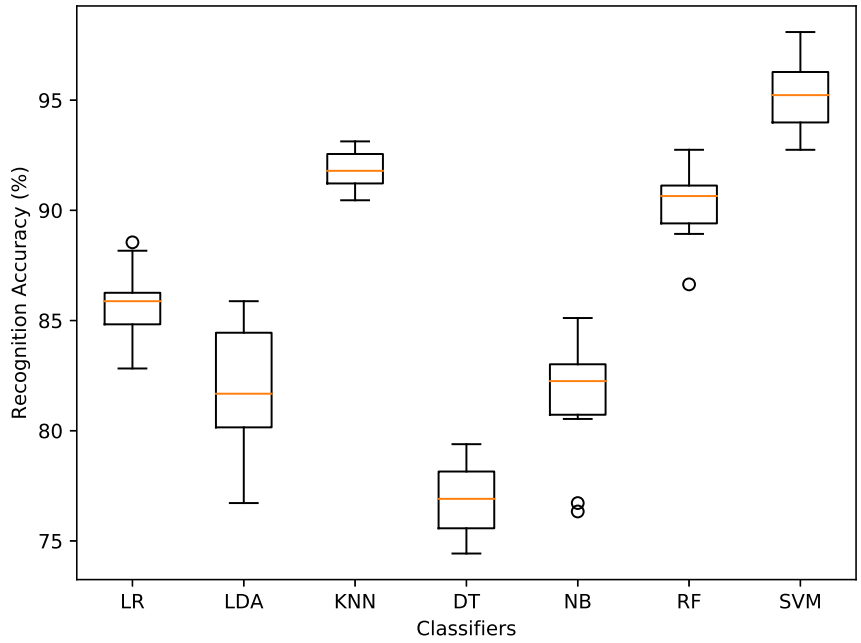

Figure 4.23: Overall recognition accuracies of the different classifiers.

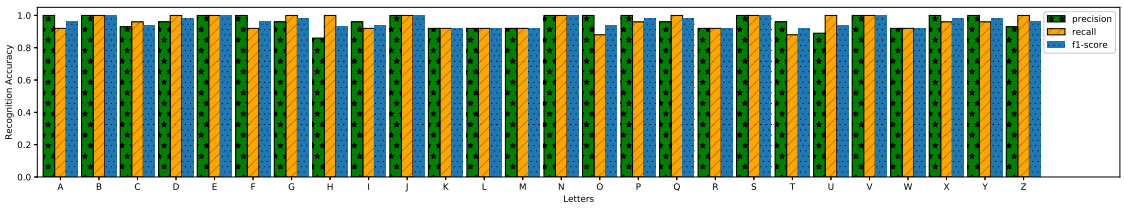

Figure 4.24: The classification results of the test set of 26 letters using SVM classifier.

The f1-score is the weighted harmonic mean of precision and recall, and calculated as $\frac{2\times P\times R}{P+R}$. The overall accuracy which is defined as $\frac{\sum_{i=1}^{C_n} TP_i}{N}$ is used for the evaluate the overall performance of the classification model, where C_n is the number of classes, and N denotes the number of all samples in the dataset.

In the first experiment, we compare the recognition performances of the different classifiers. Fig. 4.23 shows the box-plot graphs of the classification results which are obtained using 10-fold cross validation. We test our model with seven classifiers, i.e., Linear Regression (LR), Linear Discriminant Analysis (LDA), K-Nearest Neighbor (KNN), Decision Tree (DT), Naive Bayes (NB), Random Forest (RF) and Support Vector Machines (SVM), which are widely used in the machine learning applications. In the figure, the circles show the outliers, and the horizontal line in each box indicates the median of the results. The overall recognition accuracy of the SVM classifier is 95.15%. KNN and RF

algorithms achieve the accuracy of 91.87% and 90.26%, respectively. Other classifiers' accuracies are less than 85%. It is clear that the SVM classifier achieves high accuracy among the other classifiers. Hence, we present the experimental results using SVM classifier.

Fig. 4.24 shows the classification performances for each letter when using the SVM classifier. The dataset is split with the rate of 80-20 percent as training and test samples. For each letter, the number of samples is the same, therefore, balanced data is used both for training and test. The classification results shown in these figures are obtained using unseen test samples. As seen from the figures, all 26 letters are classified with varying accuracies. It can be seen in Fig. 4.24 that the f1-scores of all letters are greater than 92% when using the SVM classifier. The proposed system can recognize the 'B', 'E', 'J', 'N', 'S', and 'V' letters without any mistakes while achieving greater than 94% recognition performance for many letters. In addition, the color map of the confusion matrix of the SVM classifier for the test set is shown in Fig. 4.25. Rows and columns represent the true and the predicted labels of the letters, respectively. The diagonal cells show the correctly classified elements while off-diagonal elements show the misclassifications. Each cell of the confusion matrix presents the normalized percentage values. This confusion matrix indicates that the proposed system can accurately recognize the letters written in the air. It can be seen that 'O' and 'T' letters have lowest recognition performance since the letter formations of 'O' and 'T' letters are similar with 'U' and 'Z', respectively. It can be seen from the confusion matrix, the error rates between 'O' and 'U' letters are not symmetrical. The variance of the letter 'U' is less than the variance of the letter 'O'. Therefore, the system confuses the letter 'O' with the letter 'U', but can detect the letter 'U' without error. In addition, misclassifications between 'M' and 'W' letters, and between 'A' and 'H' letters occur due to the similarity of these letter pairs. In conclusion, the proposed system achieves an overall recognition accuracy of 96.03% by using SVM classifier for unseen test samples.

The third experiment is designed to determine how many DCT coefficients can be sufficient for the accurate air-written letter classification. In addition, the effects of the letter segmentation and feature normalization to the system performance are examined. Fig. 4.26 shows the overall recognition performance according to the number of DCT coefficients (N_c). These results are obtained using 10-fold cross-validation. As seen in

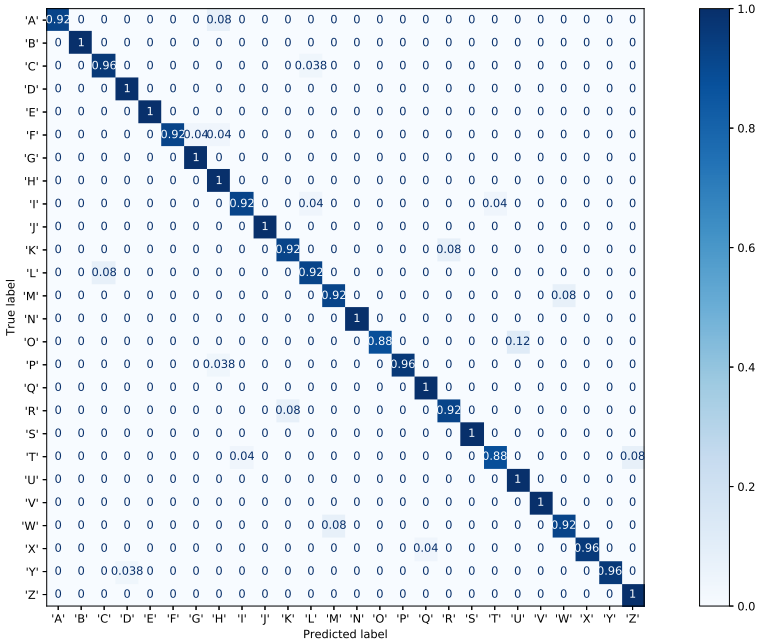

Figure 4.25: The confusion matrix of the SVM classifier for the test set.

the figure, recognition performances are unsatisfactory for all cases when using a small number of DCT coefficients ($N_c = 5$). Then, the performance improves with the increase in the number of DCT coefficients, however, after a certain value, it reaches saturation. Since the values of high-frequency DCT coefficients are quite small, they do not provide the distinctiveness. These high-frequency coefficients increase the dimension of the feature vector, but not the accuracy. Therefore, the optimum number of DCT coefficients is chosen as 10, which is sufficient to reconstruct the original signal as shown in Fig. 4.20. The segmentation of letters and the feature normalization improve the system performance as shown in the Fig. 4.26. The best recognition performance is obtained when the segmentation and normalization are applied.

Fig. 4.27 shows the overall recognition accuracies when two separate receiver structures are used. The single channel receiver system and two-channel receiver system are compared. We use a vertically polarized antenna as the receiving antenna in the single-channel system and we use two antennas with orthogonal polarization each other in the two-channel receiver. The performances which are obtained using 10-fold cross-validation are given according to the number of DCT coefficients. It can be seen that the two-channel receiver has a superior performance compared to the single-channel receiver for all the number of DCT coefficients. Especially, when using a small number of DCT

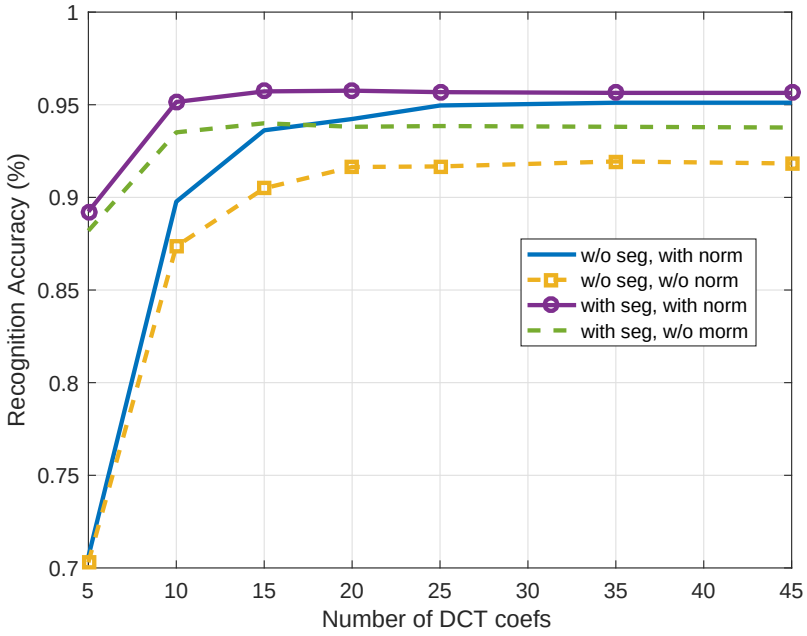

Figure 4.26: Overall recognition accuracy of the classification model according to the number of DCT coefficients.

coefficients, the difference in accuracy between the two receiver structures is more pronounced. The fact that two-channel receiver has the polarization diversity between the receiving antennas improves the classification accuracy as shown in the figure.

To evaluate the robustness and generalization of the proposed method, we collect the air-writing data in eighteen different days. Since the experiments are carried out on working days, there are people walking/existing outside the office or in the corridors, and students attending their sessions in the lab next door. We aim to illustrate that the proposed method is robust to these environmental changes. In addition, collecting all the samples belonging to a letter at a time creates uniformity in the training set, which reduces the accuracy when testing with unseen samples. In this experiment, recognition performances are obtained using the leave-one day-out validation which is a special form of cross-validation. In this validation method, samples of one day are considered as a fold and the total number of folds is equal to the number of measurement days. Then, one fold (day) of the samples is chosen for testing, the rest for training, and this process is repeated for all days. Thus, the overall recognition accuracies for each day are extracted. Fig. 4.28 shows the overall recognition accuracies for each measurement day. It can be seen that accuracies of only four days are less than 91%, which are Day-1, Day-5,

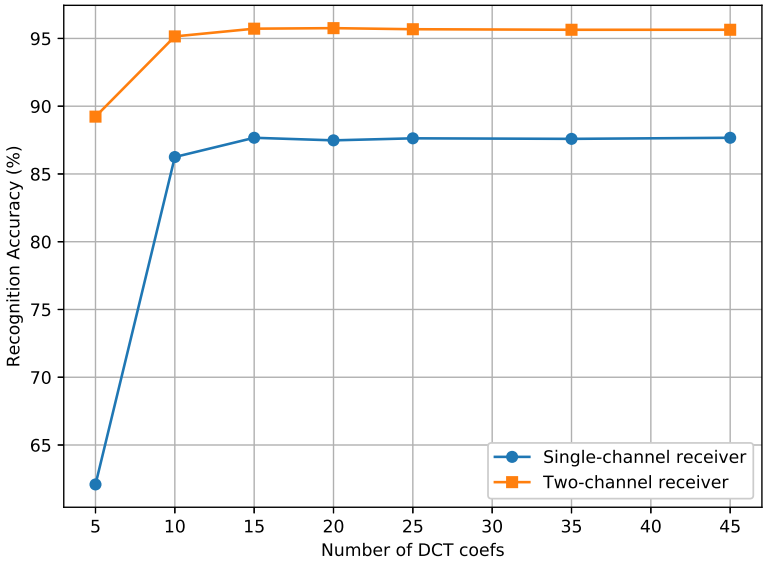

Figure 4.27: Performance comparison of single channel and two-channel receiver.

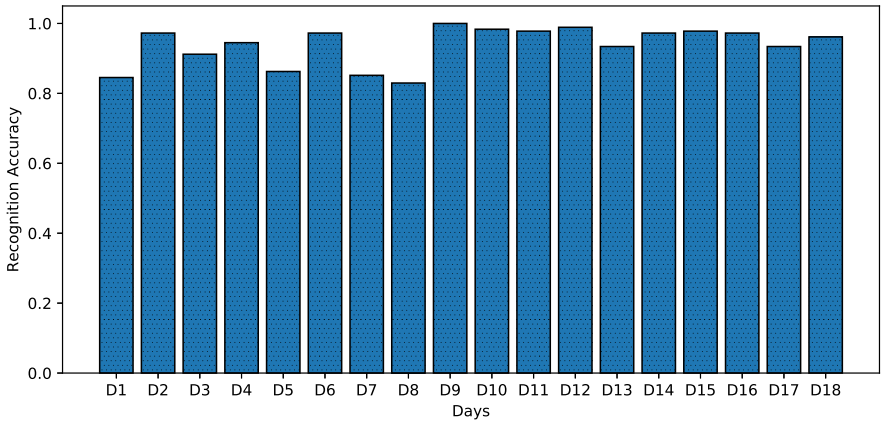

Figure 4.28: Overall recognition accuracies for different measurement days.

Day-7, and Day-8. The reason may be that there is more movement in the environment that increase the interferences on the signal in these days. On the other hand, the proposed method achieves high accuracy in the remaining days, indicating that the method is robust to environmental changes.

We investigate the effect of the training sample size to the recognition performance. Fig. 4.29 shows the overall recognition accuracy of the proposed method according to the different sizes of training sets which consist of 30, 50, 70, and 100 samples per letter. The overall recognition accuracies are obtained by using 10-fold cross-validation. For 30 samples, the overall recognition accuracy is 90.50%. It is seen in the figure that the recognition accuracy increases with the increasing of the training sample size. If the

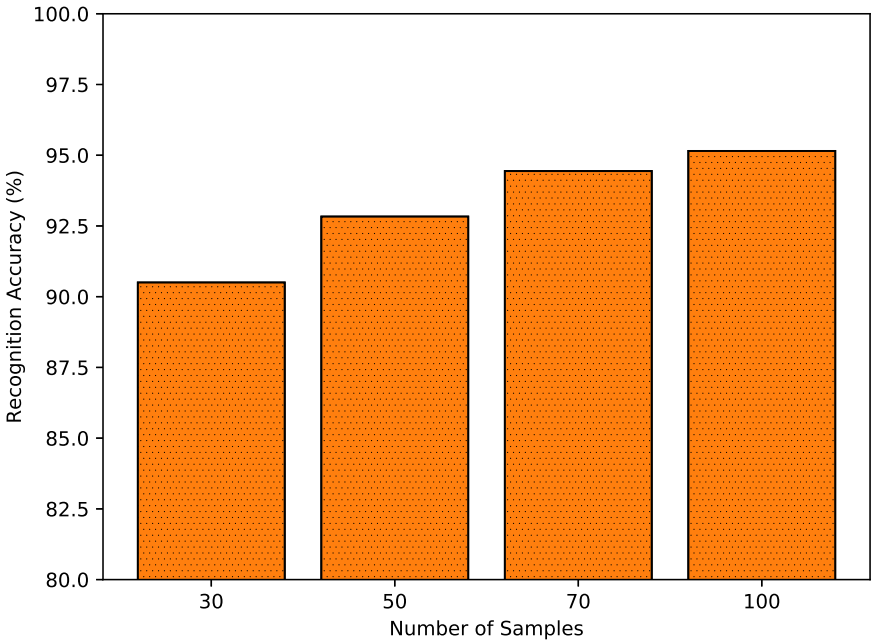

Figure 4.29: The overall recognition accuracies according to the size of training samples.

sample size is chosen to be 100, the overall recognition accuracy increases to 95.15%.

In order to evaluate the generalization of the proposed system, we designed an experiment in which training and test data are collected from different environments. In this experiment, the model is trained with data collected in the office room shown in Fig. 4.22(a), and tested with data collected in a laboratory whose layout shown in Fig. 4.22(c). In the laboratory, the distance between the transmitter and receiver and the placement of the antennas are adjusted in accordance with the office room. The proposed system is also compared with the method that uses Discrete Wavelet Transform (DWT)-based features [165]. In this method, Daubechies-3 wavelet is used as the mother wavelet and decomposition level is selected as 9. Fig. 4.30 shows the overall recognition accuracies of the proposed method and DWT-based method when the training and test samples are obtained from same and different environments. It can be seen in the figure that the performances of both the proposed method and DWT-based method are satisfactory when training and test samples collected from the same environment are used. In this situation, the proposed method and DWT-based method achieve the overall accuracy of 95% and 85%, respectively. However, if the test samples collected from the laboratory are used, the overall accuracy of DWT-based method reduces to 20% while the proposed method achieves 92% accuracy which is still satisfactory. This shows that it is required to re-

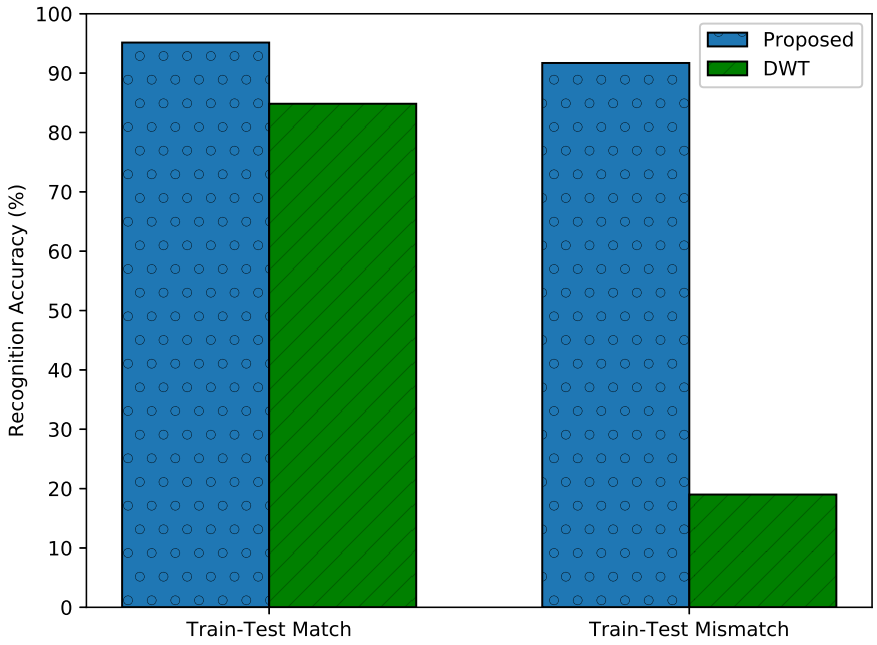

Figure 4.30: Performance comparison between the proposed method and DWT [165] in training and testing locations.

train the model for the different environments when DWT-based features are used. In the DWT-based method, the signal waveforms in the time domain are used as the features. Time-domain features are easily affected by environmental changes. In addition, the proposed segmentation algorithm cannot be applied to the DWT-based method as the letter segments are of different lengths, which reduces the accuracy. Although the environments are very different, the proposed system achieves high overall accuracy in the classification of 26 air-written letters.

4.2.6. Conclusion

In this thesis, the potentials of RF waves for air-writing applications are investigated. We propose a novel device-free air-writing recognition system with SDR modules. The proposed system utilizes a receiver structure with two antennas that are placed orthogonal to each other which provides polarization diversity. The user writes 26 letters into an imaginary air box of 15 $\times$ 15 cm with no sensor/device to be held. After collecting data we perform DWT for removing the noise from the signal. We apply a letter segmentation method based on variance-thresholding to distinguish the data segments that contain air-writing activity. After segmentation, we extracted DCT coefficients as the discriminative

spectral features representing the RF waveform. The machine learning based recognition system uses 126 samples for each letter. We use SVM classifier to recognize the air-written letters. It is shown with the experiments that the proposed air-writing recognition system achieves 95.15% overall accuracy for a reasonable size writing area. It is also shown that the proposed method can recognize the air-written letters in a different place from the environment where the model is trained, with a slight loss of performance, and leveraging polarization diversity improves the overall accuracy of the system.

5. CONCLUSION

In this thesis, the RF signals are investigated as a new technology for the human activity recognition and monitoring. In particular, we mainly focus on noncontact vital respiratory rate (RR) monitoring using different signal models, and through-the-wall (TTW) static human detection and device free air-writing recognition applications. In all these applications SDR modules are used for the measurements of the received narrow-band RF signal with a noncontact (wireless) and device free manner. This study offers novel contributions and solutions to these new and challenging problems.

In this thesis, we first investigate the problem of noncontact RR estimation. Three RF-based RR estimation methods are presented. The presented methods which exploit the periodic patterns caused by breathing on RF signals are derived from three different signal models for the noisy breathing signal. First, the high resolution subspace techniques, ESPRIT and MUSIC, which are derived from covariance matrix model are first time applied to the RR estimation in literature. It is shown that ESPRIT is computationally efficient and works approximately 49 times faster than the MUSIC algorithm. The proposed system is validated with real data collected using ten participants and realistic scenarios that examine the practical factors affecting RR estimation performance. It is shown that the high resolution technique achieves 0.13 bpm error rate with the limited number of data and significantly improve the RR estimation accuracy according to the benchmark (periodogram) method in literature. In addition, it is shown that high resolution techniques can be able to estimate the closely spaced RRs of two subjects, which is a challenging task, while the periodogram fails due to its inherent resolution potential. Then, the ARMA (2,2) model-based Quinn and Fernandes (QF) method is firstly adapted and used for the noncontact RR monitoring during sleep. In addition, a simple method for the detection of three sleep events is developed. It is shown in various real experiments that the proposed QF method achieves 0.15 bpm error rate with 20 seconds of measurement and is also effective for different distances and sleeping postures. These methods derived from the first two models benefit from the windowing approach where the RR is stationary along the window length. RR is a time-varying parameter. Assuming the RR as a longtime constant causes delays in monitoring the parameter; this can be a

critical problem in emergencies. Although the subspace techniques reduce the latency and improve the accuracy according to the periodogram, a real-time tracking is still an important requirement. In the end, the nonlinear model-based Kalman Filter (KF) approach which is capable of estimating and tracking the RR with a low steady-state error is proposed. For real-time monitoring, we modify the standard joint unscented Kalman filter method which uses third-order state-space model. Due to the nonlinear structure of the RR estimation problem with respect to the measurements, a novel modification is proposed to transform measurement errors into parameter errors by using the hyperbolic tangent function. It is shown in the experiments conducted with real measurements taken using healthy volunteers that the proposed ModJUKF method offers both a decrease in computational complexity of 8.54% and an increase in accuracy of 36.7% according to the JUKF method. It is also shown that the proposed ModJUKF method outperforms the windowing-based methods in the time-varying RR scenario.

In the second part of thesis, we exploit machine learning techniques for TTW human detection and air-writing recognition. First, the presence detection of static/moving human through-the-wall is performed as a classification process applied to the feature set. The presented system considers separating the three states: 1) Static Human, 2) Human-free, 3) Moving Human. The presented system is tested with a double TTW (DTTW) configuration, which is a more challenging scenario, to demonstrate the robustness against signal attenuation. Since the periodic structure of human breathing causes a periodic pattern on RF signals, this can be used as a distinctive feature for the presence detection of static human behind the wall. When there is a moving person in the environment, very obvious changes are observed on the received signal. Therefore, the variance of the signal can be used to separate the moving human state from the others. It is shown in various experiments that the proposed machine learning-based method achieves over 99% accuracy for the detection of both static and moving human in double TTW scenario. It is also validated with the real experiments that the proposed system can be used in a new environment without retraining the machine learning model. Second, we present a human-machine interaction application which is a device-free air-writing recognition system that classifies 26 capital letters using RF signals. The potentials of use of RF signals for air-writing applications are investigated. In the receiver, two oppositely polarized (horizontal and vertical) antennas are placed. Thus, a polarization diversity is provided. The

polarization diversity improves the recognition accuracy of the proposed system. The user does not need to hold a sensor or device while writing the letters in the air. In addition, we develop a letter segmentation algorithm based on variance-thresholding to distinguish the data segments that contain air-writing activity. The letter segmentation provides an exact matching of the DCT coefficients belonging the same letter written in different speed and magnitude. The machine learning-based recognition system uses 126 samples for each letter. We use SVM classifier to recognize the air-written letters. It is shown with experiments conducted with real measurements that the proposed system achieves 95.15% accuracy for a reasonable size writing area in the classification of 26 air-written letters and outperforms the fairly new WiFi-based air-writing recognition approaches. It is also shown that the proposed method can recognize the air-written letters in a different place from the environment where the model is trained, with a slight loss of performance, and leveraging polarization diversity improves the overall accuracy of the system.

5.1. Future Works

The presented systems in this thesis contain some limitations that will be interesting to explore in the future. In this section, we review these limitations for future research. In the proposed RR estimation systems, the monitored person is expected to be as motionless as possible. Signal changes caused by large-scale body movements suppress small changes due to breathing, which causes the system to miss minute movements such as breathing at these moments. If the person moves, the motion detection algorithm can sense these movements, and the RR estimation algorithm is not performed in the time of the movement. However, RR estimation is still not possible in the presence of any type of large-scale body movements and environmental motions. Therefore, the problem of RR estimation when there is a motion in the environment is an open research field. Another open research problem is multi-person RR monitoring which is not explored enough yet. Most of the existing studies are built on the idea of monitoring one person. However, this is not compatible with practical scenarios. It is an important requirement to be able to monitor more than one person's RR at the same time. In the proposed air-writing recognition system, the performance of the system is affected by the position of the person. However, a larger data set can be created by taking measurements for different positions of the person, and a highly accurate and robust system can be developed using this data set

in deep learning techniques. In this thesis, the effect of practical factors such as distance and carrier frequency on the performances of RF-based applications has been investigated. In addition, the theoretical limitations of these factors and analysis of frequency are left to future works. In addition, the proposed RF-based systems can be fused with systems that use different sensor technologies. Using combined data of different type sensors can increase the diversity and improve the system accuracy. In addition, the data sets collected for all RF-based applications performed in this thesis will be shared publicly to ensure the reproducibility of the results.

REFERENCES

[1] F. Q. AL-Khalidi, R. Saatchi, D. Burke, H. Elphick, and S. Tan, "Respiration rate monitoring methods: A review," *Pediatric pulmonology*, vol. 46, no. 6, pp. 523–529, 2011.

[2] A. Gaucher, D. Frasca, O. Mimoz, and B. Debaene, "Accuracy of respiratory rate monitoring by capnometry using the capnomask® in extubated patients receiving supplemental oxygen after surgery," *British journal of anaesthesia*, vol. 108, no. 2, pp. 316–320, 2012.

[3] D. A. Birrenkott, M. A. Pimentel, P. J. Watkinson, and D. A. Clifton, "A robust fusion model for estimating respiratory rate from photoplethysmography and electrocardiography," *IEEE Transactions on Biomedical Engineering*, vol. 65, no. 9, pp. 2033–2041, 2018.

[4] H.-H. Chang, C.-C. Hsu, C.-Y. Chen, W.-K. Lee, H.-T. Hsu, K.-K. Shyu, J.-R. Yeh, P.-J. Lin, and P.-L. Lee, "A method for respiration rate detection in wrist ppg signal using holo-hilbert spectrum," *IEEE Sensors Journal*, vol. 18, no. 18, pp. 7560–7569, 2018.

[5] W. Karlen, C. J. Brouse, E. Cooke, J. M. Ansermino, and G. A. Dumont, "Respiratory rate estimation using respiratory sinus arrhythmia from photoplethysmography," in *2011 Annual International Conference of the IEEE Engineering in Medicine and Biology Society*, pp. 1201–1204, IEEE, 2011.

[6] P. Corbishley and E. Rodriguez-Villegas, "Breathing detection: towards a miniaturized, wearable, battery-operated monitoring system," *IEEE Transactions on Biomedical Engineering*, vol. 55, no. 1, pp. 196–204, 2007.

[7] Y. Nam, B. A. Reyes, and K. H. Chon, "Estimation of respiratory rates using the built-in microphone of a smartphone or headset," *IEEE journal of biomedical and health informatics*, vol. 20, no. 6, pp. 1493–1501, 2015.

[8] S. Sigg, M. Scholz, S. Shi, Y. Ji, and M. Beigl, "Rf-sensing of activities from non-cooperative subjects in device-free recognition systems using ambient and local signals," *IEEE Transactions on Mobile Computing*, vol. 13, no. 4, pp. 907–920, 2014.

[9] O. D. Lara and M. A. Labrador, "A survey on human activity recognition using wearable sensors," *IEEE communications surveys & tutorials*, vol. 15, no. 3, pp. 1192–1209, 2012.

[10] W. Tao, T. Liu, R. Zheng, and H. Feng, "Gait analysis using wearable sensors," *Sensors*, vol. 12, no. 2, pp. 2255–2283, 2012.

[11] L. Bao and S. S. Intille, "Activity recognition from user-annotated acceleration data," in *International conference on pervasive computing*, pp. 1–17, Springer, 2004.

[12] M. Yu, A. Rhuma, S. M. Naqvi, L. Wang, and J. Chambers, "A posture recognition-based fall detection system for monitoring an elderly person in a smart home environment," *IEEE transactions on information technology in biomedicine*, vol. 16, no. 6, pp. 1274–1286, 2012.

[13] K. S. Tan, R. Saatchi, H. Elphick, and D. Burke, "Real-time vision based respiration monitoring system," in *2010 7th International Symposium on Communication Systems, Networks & Digital Signal Processing (CSNDSP 2010)*, pp. 770–774, IEEE, 2010.

[14] S. Banerjee, F. Steenkeste, P. Couturier, M. Debray, and A. Franco, "Telesurveillance of elderly patients by use of passive infra-red sensors in a'smart'room," *Journal of telemedicine and telecare*, vol. 9, no. 1, pp. 23–29, 2003.

[15] B. U. Toreyin, A. B. Soyer, I. Onaran, and E. E. Cetin, "Falling person detection using multi-sensor signal processing," *EURASIP Journal on Advances in Signal Processing*, vol. 2008, pp. 1–7, 2007.

[16] A. Yazar, F. Keskin, B. U. Töreyin, and A. E. Çetin, "Fall detection using single-tree complex wavelet transform," *Pattern Recognition Letters*, vol. 34, no. 15, pp. 1945–1952, 2013.

[17] H. Abdelnasser, K. Harras, and M. Youssef, "A ubiquitous wifi-based fine-grained gesture recognition system," *IEEE Transactions on Mobile Computing*, vol. 18, no. 11, pp. 2474–2487, 2018.

[18] X. Liu, J. Cao, S. Tang, J. Wen, and P. Guo, "Contactless Respiration Monitoring Via Off-the-Shelf WiFi Devices," *IEEE Transactions on Mobile Computing*, vol. 15, no. 10, pp. 2466–2479, 2016.

[19] N. Patwari, J. Wilson, S. Ananthanarayanan, S. K. Kasera, and D. R. Westenskow, "Monitoring breathing via signal strength in wireless networks," *IEEE Transactions on Mobile Computing*, vol. 13, no. 8, pp. 1774–1786, 2014.

[20] C. Uysal and T. Filik, "MUSIC algorithm for respiratory rate estimation using RF signals," *Electrica*, vol. 18, no. 2, pp. 300–309, 2018.

[21] C. Uysal and T. Filik, "Rf-based noncontact respiratory rate monitoring with parametric spectral estimation," *IEEE Sensors Journal*, vol. 19, no. 21, pp. 9841–9849, 2019.

[22] C. Uysal, A. Onat, and T. Filik, "Non-contact respiratory rate estimation in real-time with modified joint unscented kalman filter," *IEEE Access*, vol. 8, pp. 99445–99457, 2020.

[23] C. Uysal and T. Filik, "An efficient noncontact method for monitoring of respiratory rate during sleep using wireless signals," in *2019 11th International Conference on Electrical and Electronics Engineering (ELECO)*, pp. 963–967, IEEE, 2019.

[24] C. Uysal and T. Filik, "Through the wall static human detection using rf signals," *in preparation*.

[25] C. Uysal and T. Filik, "Device-free air-writing recognition with dct by leveraging polarization diversity," *in preparation*.

[26] T. S. Rappaport *et al.*, *Wireless communications: principles and practice*, vol. 2. prentice hall PTR New Jersey, 1996.

[27] A. Goldsmith, *Wireless communications*. Cambridge university press, 2005.

[28] A. J. Wilson, *Device-free localization with received signal strength measurements in wireless networks*. PhD thesis, University of Utah, College of Engineering, 2010.

[29] H. Hashemi, "The indoor radio propagation channel," *Proceedings of the IEEE*, vol. 81, no. 7, pp. 943–968, 1993.

[30] H. Yiğitler *et al.*, "Narrowband radio frequency inference: Physical modeling and measurement processing," 2018.

[31] O. Kaltiokallio *et al.*, "Gaining situational awareness in indoor environments using narrowband radio signal measurements," 2017.

[32] A. J. Wilson, *Device-free localization with received signal strength measurements in wireless networks*. PhD thesis, University of Utah, College of Engineering, 2010.

[33] B. Mrazovac12, B. M. Todorović, D. Kukolj12, and M. Temerinac12, "Device-free human presence detection using frequency domain," 2015.

[34] S. Depatla, A. Muralidharan, and Y. Mostofi, "Occupancy estimation using only wifi power measurements," *IEEE Journal on Selected Areas in Communications*, vol. 33, no. 7, pp. 1381–1393, 2015.

[35] B. Mager, N. Patwari, and M. Bocca, "Fall detection using rf sensor networks," in *Personal Indoor and Mobile Radio Communications (PIMRC), 2013 IEEE 24th International Symposium on*, pp. 3472–3476, IEEE, 2013.

[36] D. Wu, D. Zhang, C. Xu, H. Wang, and X. Li, "Device-free wifi human sensing: From pattern-based to model-based approaches," *IEEE Communications Magazine*, vol. 55, no. 10, pp. 91–97, 2017.

[37] H. Abdelnasser, K. A. Harras, and M. Youssef, "UbiBreathe," in *Proceedings of the 16th ACM International Symposium on Mobile Ad Hoc Networking and Computing - MobiHoc '15*, (New York, New York, USA), pp. 277–286, ACM Press, 2015.

[38] C. Wu, Z. Yang, Z. Zhou, X. Liu, Y. Liu, and J. Cao, "Non-invasive detection of moving and stationary human with WiFi," *IEEE Journal on Selected Areas in Communications*, vol. 33, no. 11, pp. 2329–2342, 2015.

[39] E. Cianca, M. De Sanctis, and S. Di Domenico, "Radios as sensors," *IEEE Internet of Things Journal*, vol. 4, no. 2, pp. 363–373, 2016.

[40] K. Wu, J. Xiao, Y. Yi, D. Chen, X. Luo, and L. M. Ni, "Csi-based indoor localization," *IEEE Transactions on Parallel and Distributed Systems*, vol. 24, no. 7, pp. 1300–1309, 2012.

[41] S. Sigg, M. Scholz, Shuyu Shi, Yusheng Ji, and M. Beigl, "RF-Sensing of Activities from Non-Cooperative Subjects in Device-Free Recognition Systems Using Ambient and Local Signals," *IEEE Transactions on Mobile Computing*, vol. 13, pp. 907–920, apr 2014.

[42] Q. Pu, S. Gupta, S. Gollakota, and S. Patel, "Whole-home gesture recognition using wireless signals," in *Proceedings of the 19th annual international conference on Mobile computing & networking*, pp. 27–38, ACM, 2013.

[43] F. Adib, H. Mao, Z. Kabelac, D. Katabi, and R. C. Miller, "Smart homes that monitor breathing and heart rate," in *Proceedings of the 33rd annual ACM conference on human factors in computing systems*, pp. 837–846, ACM, 2015.

[44] R. Ravichandran, E. Saba, K. Y. Chen, M. Goel, S. Gupta, and S. N. Patel, "WiBreathe: Estimating respiration rate using wireless signals in natural settings in the home," in *2015 IEEE International Conference on Pervasive Computing and Communications, PerCom 2015*, pp. 131–139, 2015.

[45] M. Scholz, S. Sigg, H. R. Schmidtke, and M. Beigl, "Challenges for device-free radio-based activity recognition," in *Workshop on Context Systems, Design, Evaluation and Optimisation*, 2011.

[46] A. Popleteev, "Device-free indoor localization using ambient radio signals," in *Proceedings of the 2013 ACM conference on Pervasive and ubiquitous computing adjunct publication*, pp. 549–552, 2013.

[47] S. Palipana, B. Pietropaoli, and D. Pesch, "Recent advances in rf-based passive device-free localisation for indoor applications," *Ad Hoc Networks*, vol. 64, pp. 80–98, 2017.

[48] Q. Zhou, J. Liu, A. Host-Madsen, O. Boric-Lubecke, and V. Lubecke, "Detection of multiple heartbeats using doppler radar," in *2006 IEEE International Conference on Acoustics Speech and Signal Processing Proceedings*, vol. 2, pp. II–II, IEEE, 2006.

[49] M. Amin, P. Zemany, P. Setlur, and F. Ahmad, "Moving target localization for indoor imaging using dual frequency cw radars," in *Fourth IEEE Workshop on Sensor Array and Multichannel Processing, 2006.*, pp. 367–371, IEEE, 2006.

[50] X. Wang, X. Wang, and S. Mao, "Rf sensing in the internet of things: A general deep learning framework," *IEEE Communications Magazine*, vol. 56, no. 9, pp. 62–67, 2018.

[51] I. Immoreev and T. H. Tao, "UWB radar for patient monitoring," in *IEEE Aerospace and Electronic Systems Magazine*, vol. 23, pp. 11–18, 2008.

[52] S. Venkatesh, C. R. Anderson, N. V. Rivera, and R. M. Buehrer, "Implementation and analysis of respiration-rate estimation using impulse-based UWB," in *Proceedings - IEEE Military Communications Conference MILCOM*, vol. 2005, 2005.

[53] F. Adib, Z. Kabelac, and D. Katabi, "Multi-person localization via {RF} body reflections," in *12th {USENIX} Symposium on Networked Systems Design and Implementation ({NSDI} 15)*, pp. 279–292, 2015.

[54] M. A. Cretikos, R. Bellomo, K. Hillman, J. Chen, S. Finfer, and A. Flabouris, "Respiratory rate: the neglected vital sign," *Medical Journal of Australia*, vol. 188, no. 11, pp. 657–659, 2008.

[55] J. J. Liu, M.-C. Huang, W. Xu, X. Zhang, L. Stevens, N. Alshurafa, and M. Sarrafzadeh, "Breathsens: A continuous on-bed respiratory monitoring system with torso localization using an unobtrusive pressure sensing array," *IEEE Journal of Biomedical and Health Informatics*, vol. 19, no. 5, pp. 1682–1688, 2014.

[56] Y. Wang, K. Wu, and L. M. Ni, "WiFall: Device-Free Fall Detection by Wireless Networks," *IEEE Transactions on Mobile Computing*, vol. 16, pp. 581–594, feb 2017.

[57] N. Patwari and J. Wilson, "Rf sensor networks for device-free localization: Measurements, models, and algorithms," *Proceedings of the IEEE*, vol. 98, no. 11, pp. 1961–1973, 2010.

[58] S. Wang, A. Pohl, T. Jaeschke, M. Czaplik, M. Kony, S. Leonhardt, and N. Pohl, "A novel ultra-wideband 80 GHz FMCW radar system for contactless monitoring of vital signs," in *Proceedings of the Annual International Conference of the IEEE Engineering in Medicine and Biology Society, EMBS*, vol. 2015-November, pp. 4978–4981, 2015.

[59] M. He, Y. Nian, and Y. Gong, "Novel signal processing method for vital sign monitoring using FMCW radar," *Biomedical Signal Processing and Control*, vol. 33, pp. 335–345, 2017.

[60] A. D. Droitcour, O. Boric-lubecke, and G. T. a. Kovacs, "Signal-to-Noise Ratio in Doppler Radar System for Heart and Respiratory Rate Measurements," *IEEE Transactions on Microwave Theory and Techniques*, vol. 57, no. 10, pp. 2498–2507, 2009.

[61] Y. Xiao, C. Li, and J. Lin, "A portable noncontact heartbeat and respiration monitoring system using 5-ghz radar," *IEEE Sensors Journal*, vol. 7, no. 7, pp. 1042–1043, 2007.

[62] C. Li, J. Ling, J. Li, and J. Lin, "Accurate doppler radar noncontact vital sign detection using the RELAX algorithm," *IEEE Transactions on Instrumentation and Measurement*, vol. 59, no. 3, pp. 687–695, 2010.

[63] M. Zakrzewski, A. Vehkaoja, A. S. Joutsen, K. T. Palovuori, and J. J. Vanhala, "Noncontact respiration monitoring during sleep with microwave doppler radar," *IEEE Sensors Journal*, vol. 15, no. 10, pp. 5683–5693, 2015.

[64] W.-P. Hung, C.-H. Chang, and T.-H. Lee, "Real-time and noncontact impulse radio radar system for μm movement accuracy and vital-sign monitoring applications," *IEEE Sensors Journal*, vol. 17, no. 8, pp. 2349–2358, 2017.

[65] K.-K. Shyu, L.-J. Chiu, P.-L. Lee, T.-H. Tung, and S.-H. Yang, "Detection of breathing and heart rates in uwb radar sensor data using fvpief-based two-layer eemd," *IEEE Sensors Journal*, vol. 19, no. 2, pp. 774–784, 2018.

[66] O. Kaltiokallio, H. Yiğitler, R. Jäntti, and N. Patwari, "Non-invasive respiration rate monitoring using a single COTS TX-RX pair," in *IPSN 2014 - Proceedings of the 13th International Symposium on Information Processing in Sensor Networks (Part of CPS Week)*, pp. 59–69, 2014.

[67] X. Liu, J. Cao, S. Tang, and J. Wen, "Wi-sleep: Contactless sleep monitoring via WiFi signals," in *Proceedings - Real-Time Systems Symposium*, vol. 2015-January, pp. 346–355, 2015.

[68] J. Liu, Y. Wang, Y. Chen, J. Yang, X. Chen, and J. Cheng, "Tracking vital signs during sleep leveraging off-the-shelf wifi," in *Proceedings of the 16th ACM International Symposium on Mobile Ad Hoc Networking and Computing*, pp. 267–276, ACM, 2015.

[69] H. Wang, D. Zhang, J. Ma, Y. Wang, Y. Wang, D. Wu, T. Gu, and B. Xie, "Human respiration detection with commodity wifi devices," in *Proceedings of the 2016 ACM International Joint Conference on Pervasive and Ubiquitous Computing - UbiComp '16*, (New York, New York, USA), pp. 25–36, ACM Press, 2016.

[70] C. Chen, Y. Han, Y. Chen, H. Q. Lai, F. Zhang, B. Wang, and K. J. Liu, "TR-BREATH: Time-Reversal Breathing Rate Estimation and Detection," *IEEE Transactions on Biomedical Engineering*, vol. 65, no. 3, pp. 489–501, 2018.

[71] X. Wang, C. Yang, and S. Mao, "Tensorbeat: Tensor decomposition for monitoring multiperson breathing beats with commodity wifi," *ACM Trans. Intell. Syst. Technol.*, vol. 9, pp. 8:1–8:27, Sept. 2017.

[72] X. Wang, C. Yang, and S. Mao, "PhaseBeat: Exploiting CSI Phase Data for Vital Sign Monitoring with Commodity WiFi Devices," in *Proceedings - International Conference on Distributed Computing Systems*, pp. 1230–1239, 2017.

[73] S. D. Min, J. K. Kim, H. S. Shin, Y. H. Yun, C. K. Lee, and M. Lee, "Noncontact respiration rate measurement system using an ultrasonic proximity sensor," *IEEE Sensors Journal*, vol. 10, no. 11, pp. 1732–1739, 2010.

[74] B. A. Reyes, N. Reljin, Y. Kong, Y. Nam, and K. H. Chon, "Tidal volume and instantaneous respiration rate estimation using a volumetric surrogate signal acquired via a smartphone camera," *IEEE Journal of Biomedical and Health Informatics*, vol. 21, no. 3, pp. 764–777, 2016.

[75] Z. Zhu, J. Fei, and I. Pavlidis, "Tracking human breath in infrared imaging," in *Proceedings - BIBE 2005: 5th IEEE Symposium on Bioinformatics and Bioengineering*, vol. 2005, pp. 227–231, 2005.

[76] W. Hu, Z. Zhao, Y. Wang, H. Zhang, and F. Lin, "Noncontact accurate measurement of cardiopulmonary activity using a compact quadrature doppler radar sensor," *IEEE Transactions on Biomedical Engineering*, vol. 61, no. 3, pp. 725–735, 2014.

[77] Y. Wang, Q. Liu, and A. E. Fathy, "Simultaneous localization and respiration detection of multiple people using low cost UWB biometric pulse Doppler radar sensor," in *IEEE MTT-S International Microwave Symposium Digest*, 2012.

[78] R. Roy, A. Paulraj, and T. Kailath, "Estimation of signal parameters via rotational invariance techniques-ESPRIT," *IEEE Transactions on Acoustics, Speech and Signal Processing*, vol. 37, no. 7, pp. 94–101, 1989.

[79] R. Schmidt, "Multiple emitter location and signal parameter estimation," *IEEE Transactions on Antennas and Propagation*, vol. 34, pp. 276–280, mar 1986.

[80] B. Quinn and J. Fernandes, "A fast efficient technique for the estimation of frequency," *Biometrika*, vol. 78, no. 3, pp. 489–497, 1991.

[81] F. Daum, "Nonlinear filters: beyond the kalman filter," *IEEE Aerospace and Electronic Systems Magazine*, vol. 20, no. 8, pp. 57–69, 2005.

[82] M. I. Owis, A. H. Abou-Zied, A.-B. Youssef, and Y. M. Kadah, "Study of features based on nonlinear dynamical modeling in ecg arrhythmia detection and classifica-

tion," *IEEE transactions on Biomedical Engineering*, vol. 49, no. 7, pp. 733–736, 2002.

[83] A. G. Polak and J. Mroczka, "Nonlinear model for mechanical ventilation of human lungs," *Computers in biology and medicine*, vol. 36, no. 1, pp. 41–58, 2006.

[84] F.-Y. Wang, N. Jin, D. Liu, and Q. Wei, "Adaptive dynamic programming for finite-horizon optimal control of discrete-time nonlinear systems with ε-error bound," *IEEE Transactions on Neural Networks*, vol. 22, no. 1, pp. 24–36, 2010.

[85] X. Liu, L. Li, Z. Li, X. Chen, T. Fernando, H. H.-C. Iu, and G. He, "Event-trigger particle filter for smart grids with limited communication bandwidth infrastructure," *IEEE Transactions on Smart Grid*, vol. 9, no. 6, pp. 6918–6928, 2017.

[86] S. Li, L. Li, Z. Li, X. Chen, T. Fernando, H. H.-C. Iu, G. He, Q. Wang, and X. Liu, "Event-trigger heterogeneous nonlinear filter for wide-area measurement systems in power grid," *IEEE Transactions on Smart Grid*, vol. 10, no. 3, pp. 2752–2764, 2018.

[87] M. I. Ribeiro, "Kalman and extended kalman filters: Concept, derivation and properties," *Institute for Systems and Robotics*, vol. 43, 2004.

[88] E. A. Wan and A. T. Nelson, "Dual extended kalman filter methods," *Kalman filtering and neural networks*, vol. 123, 2001.

[89] S. J. Julier and J. K. Uhlmann, "New extension of the kalman filter to nonlinear systems," in *Signal processing, sensor fusion, and target recognition VI*, vol. 3068, pp. 182–193, International Society for Optics and Photonics, 1997.

[90] E. A. Wan and R. Van Der Merwe, "The unscented kalman filter for nonlinear estimation," in *Proceedings of the IEEE 2000 Adaptive Systems for Signal Processing, Communications, and Control Symposium (Cat. No. 00EX373)*, pp. 153–158, Ieee, 2000.

[91] E. Saatci and A. Akan, "Dual unscented kalman filter and its applications to respiratory system modelling," *Kalman Filter: Recent Advances and Applications*, pp. 205–228, 2009.

[92] E. Saatci and A. Akan, "Lung model parameter estimation by unscented kalman filter," in *2007 29th Annual International Conference of the IEEE Engineering in Medicine and Biology Society*, pp. 2556–2559, IEEE, 2007.

[93] J. L. Crassidis and F. L. Markley, "Unscented filtering for spacecraft attitude estimation," *Journal of guidance, control, and dynamics*, vol. 26, no. 4, pp. 536–542, 2003.

[94] R. Zhan and J. Wan, "Iterated unscented kalman filter for passive target tracking," *IEEE Transactions on Aerospace and Electronic Systems*, vol. 43, no. 3, pp. 1155–1163, 2007.

[95] G. Valverde and V. Terzija, "Unscented kalman filter for power system dynamic state estimation," *IET generation, transmission & distribution*, vol. 5, no. 1, pp. 29–37, 2011.

[96] A. K. Singh and B. C. Pal, "Decentralized dynamic state estimation in power systems using unscented transformation," *IEEE Transactions on Power Systems*, vol. 29, no. 2, pp. 794–804, 2013.

[97] G. Hu, L. Ni, B. Gao, X. Zhu, W. Wang, and Y. Zhong, "Model predictive based unscented kalman filter for hypersonic vehicle navigation with ins/gnss integration," *IEEE Access*, 2019.

[98] B. Gao, S. Gao, G. Hu, Y. Zhong, and C. Gu, "Maximum likelihood principle and moving horizon estimation based adaptive unscented kalman filter," *Aerospace Science and Technology*, vol. 73, pp. 184–196, 2018.

[99] B. Gao, G. Hu, S. Gao, Y. Zhong, and C. Gu, "Multi-sensor optimal data fusion for ins/gnss/cns integration based on unscented kalman filter," *International Journal of Control, Automation and Systems*, vol. 16, no. 1, pp. 129–140, 2018.

[100] J. He, A. Khedher, and P. Spreij, "A kalman particle filter for online parameter estimation with applications to affine models," *arXiv preprint arXiv:1905.08552*, 2019.

[101] C.-l. Wang, X. Xiong, and H.-j. Liu, "Target tracking algorithm of automotive radar based on iterated square-root ckf," in *Journal of Physics: Conference Series*, vol. 976, p. 012010, IOP Publishing, 2018.

[102] H. Chen, "Adaptive cubature kalman filter for nonlinear state and parameter estimation," in *2012 15th International Conference on Information Fusion*, pp. 1413–1420, IEEE, 2012.

[103] S. Li, Y. Hu, L. Zheng, Z. Li, X. Chen, T. Fernando, H. H. Iu, Q. Wang, and X. Liu, "Stochastic event-triggered cubature kalman filter for power system dynamic state estimation," *IEEE Transactions on Circuits and Systems II: Express Briefs*, vol. 66, no. 9, pp. 1552–1556, 2018.

[104] M. Roth, C. Fritsche, G. Hendeby, and F. Gustafison, "The ensemble kalman filter and its relations to other nonlinear filters," in *2015 23rd European Signal Processing Conference (EUSIPCO)*, pp. 1236–1240, IEEE, 2015.

[105] H. Jiang, G. Liu, J. Li, T. Zhang, C. Wang, and K. Ren, "Model based fault diagnosis for drillstring washout using iterated unscented kalman filter," *Journal of Petroleum Science and Engineering*, vol. 180, pp. 246–256, 2019.

[106] X. Peng, B. Zhang, and L. Rong, "A robust unscented kalman filter and its application in estimating dynamic positioning ship motion states," *Journal of Marine Science and Technology*, vol. 24, no. 4, pp. 1265–1279, 2019.

[107] J. Zhao and L. Mili, "Robust unscented kalman filter for power system dynamic state estimation with unknown noise statistics," *IEEE Transactions on Smart Grid*, vol. 10, no. 2, pp. 1215–1224, 2017.

[108] J. Zhao and L. Mili, "A decentralized h-infinity unscented kalman filter for dynamic state estimation against uncertainties," *IEEE Transactions on Smart Grid*, vol. 10, no. 5, pp. 4870–4880, 2018.

[109] M. Wielitzka, M. Dagen, and T. Ortmaier, "Joint unscented kalman filter for state and parameter estimation in vehicle dynamics," in *2015 IEEE Conference on Control Applications (CCA)*, pp. 1945–1950, IEEE, 2015.

[110] Y. Yuan, G. Fu, and W. Zhang, "Extended and unscented kalman filters for parameter estimation of a hydrodynamic model of vessel," in *2016 35th Chinese Control Conference (CCC)*, pp. 2051–2056, IEEE, 2016.

[111] A. Onat, P. Voltr, and M. Lata, "A new friction condition identification approach for wheel–rail interface," *International Journal of Rail Transportation*, vol. 5, no. 3, pp. 127–144, 2017.

[112] A. Onat, P. Voltr, and M. Lata, "An unscented kalman filter-based rolling radius estimation methodology for railway vehicles with traction," *Proceedings of the Institution of Mechanical Engineers, Part F: Journal of Rail and Rapid Transit*, vol. 232, no. 6, pp. 1686–1702, 2018.

[113] A. Nikoofard, U. J. F. Aarsnes, T. A. Johansen, and G.-O. Kaasa, "State and parameter estimation of a drift-flux model for underbalanced drilling operations," *IEEE Transactions on Control Systems Technology*, vol. 25, no. 6, pp. 2000–2009, 2017.

[114] A. Onat, "A novel and computationally efficient joint unscented kalman filtering scheme for parameter estimation of a class of nonlinear systems," *IEEE Access*, vol. 7, pp. 31634–31655, 2019.

[115] S. J. Julier, J. K. Uhlmann, and H. F. Durrant-Whyte, "A new approach for filtering nonlinear systems," in *American Control Conference, Proceedings of the 1995*, vol. 3, pp. 1628–1632, IEEE, 1995.

[116] E. Wan and R. Van Der Merwe, "Chapter 7: The unscented kalman filter," *Kalman Filtering and Neural Networks*, pp. 221–280, 2001.

[117] S. J. Julier and J. K. Uhlmann, "Unscented filtering and nonlinear estimation," *Proceedings of the IEEE*, vol. 92, no. 3, pp. 401–422, 2004.

[118] B. Matzuka, M. Aoi, A. Attarian, and H. T. Tran, "Nonlinear filtering methodologies for parameter estimation," tech. rep., North Carolina State University. Center for Research in Scientific Computation, 2012.

[119] P. Ramachandran, B. Zoph, and Q. V. Le, "Searching for activation functions," *arXiv preprint arXiv:1710.05941*, 2017.

[120] M. M. Lau and K. H. Lim, "Investigation of activation functions in deep belief network," in *2017 2nd international conference on control and robotics engineering (ICCRE)*, pp. 201–206, IEEE, 2017.

[121] C. Lowanichkiattikul, M. Dhanachai, C. Sitathanee, S. Khachonkham, and P. Khaothong, "Impact of chest wall motion caused by respiration in adjuvant radiotherapy for postoperative breast cancer patients," *SpringerPlus*, vol. 5, no. 1, p. 144, 2016.

[122] P. Stoica, R. L. Moses, *et al.*, *Spectral analysis of signals*, vol. 1. Pearson Prentice Hall Upper Saddle River, NJ, 2005.

[123] S. Corbetta, A. Dardanelli, I. Boniolo, S. M. Savaresi, and S. Bittanti, "Frequency estimation of narrow band signals in gaussian noise via unscented kalman filter," in *Decision and Control (CDC), 2010 49th IEEE Conference on*, pp. 2869–2874, IEEE, 2010.

[124] R. Yates and R. Lyons, "Dc blocker algorithms [dsp tips & tricks]," *IEEE Signal Processing Magazine*, vol. 25, no. 2, pp. 132–134, 2008.

[125] J. O. Smith, *Introduction to Digital Filters with Audio Applications*. http://www.w3k.org/books/: W3K Publishing, 2007.

[126] L. Davies and U. Gather, "The identification of multiple outliers," *Journal of the American Statistical Association*, vol. 88, no. 423, pp. 782–792, 1993.

[127] M. Ettus *et al.*, "Ettus research, LLC," *Online information on USRP board). http://www. ettus. com*, 2008.

[128] F. C. Commission *et al.*, "Part 15–radio frequency devices," *FCC, Washington, DC*, 2003.

[129] B. G. Quinn and E. J. Hannan, *The estimation and tracking of frequency*, vol. 9. Cambridge University Press, 2001.

[130] R. Van Der Merwe, *Sigma-point Kalman filters for probabilistic inference in dynamic state-space models*. PhD thesis, Oregon Health & Science University, 2004.

[131] A. Nikoofard, T. A. Johansen, and A. Molaei, "Reservoir characterization in under-balanced drilling with nonlinear moving horizon estimation with manual and automatic control conditions," *Journal of Petroleum Science and Engineering*, p. 107248, 2020.

[132] J. Wang, Q. Gao, M. Pan, and Y. Fang, "Device-free wireless sensing: Challenges, opportunities, and applications," *IEEE Network*, vol. 32, no. 2, pp. 132–137, 2018.

[133] L. Deng and X. Li, "Machine learning paradigms for speech recognition: An overview," *IEEE Transactions on Audio, Speech, and Language Processing*, vol. 21, no. 5, pp. 1060–1089, 2013.

[134] J. Padmanabhan and M. J. Johnson Premkumar, "Machine learning in automatic speech recognition: A survey," *IETE Technical Review*, vol. 32, no. 4, pp. 240–251, 2015.

[135] G. Guo, S. Z. Li, and K. Chan, "Face recognition by support vector machines," in *Proceedings fourth IEEE international conference on automatic face and gesture recognition (cat. no. PR00580)*, pp. 196–201, IEEE, 2000.

[136] C. Topal, S. Gunal, O. Koçdeviren, A. Doğan, and Ö. N. Gerek, "A low-computational approach on gaze estimation with eye touch system," *IEEE transactions on cybernetics*, vol. 44, no. 2, pp. 228–239, 2013.

[137] J. Peters, "Machine learning for motor skills in robotics," *KI-Künstliche Intelligenz*, vol. 2008, no. 4, pp. 41–43, 2008.

[138] S. Di Domenico, M. De Sanctis, E. Cianca, and M. Ruggieri, "Wifi-based through-the-wall presence detection of stationary and moving humans analyzing the doppler spectrum," *IEEE Aerospace and Electronic Systems Magazine*, vol. 33, no. 5-6, pp. 14–19, 2018.

[139] J. Li, Z. Zeng, J. Sun, and F. Liu, "Through-wall detection of human being's movement by uwb radar," *IEEE Geoscience and Remote Sensing Letters*, vol. 9, no. 6, pp. 1079–1083, 2012.

[140] S. D. Liang, "Sense-through-wall human detection based on uwb radar sensors," *Signal Processing*, vol. 126, pp. 117–124, 2016.

[141] K. Chetty, G. E. Smith, and K. Woodbridge, "Through-the-wall sensing of personnel using passive bistatic wifi radar at standoff distances," *IEEE Transactions on Geoscience and Remote Sensing*, vol. 50, no. 4, pp. 1218–1226, 2011.

[142] X. Wu, Z. Chu, P. Yang, C. Xiang, X. Zheng, and W. Huang, "Tw-see: Human activity recognition through the wall with commodity wi-fi devices," *IEEE Transactions on Vehicular Technology*, vol. 68, no. 1, pp. 306–319, 2018.

[143] J. Wilson and N. Patwari, "See-through walls: Motion tracking using variance-based radio tomography networks," *IEEE Transactions on Mobile Computing*, vol. 10, no. 5, pp. 612–621, 2010.

[144] F. Adib and D. Katabi, "See through walls with wifi!," in *Proceedings of the ACM SIGCOMM 2013 conference on SIGCOMM*, pp. 75–86, 2013.

[145] H. Zhu, F. Xiao, L. Sun, R. Wang, and P. Yang, "R-ttwd: Robust device-free through-the-wall detection of moving human with wifi," *IEEE Journal on Selected Areas in Communications*, vol. 35, no. 5, pp. 1090–1103, 2017.

[146] J. Wilson and N. Patwari, "Radio tomographic imaging with wireless networks," *IEEE Transactions on Mobile Computing*, vol. 9, no. 5, pp. 621–632, 2010.

[147] J. Wilson and N. Patwari, "A fade-level skew-laplace signal strength model for device-free localization with wireless networks," *IEEE Transactions on Mobile Computing*, vol. 11, no. 6, pp. 947–958, 2012.

[148] A. E. Kosba, A. Saeed, and M. Youssef, "Rasid: A robust wlan device-free passive motion detection system," in *2012 IEEE International Conference on Pervasive Computing and Communications*, pp. 180–189, IEEE, 2012.

[149] J. Xiao, K. Wu, Y. Yi, L. Wang, and L. M. Ni, "Fimd: Fine-grained device-free motion detection," in *2012 IEEE 18th International Conference on Parallel and Distributed Systems*, pp. 229–235, IEEE, 2012.

[150] K. Qian, C. Wu, Z. Yang, Y. Liu, and Z. Zhou, "Pads: Passive detection of moving targets with dynamic speed using phy layer information," in *2014 20th IEEE international conference on parallel and distributed systems (ICPADS)*, pp. 1–8, IEEE, 2014.

[151] H. Zhu, F. Xiao, L. Sun, X. Xie, and R. Wang, "Robust passive static human detection with commodity wifi devices," in *2017 IEEE 36th International Performance Computing and Communications Conference (IPCCC)*, pp. 1–8, IEEE, 2017.

[152] S. Depatla and Y. Mostofi, "Crowd counting through walls using wifi," in *2018 IEEE International Conference on Pervasive Computing and Communications (PerCom)*, pp. 1–10, IEEE, 2018.

[153] C. M. Bishop, *Pattern recognition and machine learning*. springer, 2006.

[154] L. Breiman, J. Friedman, C. J. Stone, and R. A. Olshen, *Classification and regression trees*. CRC press, 1984.

[155] W.-Y. Loh, "Classification and regression trees," *Wiley Interdiscip. Rev. Data Min. Knowl. Discov.*, vol. 1, pp. 14–23, 2011.

[156] S. S. Rautaray and A. Agrawal, "Vision based hand gesture recognition for human computer interaction: a survey," *Artificial Intelligence Review*, vol. 43, pp. 1–54, Jan 2015.

[157] L. Sun, S. Sen, D. Koutsonikolas, and K.-H. Kim, "Widraw: Enabling hands-free drawing in the air on commodity wifi devices," in *Proceedings of the 21st Annual International Conference on Mobile Computing and Networking*, pp. 77–89, ACM, 2015.

[158] Z. Fu, J. Xu, Z. Zhu, A. X. Liu, and X. Sun, "Writing in the air with wifi signals for virtual reality devices," *IEEE Transactions on Mobile Computing*, vol. 18, no. 2, pp. 473–484, 2018.

[159] A. Graves, A. Mohamed, and G. Hinton, "Speech recognition with deep recurrent neural networks," in *2013 IEEE International Conference on Acoustics, Speech and Signal Processing*, pp. 6645–6649, May 2013.

[160] X. Liu, J. Cao, S. Tang, and J. Wen, "Wi-sleep: Contactless sleep monitoring via wifi signals," in *2014 IEEE Real-Time Systems Symposium*, pp. 346–355, IEEE, 2014.

[161] Y. Wang, K. Wu, and L. M. Ni, "Wifall: Device-free fall detection by wireless networks," *IEEE Transactions on Mobile Computing*, vol. 16, no. 2, pp. 581–594, 2016.

[162] C. Amma, D. Gehrig, and T. Schultz, "Airwriting recognition using wearable motion sensors," in *Proceedings of the 1st Augmented Human international Conference*, p. 10, ACM, 2010.

[163] M. Chen, G. AlRegib, and B.-H. Juang, "Air-writing recognition—part i: Modeling and recognition of characters, words, and connecting motions," *IEEE Transactions on Human-Machine Systems*, vol. 46, no. 3, pp. 403–413, 2015.

[164] A. Schick, D. Morlock, C. Amma, T. Schultz, and R. Stiefelhagen, "Vision-based handwriting recognition for unrestricted text input in mid-air," in *Proceedings of the 14th ACM international conference on Multimodal interaction*, pp. 217–220, ACM, 2012.

[165] X. Cao, B. Chen, and Y. Zhao, "Wi-wri: Fine-grained writing recognition using wi-fi signals," in *2016 IEEE Trustcom/BigDataSE/ISPA*, pp. 1366–1373, IEEE, 2016.

[166] S. Ma, T. Huang, S. Li, J. Huang, T. Ma, and J. Liu, "Mcsm-wri: A small-scale motion recognition method using wifi based on multi-scale convolutional neural network," *Sensors*, vol. 19, no. 19, p. 4162, 2019.

[167] A. B. Watson, "Image compression using the discrete cosine transform," *Mathematica journal*, vol. 4, no. 1, p. 81, 1994.

[168] X.-Y. Jing and D. Zhang, "A face and palmprint recognition approach based on discriminant dct feature extraction," *IEEE Transactions on Systems, Man, and Cybernetics, Part B (Cybernetics)*, vol. 34, no. 6, pp. 2405–2415, 2004.

[169] Z. He and L. Jin, "Activity recognition from acceleration data based on discrete consine transform and svm," in *2009 IEEE International Conference on Systems, Man and Cybernetics*, pp. 5041–5044, IEEE, 2009.

[170] I. Batal and M. Hauskrecht, "A supervised time series feature extraction technique using dct and dwt," in *2009 international conference on machine learning and applications*, pp. 735–739, IEEE, 2009.

[171] C. Wang, Z. Liu, and S.-C. Chan, "Superpixel-based hand gesture recognition with kinect depth camera," *IEEE transactions on multimedia*, vol. 17, no. 1, pp. 29–39, 2014.

[172] G. Marin, F. Dominio, and P. Zanuttigh, "Hand gesture recognition with leap motion and kinect devices," in *2014 IEEE International conference on image processing (ICIP)*, pp. 1565–1569, IEEE, 2014.

[173] S. Gupta, D. Morris, S. Patel, and D. Tan, "Soundwave: using the doppler effect to sense gestures," in *Proceedings of the SIGCHI Conference on Human Factors in Computing Systems*, pp. 1911–1914, 2012.

[174] D. Kim, O. Hilliges, S. Izadi, A. D. Butler, J. Chen, I. Oikonomidis, and P. Olivier, "Digits: freehand 3d interactions anywhere using a wrist-worn gloveless sensor," in *Proceedings of the 25th annual ACM symposium on User interface software and technology*, pp. 167–176, 2012.

[175] W. He, K. Wu, Y. Zou, and Z. Ming, "Wig: Wifi-based gesture recognition system," in *2015 24th International Conference on Computer Communication and Networks (ICCCN)*, pp. 1–7, IEEE, 2015.

[176] M. A. A. Al-qaness and F. Li, "Wiger: Wifi-based gesture recognition system," *ISPRS International Journal of Geo-Information*, vol. 5, no. 6, p. 92, 2016.

[177] L. Kane and P. Khanna, "Vision-based mid-air unistroke character input using polar signatures," *IEEE Transactions on Human-Machine Systems*, vol. 47, no. 6, pp. 1077–1088, 2017.

[178] D. Wu, R. Gao, Y. Zeng, J. Liu, L. Wang, T. Gu, and D. Zhang, "Fingerdraw: Sub-wavelength level finger motion tracking with wifi signals," *Proceedings of the ACM on Interactive, Mobile, Wearable and Ubiquitous Technologies*, vol. 4, no. 1, pp. 1–27, 2020.

[179] D. Ren, Y. Zhang, N. Xiao, H. Zhou, X. Li, J. Qian, and P. Yang, "Word-fi: Accurate handwrite system empowered by wireless backscattering and machine learning," *IEEE Network*, vol. 32, no. 4, pp. 47–53, 2018.

[180] A. Bensky, *Short-range wireless communication*. Newnes, 2019.

[181] C. A. Balanis, *Antenna theory: analysis and design*. John wiley & sons, 2016.

[182] Y. Xiong and F. Quek, "Hand motion gesture frequency properties and multimodal discourse analysis," *International Journal of Computer Vision*, vol. 69, no. 3, pp. 353–371, 2006.

[183] S. Mallat, *A wavelet tour of signal processing*. Elsevier, 1999.

[184] I. Daubechies, *Ten lectures on wavelets*, vol. 61. Siam, 1992.

[185] N. Ahmed, T. Natarajan, and K. R. Rao, "Discrete cosine transform," *IEEE transactions on Computers*, vol. 100, no. 1, pp. 90–93, 1974.

[186] A. R. Webb, *Statistical pattern recognition*. John Wiley & Sons, 2003.

[187] B. Scholkopf and A. J. Smola, *Learning with kernels: support vector machines, regularization, optimization, and beyond*. MIT press, 2001.

CV

Name:	Can Uysal
Foreign Languages:	English
Birth date and place:	01/02/1986, Çanakkale
E-mail:	canuysal@eskisehir.edu.tr

Education

- PhD (2015–2020), Eskisehir Technical University, Department of Electrical and Electronics Engineering
- MSc (2012–2015), Anadolu University, Department of Electrical and Electronics Engineering
- BSc (2005–2009), Kocaeli University, Department of Electronics and Communication Engineering
- High School (1997 – 2004) Milli Piyango Anatolian High School, Çanakkale

Employment

- Research Assistant (2018—), Eskisehir Technical University, Department of Electrical and Electronics Engineering
- Research Assistant (2012—2018), Anadolu University, Department of Electrical and Electronics Engineering
- RF Optimization Engineer (2011—2012), ETC Telecommunication (Turkcell-Consultant)

Publications

- C. Uysal, A. Onat and T. Filik, "Non-contact respiratory rate estimation in real-time with modified joint unscented Kalman Filter," in *IEEE Access*, vol. 8, pp. 99445-99457, 2020
- C. Uysal and T. Filik, "RF-based noncontact respiratory rate monitoring with parametric spectral estimation," *IEEE Sensors Journal*, vol. 19, no. 21, pp. 9841–9849, 2019
- C. Uysal and T. Filik, "An efficient noncontact method for monitoring of respiratory rate during sleep using wireless signals," in *11th International Conference on Electrical and Electronics Engineering (ELECO)*, pp. 963–967, IEEE, 2019
- C. Uysal and T. Filik, "MUSIC algorithm for respiratory rate estimation using RF signals," *Electrica*, vol. 18, no. 2, pp. 300–309, 2018

- C. Uysal and T. Filik. "Contactless respiration rate estimation with phase difference." *26th Signal Processing and Communications Applications Conference (SIU). IEEE*, 2018

- C. Uysal and T. Filik. "Contactless respiration rate estimation using MUSIC algorithm." *10th International Conference on Electrical and Electronics Engineering (ELECO). IEEE,* 2017

- C. Uysal and T. Filik. "The localization of LPI signals using sparse TDOA estimates." *24th Signal Processing and Communication Application Conference (SIU). IEEE*, 2016

- C. Uysal and T. Filik. "A joint detection and localization method for non-cooperative DS-SS signals." *IEEE Military Communications Conference (MILCOM). IEEE*, 2015

- C. Uysal and T. Filik. "A sparse approach for the presence detection of long-code DS-SS signals." *23nd Signal Processing and Communications Applications Conference (SIU). IEEE*, 2015

- C. Uysal and T. Filik. "Presence detection of long-and-short-code DS-SS signals using the phase linearity of multichannel sensors." *19th International Conference on Digital Signal Processing (DSP). IEEE*, 2014

- C. Uysal and T. Filik. "Detection of low probability of intercept signals in low SNR using multichannel sensor arrays." *22nd Signal Processing and Communications Applications Conference (SIU). IEEE*, 2014